FOG

Freiberg Online Geology

FOG is an electronic journal registered under
ISSN 1434-7512

2010, VOL 26

Nadja Schmidt

Hydrogeological and hydrochemical investigations at the Salar de Uyuni (Bolivia) with regard to the extraction of lithium

131 pages, 58 figures, 30 tables, 62 references

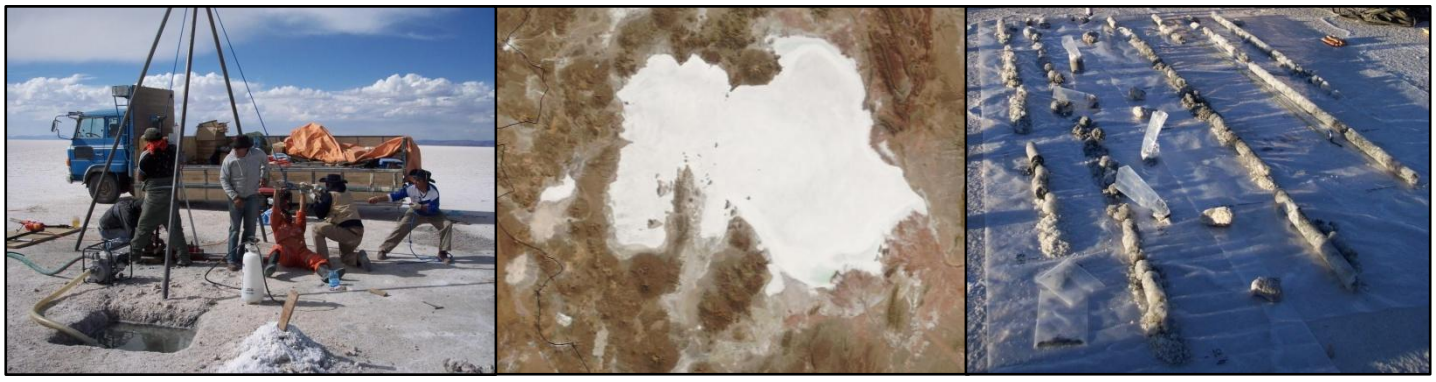

Acknowledgements

First of all, my thanks go to Prof. Broder Merkel, my first supervisor, for providing the amazing topic and thus giving me the opportunity to work abroad, and for his support especially during the fieldwork and back in Germany.

Further I want to sincerely thank Dipl.Geoökol. Robert Sieland for his engagement, his consequent advice and encouragement during the stay in Bolivia and the completion of the thesis in Freiberg.

My special thanks go to Dr. Jaime Claros from the UATF in Potosí, who organized my stay and the field trips in Bolivia. The kind hospitality of him and his family and his support in any form made my stay an impressive experience.

My acknowledgements go to Juan Carlos Erquisia and Dr. Pedro Lopez from the UATF for introducing me into the investigation area, for their assistance in the field and for providing far more than scientific advice.

I honestly enjoyed the interdisciplinary work in an international team as a valuable experience. Therefore, I owe thanks to all members of the field trips, German and Bolivian students as well as Alberto, Gari and Fidel, for their engagement in the physically demanding work under challenging conditions.

Further I generally want to thank the university of Potosí in Bolivia, and especially the rector Juan J. R. Bohorquez for permanent support, be it in material, personal or financial form.

My thanks go to the Bundesanstalt für Geowissenschaften und Rohstoffe in Hannover, especially to Mr. Schramm und Mr. Hammer, for the financial support of the field trip and for performing important parts of the analytical work.

For laboratory assistance with the water analyses in Freiberg, I want to thank H.J. Peter and Dr. S. Kummer, as well as J. Hubálkova for the advice with the CT analyses.

I also want to thank the German Academic Exchange Survey (DAAD) for providing the financial base that actually made this stay abroad possible.

Great thanks go to the team of chemistry students in Potosí for introducing me into the Bolivian culture, the way of life and the language.

Of course, my sincere thanks go to my friends and my family, especially my parents, for their patience and mental support as well as for their willing to listen in good and in bad times.

Table of Contents

1 Introduction 1
1.1 Motivation 1
1.2 Universitary cooperation project “Salar de Uyuni” 4
1.3 Objectives of the work 5

2 Description of the study area 6
2.1 Geographic and geologic background 6
2.2 Contemporary hydrologic setting of the Altiplano 8
2.3 Climatic conditions 10
2.4 Sedimentology and Paleolakes 12
2.5 Brine chemistry and origin of solutes 14

3 Methods 16
3.1 Drilling procedure 16
3.1.1 First attempt 16
3.1.2 Second attempt 17
3.1.3 Distribution of boreholes and drilling patterns 19
3.1.4 Sampling of salt cores 22
3.2 Well casing 23
3.3 Field analyses and brine sampling 24
3.4 Laboratory analyses 27
3.4.1 Analyses of the core samples 27
3.4.1.1 Geochemical and mineralogical composition 27
3.4.1.2 Computer tomography 27
3.4.2 Analyses of the brine samples 29
3.4.2.1 Ion chromatography 29
3.4.2.2 Total inorganic and dissolved organic carbon 29
3.4.2.3 Mass spectrometry with inductively coupled plasma 30
3.4.2.4 Determination of viscosity and density 31
3.4.3 Methods of evaluation 32
3.4.3.1 Check for plausibility 32
3.4.3.2 Statistical data treatment 32
3.5 Pumping Tests 34

4 Results and Evaluation 35
4.1 Core samples 35
4.1.1 Stratigraphy 35
4.1.1.1 Drilling location SLT-01 36

4.1.1.2 Drilling location SLT-03 39
4.1.2 Rock quality and core loss 41
4.1.3 Chemical and mineralogical composition 44
4.1.4 Porosity 49
4.2 Hydraulic conductivity 53
4.3 Brine samples 60
4.3.1 On-Site parameters 60
4.3.2 Photometry 62
4.3.3 Total dissolved solids 63
4.3.4 Main anions and cations 64
4.3.5 Minor and trace elements 70
4.3.6 Evaluation of errors and check for plausibility 71
4.3.7 Statistical evaluation 74
4.3.8 Modelling with PhreeqC 76
4.3.8.1 Ionic strength 76
4.3.8.2 Saturation index 77
4.3.9 Physical parameters 80
4.3.9.1 Viscosity 80
4.3.9.2 Density 82
5 Discussion and conclusions 84
5.1 Review of salt deposits 85
5.2 Factors concerning brine evaporation 87
5.3 Chemical aspects of lithium recovery 91
5.4 Environmental considerations 92
6 Perspectives and recommendations 93
7 Literature 95
Appendix 102

List of Figures

Fig. 1: Application of lithium in different industries (modified after Roskill 2009, in Angerer et al. 2009) 2
Fig. 2: Schematic map of the Altiplano with main drainage basins (after Risacher & Fritz 2000) 6
Fig. 3: Satellite image of the Salar de Uyuni with laterally adjacent mountain ranges and volcano summits, captured by the MODUS sensor of the satellite Terra (source: NASA) 7
Fig. 4: N-S cross section of the northern and central basins of the Altiplano with recent and past lake levels (from Risacher & Fritz 2000) 8
Fig. 5: Climate diagrams for 3 locations in the Altiplano from north to south (data from www.worldclimate.com) 10
Fig. 6: Log of the drilling hole in the centre of the Salar de Uyuni reflecting the stratigraphy and thickness of each layer (after Fornari et al. 2001) 12
Fig. 7: Drilling machine of the Bolivian drilling company (left), pump for drilling fluid (top right), core barrel for cores with a length of 1 m and a diameter of 4” (down right) 17
Fig. 8: Diamasa drilling machine (left); fixation of the drill rig with anchors (middle); using the support of the tripod (right) 18
Fig. 9: Distribution of performed and planned drillings on the Salar de Uyuni (modified after Risacher & Fritz 2000) 19
Fig. 10: Depths of the drillings in location SLT-01 (left) as well as arrangement of the boreholes (right) 21
Fig. 11: Depths of the drillings in location SLT-03 (left) as well as arrangement of the boreholes (right) 21
Fig. 12: Schema of the well casing (not to scale) 23
Fig. 13: Determination of field parameters of the brine in a flow through cell 24
Fig. 14: Fixation of the core sample in the instrument 27
Fig. 15: Viscometer with UL adapter 31
Fig. 16: Upper crust of SLT-01A (left) with a length of 10 cm, SLT-03C (middle) and SLT-03A (right) with a length of 25 cm each 36
Fig. 17: Core documentation for drilling hole SLT-01E for the upper 2.70 m 38
Fig. 18: Profile of the deepest drillings from SLT-01 and SLT-03 in comparison to the drilling UA in the central part of the Salar 40
Fig. 19: Gradient of the rock quality after Meier (1999) with sampling depth for selected drilling points from SLT-01 and SLT-03 42
Fig. 20: Distribution of minerals determined in the core samples from SLT-01A in dependency of the depth and the splitting of the fraction summarized as other minerals 45
Fig. 21: Pictures of core samples associated to layers with low content of halite 46
Fig. 22: Comparison of the bromine content in halite in core samples from SLT-01A analysed by the BGR and from a point with a low distance to SLT-01A according to Risacher 47
Fig. 23: 3-dimensional images of the upper crust sample from SLT-03: slant side view (left), the same core sample longitudinally cut to show connected pores (right) 49

Fig. 24: 3-dimensional images of the sample from a depth of 3 m from SLT-03: side view showing vertical cavity (left); top view (right) 50
Fig. 25: Processing of the raw images derived from CT analyses 51
Fig. 26: Drawdown curve in observation well SLT-03B for a pumping duration of 160 min 54
Fig. 27: Curve of drawdown versus time for the recovery test in well SLT-01A, the Δh_s for the determination of T_M is obtained from a logarithmic time decade 57
Fig. 28: E_H/pH-diagram with upper and lower stability limits of water (closed line), borders of E_H for oxidizing and reducing conditions (dashed line)..... 61
Fig. 29: Contents of total dissolved solids in the samples and comparative values of brines from other saline pans in South America (after Warren 2006)..... 63
Fig. 30: Concentration ranges in mmol/L of main cations and anions in the nine brine samples (numbers below elements are the standard deviations of the data in % of the mean) 64
Fig. 31: Concentrations of sodium and calcium plotted against lithium contents in the brine samples, points in dashed circles indicate the sampling location .. 66
Fig. 32: Concentrations of Mg, K and SO_4 plotted against the content of lithium in the brine samples..... 67
Fig. 33: Concentrations of Br and B plotted against the content of lithium in the brine samples..... 69
Fig. 34: Enrichment and depletion of elements at SLT-03 and SLT-S compared to SLT-01 71
Fig. 35: Percent charge errors of the brine analyses computed with PhreeqC (Pitzer database)..... 72
Fig. 36: Electric conductivity (at 25°C) of a standard solution of NaCl in dependency of salt concentration and comparison to measured values of the Uyuni brine samples..... 73
Fig. 37: Dendrogram resulting from clustering with 45 parameters obtained from chemical analyses of all nine brine samples..... 75
Fig. 38: Ionic strengths of the sampled brines calculated by PhreeqC using the database based on the Pitzer equation (values for Atacama obtained from data of Boschetti et al. 2007)..... 77
Fig. 39: Averaged saturation indices for selected sulphate, carbonate and chloride mineral phases; samples are grouped together according to their location on the Salar, standard deviations for samples from SLT-01 and SLT-03 are also shown..... 79
Fig. 40: Temperature – density and temperature – viscosity relation for a standard solution (Holldorf & Baumbach 1987) and the brine samples..... 81
Fig. 41: Relation between TDS content and density of brines from the Salar de Uyuni and concentrated seawater 82
Fig. 42: Development of the saturation indices for important mineral phases with increasing evaporation rate of the brine from SLT-01 (modeled by PhreeqC)..... 88
Fig. 43: Development of the concentration of solved components with increasing evaporation rate of the brine under the assumption that oversaturated mineral phases are removed from the solution by precipitation (modeled by PhreeqC)..... 89
Fig. 44: Ratios of magnesium to lithium in brines from different salt pans (values for the Salar de Uyuni are from this study, other data are taken from King 2010)..... 91

List of Tables

Table 1: Estimated global resources and reserves of lithium (source: U.S. Geological Survey, values are from 2010) 3
Table 2: Properties of the drilling machine 18
Table 3: GPS-positions of important points (geographic coordinates converted from UTM, geodetic datum: Prov S Am'56) 20
Table 4: Parameters of the single methods used for photometry 26
Table 5: Core losses for the documented drilling profiles 41
Table 6: Volume of the pores in both cores obtained by computer tomography 50
Table 7: Parameters for the determination of k_f 55
Table 8: Summary of parameters determined in the field including the standard deviation 60
Table 9: Results of photometrical analyses performed in the field: average values of the samples from each drilling location with standard deviation (all values in mg/L) 62
Table 10: Classification of determined species according to their concentration 70
Table 11: Exclusion of species based on the measured concentration of opposite species (source: DVWK rules 128, 1992) 73
Table 12: Comparison of lithium contents for different calibration methods 74
Table 13: Results of the Kruskal-Wallis-Test for clustering the data into three clusters 75
Table 14: Comparison of the number of under- and oversaturated mineral phases for the three sample groups 78
Table 15: Dynamic viscosity of the samples, of deionized water (dH_2O) and of a reference value with a defined composition (from Lide 2008) 80
Table 16: Estimated concentrations c of solutes in precipitation and surface inflow from the Rio Grande, and contributions M of solutes per year to the Salar (see text for explanations) 86

Symbols and Abbreviations

Δh_S	difference in drawdown [m]
asl	above sea level
BGR	Bundesanstalt für Geowissenschaften und Rohstoffe
B.P.	before present
CT	computer tomography
D_{Br}	distribution coefficient of bromine
DL	detection limit
E_0	standard redox potential [mV]
E_H	redox potential [mV]
E_{pot}	potential evaporation
EC	electrical conductivity [mS/cm]
EDL	estimated detection limit
EMK	electromotive force [mV]
g	gravity [m/s²]
GPS	Global Positioning System
h_S	drawdown [m]
HDPE	high-density polyethylene
I_{AP}	ion activity product
IC	ion chromatography
ICP-MS	mass spectrometry with inductively coupled plasma
K	intrinsic permeability [m²]
k_f	hydraulic conductivity [m/s]
K_{SP}	solubility product of a mineral phase
L_M	rock quality
LOD	lower detection limit
M	thickness of the aquifer [m]
η	dynamic viscosity [mPa·s]
n	number of samples
n_{eff}	effective porosity
OES	optical emission spectrometry
ρ	density [kg/m³]
PE	polyethylene
PVC	polyvinylchloride

Q	discharge rate [m^3/s]
r	distance between wells [m]
rpm	rounds per minute
s	standard deviation
SI	saturation index
T	temperature [°C]
T_M	transmissivity [m^2/s]
TDS	total dissolved solids
TIC	total inorganic carbon [mg C/L]
TUBAF	Technische Universität Bergakademie Freiberg
UATF	Universidad Autónoma Tomás Frías
USGS	United States Geological Survey
wt%	weight %
yr	years

Abstract

The Salar de Uyuni, a salt pan located in the Bolivian Andes, was subject to hydrogeological and hydrochemical investigations between June and September 2009. During a drilling and sampling campaign halite cores were gained from different bore holes with depths between 2 and 12 m at two locations in the north eastern and the central part of the Salar (named SLT-01 and SLT-03, respectively). Brine samples, taken in different depths from the installed wells, were subject to field and laboratory analyses (IC, ICP-MS) and the determination of physical parameters (viscosity, density).

Geochemical analyses of the sediment cores from SLT-01 show the large excess of halite with minor amounts of gypsum. The underlying mud layer is characterized by a high content of water insoluble minerals. Computer tomograph analyses of selected core samples revealed significant differences between the surface-near salt crust and deeper halite layers by means of pore volume, connectivity and structure of pores. The high permeability indicated by the calculated effective pore volume of almost 20%, was roughly confirmed by the results of a pumping test performed in SLT-03, which showed an intrinsic permeability of $1.95 \cdot 10^{-10}$ m² of the uppermost halite aquifer.

Brines from the two drilling locations exhibit high differences in chemical composition, but variations with depth could not be observed. The major part of ions and minor elements is clearly enriched in SLT-03, which is located in a lower distance to the inflow delta of the Rio Grande in the south, the main tributary of the Uyuni salt flat. Concentrations of calcium and sodium show a converse trend indicating the removal from solution by the precipitation of gypsum and halite. Lithium, the element of highest economical interest, follows the trend of enrichment in southern direction and has concentrations in the brine of 0.3 g/L in SLT-01 and 1 g/L in SLT-03, which is in good accordance with results of former investigations in the area.

Zusammenfassung

Der Salar de Uyuni, eine Salzwüste im Hochland der bolivianischen Anden, war zwischen Juni und September 2009 Gegenstand hydrogeologischer und hydrochemischer Untersuchungen. Während der Kampagne wurden Salzkerne aus verschiedenen Bohrungen mit Tiefen zwischen 2 und 12 m an zwei verschiedenen Lokalitäten im nordöstlichen und im zentralen Teil des Salars (SLT-01 und SLT-03) gewonnen. Wasserproben wurden aus verschiedenen Tiefen der ausgebauten Brunnen entnommen und vor Ort sowie im Labor chemischen (IC, ICP-MS) sowie physikalischen Analysen (Viskosität, Dichte) unterzogen.

Die geochemischen Analysen der Salzkerne aus SLT-01 ergaben einen hohen Überschuss an Halit mit geringen Anteilen an Gips. Die darunter liegende lakustrine Sedimentschicht ist durch einen hohen Gehalt an wasserunlöslichen Mineralen gekennzeichnet. Computertomographische Untersuchungen ausgewählter Kernproben zeigen signifikante Unterschiede zwischen der oberflächennahen Salzkruste und tiefer anstehenden Halitschichten in Bezug auf Porenvolumen, Konnektivität und räumlicher Verteilung der Poren. Die hohe Durchlässigkeit, welche sich aus dem berechneten effektiven Porenvolumen von fast 20% ergibt, wurde durch die Ergebnisse eines Pumpversuches in SLT-03 bestätigt. Dieser ergab eine intrinsische Permeabilität von $1.95 \cdot 10^{-10}$ m² für den obersten Halit-Aquifer.

Die Grundwässer der beiden Probenahmelokalitäten weisen hohe Unterschiede in Bezug auf ihre chemische Zusammensetzung auf, Variationen mit der Tiefe wurden allerdings nicht festgestellt. Der Großteil der Elemente ist deutlich in SLT-03 angereichert, was sich durch die geringere Distanz zum Delta des Rio Grande, dem Hauptzufluss des Salar de Uyuni, erklärt. Die Ca- und Na-Konzentrationen zeigen einen gegenläufigen Trend, bedingt durch die Ausfällung von Gips und Halit bei höheren Salzkonzentrationen. Lithium, das Element von gegenwärtig höchstem wirtschaftlichem Interesse, folgt dem Trend der Anreicherung im Südosten. In SLT-01 und SLT-03 wurden Li-Konzentrationen in der Lösung von 0.3 bzw. 1 g/L gemessen, was in guter Deckung mit Ergebnisse früherer Studien im Untersuchungsgebiet ist.

1 Introduction

1.1 Motivation

The demand for energy-saving, cost-efficient technologies has brought an element into focus, that formerly played only a tributary role in industrial applications: lithium. The request for it has increased exponentially in the last two decades. According to Meridian International Research the current annual production of 90,000 t of lithium carbonate will rise to more than 300,000 t in 2020 (Tahil 2008). Up to that year, as the German government states, there will be as many as one million electric vehicles on the streets in Germany (source: “Nationaler Entwicklungsplan Elektromobilität 2009”). Progresses in the development of cars that obtain their energy from lithium based batteries are limited by the fact that the exploitable reserves of the lithium resource in the world are barely explored, for the most part difficult to access and scarcely to exploit cost-effective.

With roughly estimated 5.5 million tons of lithium the reserves of the Salar de Uyuni, the world’s biggest salt pan located in Bolivia, are considered to have huge mining potential. Due to political instabilities in the last decades and the fear of the Bolivian government of foreign investors, these resources have yet not been touched at all.

With an average amount of about 20 ppm in the upper earth crust lithium is a comparatively rare element (Vine 1980). The two main sources that contain exploitable amounts of lithium are ore deposits and brines. The first source are pegmatites which are the most abundant rocks that can obtain significant amounts of lithium. These coarse-grained igneous rocks have their origin near large magmatic intrusions and usually consist of granite (Garrett 2004). Although there are 145 minerals, that contain lithium as a major element, only three of them, lepidolite, spodumene and petalite do have contents of economic value (Yaksic & Tilton 2009). Another mineral source for lithium is hectorite clay. Although the largest known deposits in the McDermitt caldera, USA, are not mined nowadays, research is done to investigate future mining in that area.

Lithium-containing brines can be subdivided into continental brines enclosed in evaporites, geothermal and oilfield brines, whereby the last two mentioned are of inferior significance. Continental brines are associated to large closed basins whose inflows have a high and specific mineralisation caused by the leaching of volcanic rocks. The content of lithium varies greatly, as it is dependent on the extent of solar evaporation in that area (Evans 2008). Currently brines deriving from salt flats provide the majority of the global production of lithium at the lowest cost (Abell & Oppenheimer 2008). The largest amounts are mined from the Salar de Atacama in Chile and the Salar de Hombre Muerto in Argentina.

With an estimated total amount of 230 billion tons of lithium seawater has as well a high potential for the exploitation of the element lithium. Japanese researchers at the Saga University's Institute of Ocean Energy are developing a method for the extraction of lithium, but at present technologies are not yet competitive because of the low efficiency (Japan Times 2004).

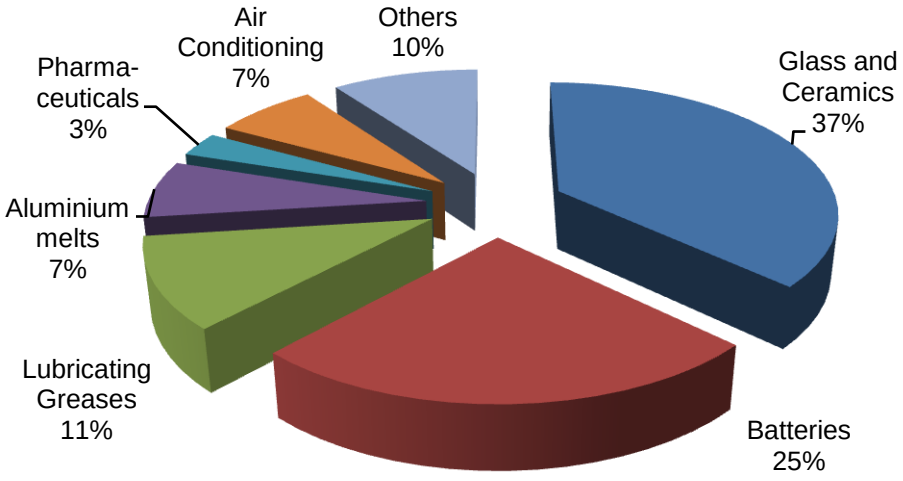

Fig. 1: Application of lithium in different industries (modified after Roskill 2009, in Angerer et al. 2009)

In 2009 lithium was mainly used in the glass and ceramic industry, followed by the use as electrolyte for cathodes in batteries, as addition to lubricating greases and aluminium melts (Fig. 1). The aspired change from conventional gasoline powered vehicles to electric vehicles (Hybrid, Plug In Hybrid and Battery Electric Vehicles) makes the ion battery sector to the industrial branch with the biggest demand for lithium in the near future.

The estimations for the present global production of lithium are very widespread. In this context it must be differentiated between resources and reserves. Reserves are the economically exploitable amounts of lithium in the crust that are obtainable with technologies available at the present (Angerer et al. 2009). They are estimated at about 15 million tonnes (Table 1). In contrast, resources also include reserves that are known but not yet exploitable under economical criteria. Estimated resources are much higher, a number of at least 24 million tons in the world gives a rough estimation. Table 1 gives an overview on the countries with the largest known deposits of lithium.

Table 1: Estimated global resources and reserves of lithium (source: U.S. Geological Survey, values are from 2010)

Country	Annual production	Resources	Reserves
Chile	10,600	7,500,000	3,000,000
Bolivia	-	9,000,000	5,400,000
Argentina	2,200	2,500,000	800,000
USA	1,700	2,500,000	38,000
Australia	4,400	350,000	170,000
China	2,300	2,500,000	540,000
Afghanistan	-	?	~ 5,000,000
Total	**21,200**	**> 24,350,00**	**~ 15,000,000**

According to this statistic more than 50% of the worldwide available lithium is located in a small region of the earth. The so-called lithium triangle, located between the borders of Argentina, Chile and Bolivia, is bounded by three large salt flats, the Salar de Hombre Muerto, the Atacama desert and the Salar de Uyuni.

Though an exploitation of the lithium reserves of the Salar de Uyuni has not yet started, it has been subject to a number of research projects done in the past years. In the 1970s Ericksen et al. (1978) discovered the presence of widespread lithium-rich brines in salt pans of the Bolivian Altiplano. Rettig, Jones and Risacher (1980) performed an extensive survey about the hydrochemical composition of brines in the Salar de Uyuni. Wolf (1988) studied the geochemical conditions at the Salar de Uyuni and discussed possible sources for the solutes.

Risacher & Fritz (1991b) put the focus on stratigraphical characteristics, the vertical and horizontal distribution of elements and the geochemical evolution from former paleolakes to the contemporary conditions.

1.2 Universitary cooperation project “Salar de Uyuni”

In 2002 the cooperation between the Universidad Autónoma Tomás Frías (UATF) in Potosí, Bolivia and the TU Bergakademie in Freiberg, Germany, concerning the exploration of the Salar de Uyuni started. In the following years plans were made to establish an initiative that comprises the investigation of the mining area, the technology for the extraction of lithium and the compatibility of human interests and environmental protection.

In recent years a technology was developed in Freiberg that differs from the conventional method of lithium exploitation by evaporation basins for example in the Salar de Atacama in Chile. The method, which is patented under the name “Verfahren und Vorrichtung zur solaren Eindampfung von Salzlösungen”, is based on the concentration of the lithium-containing brine by evaporation cones. The brine is pumped from the subsurface and then circulated to the top of evaporation cones to concentrate the brine under the prevailing climatic conditions of the Salar (high solar insolation, strong winds). Successively accompanying salts as sulphates and chlorides precipitate until a brine remains that is highly concentrated in lithium. In the following steps performed in the laboratory respectively an industrial treatment plant this brine is subject to a number of chemical processes. The further concentration, the precipitation of Li_2CO_3 and several purification steps result in a product with a high purity. Beside lithium also other economically interesting substances such as potassium, magnesium, boron and table salt may be extracted. Finally, the rest brine is planned to be returned into the Salar de Uyuni in order to avoid the accumulation of large tailings.

1.3 Objectives of the work

The main goal of this thesis was to gain a first survey about the hydrogeological and hydrochemical conditions at the Salar de Uyuni in Bolivia. Thereby, the focus was on the characterisation of the properties of the salt crust and the interstitial brine in terms of chemical and physical parameters.

The geochemical and mineralogical composition of the salt rock should be evaluated in relation to the observed stratigraphical units. The hydraulic conductivity should be estimated by different approaches. A further aim was the evaluation of the different methods applied based on the results from this work.

As the brine is the main factor for the economic potential of the lithium reserves at the Salar de Uyuni, its chemical composition had to be determined. Thereby, the spatial distribution of elements as well as the enrichment and depletion of elements in solution compared to the salt rock were regarded. Considering this background the understanding of the processes which are responsible for the accumulation of large amounts of solutes as well as their geologic origin was essential. Further the results had to be evaluated for consistency with former investigations in that area and in comparison to other Salars in South America with a similar geologic and climatic background.

Also the question if different groundwater levels are separated from each other or if a hydraulic connection exists had to be regarded. Finally, the modelling of the evaporation processes of the brine under the specific conditions of the Salar, especially the behaviour of the ionic composition, was essential for the future extraction of lithium. Thereby, an estimation of the available lithium reserves was taken into account.

2 Description of the study area

The Salar de Uyuni, comprising an area of about 10,500 km² at a height of 3,653 m, is an endorheic basin situated in the southern part of Bolivia on the Altiplano (Ballivian & Risacher 1981). It is considered to be the world's largest single salt pan and characterised by huge amounts of lithium.

2.1 Geographic and geologic background

The Altiplano is a closed high plateau basin situated between the Eastern and Western Cordilleras of the Andes, which includes parts of Bolivia, Peru and Chile (Fig. 2). It comprises an area of about 190,000 km² at an altitude between 3,650 and 3,900 m (Argollo & Mourguiart 2000). To the east the Altiplano is marked by the Cordillera Oriental with summits peaking up to 6,500 m (Nevado Illimani: 6,439 m asl). These mountain ranges are characterised by paleozoic sediments which are intruded by intermediate granitic plutons (Kussmaul et al. 1977). The mountain ranges of the Cordillera Occidental form the natural border to the west. Their origin is mainly volcanic, the underlain tertiary formations are covered with volcanoes and ignimbrites (Risacher & Fritz 1991b). The Mt. Sajama forms the highest summit with an elevation of 6,550 m asl.

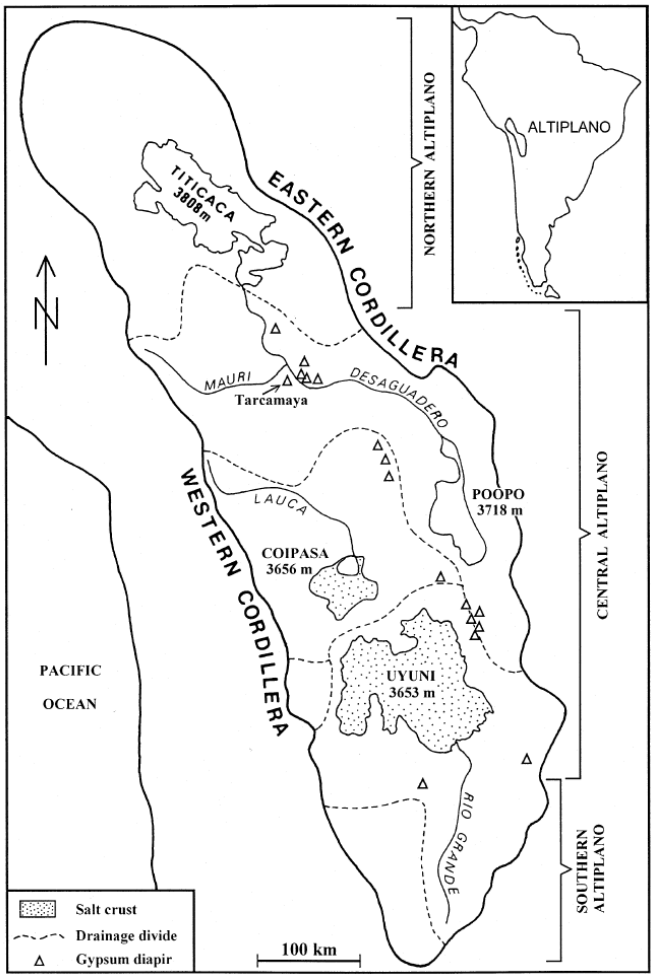

Fig. 2: Schematic map of the Altiplano with main drainage basins (after Risacher & Fritz 2000)

With a length of 1,000 km and an increasing width from about 70 km in the north to more than 220 km in the south the Altiplano basin is a large and narrow depression (Guyot et al. 1990). The basement is formed by metamorphic sediments of paleozoic age. They are overlain by limestone and terrestrial sediments of mesozoic and tertiary age as well as ignimbrites and tuffs which alternate with layers of volcanic lava rocks. During the Quaternary large composite volcanoes formed in the western and southern area. The Altiplano comprises a system of mountain ranges and interjacent sediment filled plateaus. Therefore, it can be partitioned into four different subbasins (Risacher et al. 2006). At a height of 3,810 m lake Titicaca forms the northernmost and at the same time the highest part of the Altiplano basins. To the south the plain of Oruro follows, which contains the highly saline Poopo lake. Westwards the Salar de Coipasa extends, which is bordered by a mountain range called Serrania Intersalar to the south. The largest basin and coevally the lowest point of the Altiplano is the Salar de Uyuni, following to the south of Coipasa (Fig. 3). The southern part of the Altiplano is covered by scattered volcanoes, which reach altitudes of up to 6,000 m (Kussmaul et al. 1977). The regions that form the southern limit of the Altiplano are covered by the pampas of Nor and Sud Lipez, ascending gradually to an altitude of 4,500 m and finally passing into the Puna de Atacama in Chile.

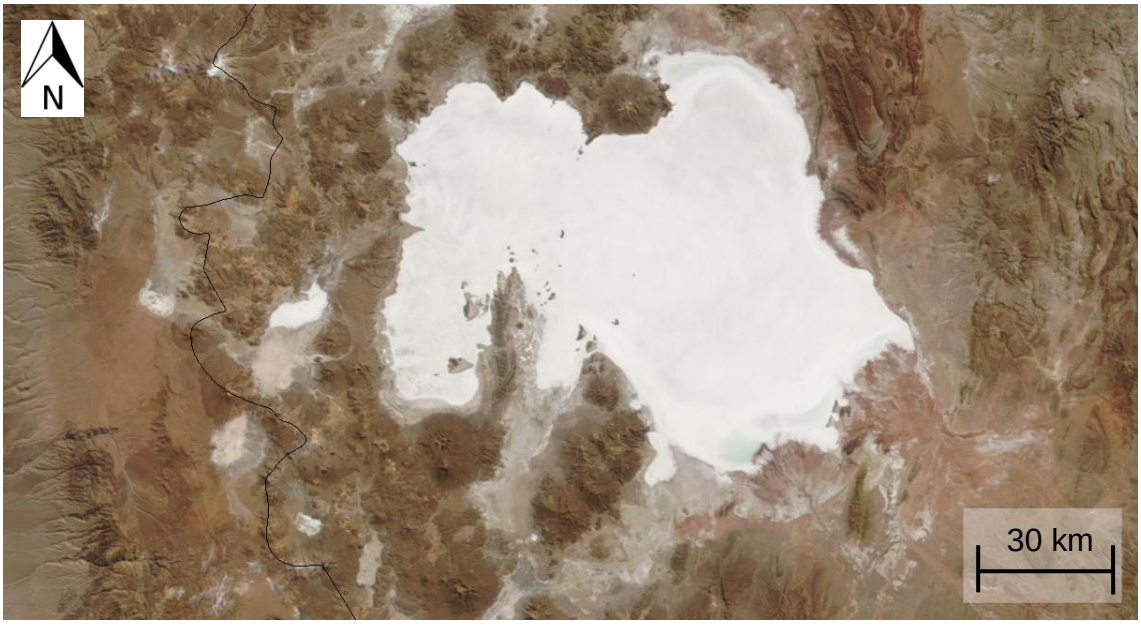

Fig. 3: Satellite image of the Salar de Uyuni with laterally adjacent mountain ranges and volcano summits, captured by the MODUS sensor of the satellite Terra (source: NASA)

2.2 Contemporary hydrologic setting of the Altiplano

A basic requirement for understanding the specific characteristics of the Salar de Uyuni is its treatment as a part of the whole, more or less connected system of the Altiplano. Hence, the understanding of the hydrologic regime of the Altiplano is vitally important. Four autonomous hydrologic regimes exist, differentiated according to the geologic, geomorphologic and climatic background (Wolf 1988). The lake Titicaca in the north of the Altiplano, situated on a height of 3,810 m, forms the baseline of the first hydrologic regime (Fig. 4). With a size of more than 8,300 km² and a maximum depth of 300 m it is at the same time the largest water-filled basin of the Altiplano. The lake receives large water masses by numerous inflows from the western cordillera, the northern and the eastern side. The Rio Desaguadero in the south-east drains the lake Titicaca and transports its outflows to the south towards the central Altiplano. Carmouze et al. (1978) stated that only 4.5% of the annual water loss from Titicaca is outflow to the south, evaporation forms the biggest part with 90%, the rest is groundwater infiltration. At a length of 383 km the river overcomes an altitude difference of 120 m, which results in a strong erosive force of the water masses and the transport of large amounts of sediment material especially in the rainy season. The lake Poopó, which forms the southern part of the first hydrologic regime, receives the waters of the Rio Desaguadero from the northern side.

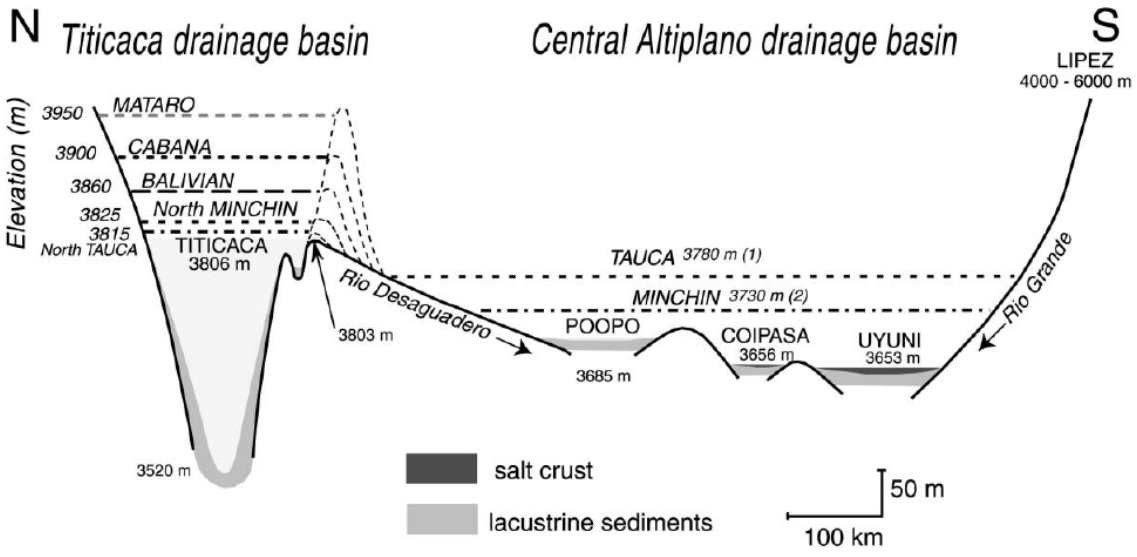

Fig. 4: N-S cross section of the northern and central basins of the Altiplano with recent and past lake levels (from Risacher & Fritz 2000)

In contrast to Titicaca, lake Poopó has no regular outflow drainage to the south meaning that 98% of the inflowing water is evaporating. This fact results in a TDS (content of total dissolved solids) which is more than 30 times higher than in lake Titicaca (Carmouze et al. 1978). Due to the unsteadiness of inflows and outflows caused by meteorological variations as well as anthropogenic disturbances the lake underlies permanent alterations in terms of extension and depth. No connection exists to the second independent hydrologic regime of the Bolivian Altiplano, the Salar de Coipasa (Rettig et al. 1980), which is located south-west of the lake Poopó. The Salar de Coipasa receives a number of inflows from the north and the west transporting large amounts of water and solid materials especially in the rainy season. The Salar de Coipasa is a basin that is covered by a salt crust, it has a surface of about 2,500 km² and is situated at an altitude of 3,655 m (Lebrun et al. 2002). South of Coipasa the third hydrologic regime, the Salar de Uyuni, is located. No obvious connection between the Salars of Coipasa and Uyuni exists. However, a superficial exchange between the water masses seems to be possible in both directions, when the salt pans are heavily flooded after massive rainfall during and shortly after the wet season. A subterraneous connection might also be considered as it is thinkable that older sediments covered by young volcanic material act as an aquifer (Wolf 1988). The salt pan of Uyuni has only one permanent surface-inflow: the Rio Grande de Lipez in the south. The fourth independent hydrologic regime comprises the south western part of Bolivia. This region is characterised by high mountains of volcanic origin interlaid by large closed basins at a height of about 4,500 m. These basins are fed by streams from the surrounding mountains and show different stages of the formation of salt pans (Wolf 1988).

2.3 Climatic conditions

Due to the Altiplano's large north-south extension of about 1,000 km a great variation of the climatic conditions in different regions occurs. When classifying the region into a climatic system by means of the latitude, three different zones can be distinguished. The northern part is characterised by tropical alternating climate with a rainy season from September to May and an annual rainfall of 600 mm. The climate diagram of Juliaca in Peru northwest of the Titicaca lake is typical for that region (Fig. 5). The central part belongs geographically to the zone of the trade winds. Precipitation occurs only between December and March, the rest of the year is almost absolutely dry (annual rainfall: 400 mm).

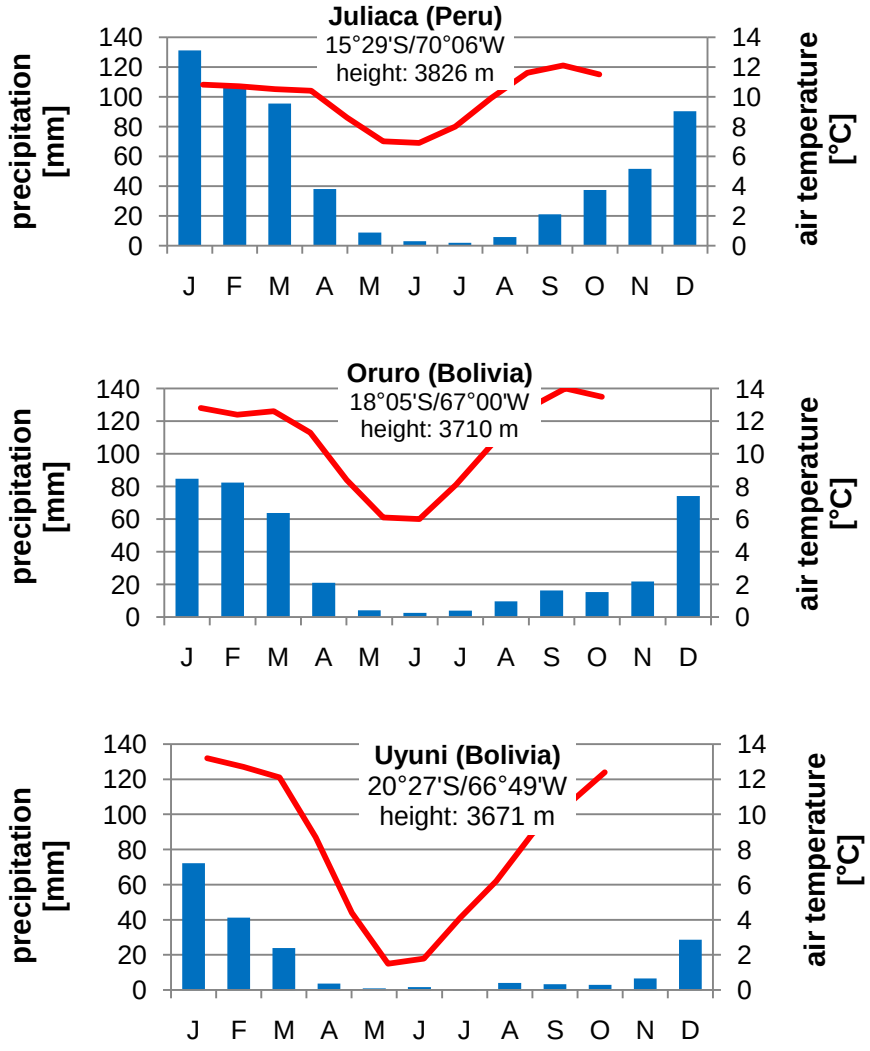

Fig. 5: Climate diagrams for 3 locations in the Altiplano from north to south (data from www.worldclimate.com)

The dates of the climatic station in the village Uyuni in the south of the Salar show a mean annual temperature of 9°C, whereat the temperature gradient at one single day can reach up to 25°C. The annual precipitation of 141 mm is very low and 90% of it occurs in only three months. In comparison, the mean annual rainfall in Germany is 770 mm, and the amount is more or less equally distributed to the months. As the potential evapotranspiration of 1,300 mm/a exceeds the precipitation on the salt flat many times over, the region is a desert. During the rainy season southward winds prevail, while the dry season is characterised by northward winds (Svendsen 2002) with an average wind speed of 8 m/s. In the southern part of the Altiplano the subtropical alternating climate dominates according to the geographic latitude.

Under the special geographic conditions of the Altiplano the theoretical climate in relation to the latitude is significant different. First, the altitude ranging from 3,500 to more than 4,500 m has a great influence on the local climate. Second, the location between the eastern and the western Cordilleras of the Andes acts as a shield, especially against the humid and warm air masses above the Amazonian rainforests (Wolf 1988). The climate diagrams from three different parts across the Bolivian Altiplano clearly show the gradient in precipitation and temperature from north to south (Fig. 5).

2.4 Sedimentology and Paleolakes

In 1986 a borehole with a depth of 121 m was drilled in the central part of the Salar de Uyuni, 10 km north of the island Incahuasi. Altogether 12 salt layers separated by 11 mud layers were registered (Fig. 6). As the drilling stopped in a salt layer in a depth of 120 m the bottom of the basin was estimated much deeper (Fornari et al. 2001). The analysis of the mineralogical composition of the salt layers showed that they mainly consist of halite with minor amounts of gypsum. In contrast, the mud layers are made up of calcium carbonate mixed with gypsum and detrital materials mainly from volcanic origin. The porosity of the salt and mud layers was estimated to 15 - 30% and 30 - 50% respectively (Fornari et al. 2001). The alternation of salt and mud layers indicates changing conditions in respect of dry and wet phases. In ancient times the Altiplano has been covered by numerous paleolakes whose expansions mainly depended on the particular climatic conditions. The oldest recorded lakes, the lake Ballivian in the northern and lake Pre-Minchin in the central part of the Altiplano, have been dated back to the early Pleistocene age, about 1.5 million yr B.P. ago. In the late Pleistocene lake Minchin (44,000 – 22,000 yr B.P.) covered an area comprising the present surfaces of lake Poopó, Coipasa and Uyuni (Clapperton et al. 1997, Fig. 4). The latest paleolake covering the central Altiplano was lake Tauca (13,000 – 18,000 yr B.P.), from which the present upper salt crust of Uyuni and Coipasa are a remnant (Baker & Rigsby 2001).

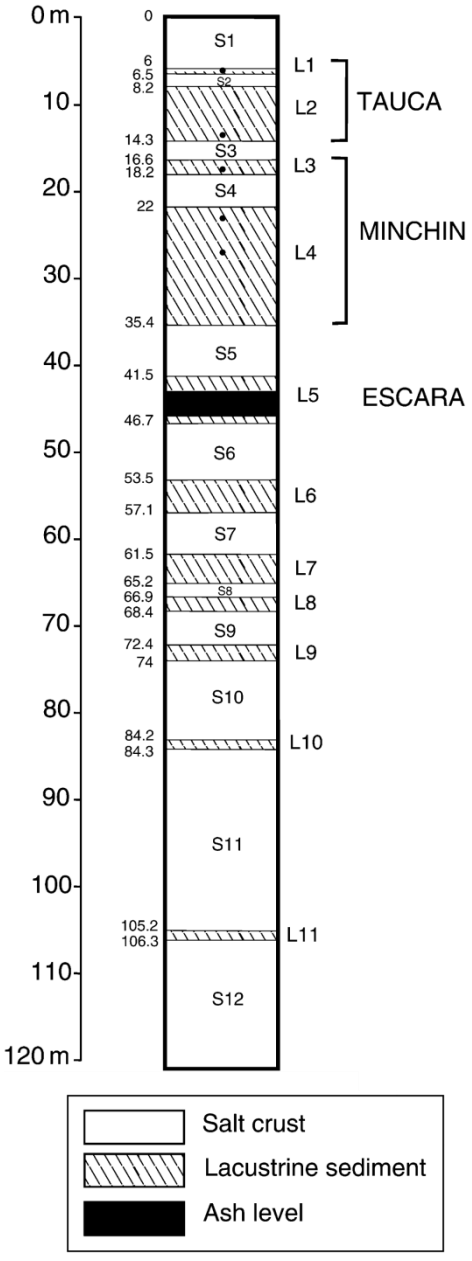

Fig. 6: Log of the drilling hole in the centre of the Salar de Uyuni reflecting the stratigraphy and thickness of each layer (after Fornari et al. 2001)

The levels of former lakes are well preserved in form of carbonatic terraces in the surrounding of the Salars as well as on islands (Ericksen et al. 1978). So it can be observed that for example lake Tauca exceeded the present level of the Salar de Uyuni for more than 100 m (Fig. 4). The age determination is challenging as it is difficult to obtain datable material in the Bolivian Altiplano. Since wood samples are rare, radiocarbon dating was performed with carbonate shells, disseminated organic material and calcareous crust as well as algal mats. However, these carbon sources provide only a limited accuracy due to possible alteration processes which lead to a falsification of the real ages (Fornari et al. 2001).

The thickness of the different mud layers rises significantly with time (Fig. 6). This suggests that the duration of lacustrine phases constantly increased during the Pleistocene (Fornari et al. 2001). For this trend, local climatic changes may be the reason. Though, an opposite development is observed in the Titicaca basin, meaning that the duration of lake phases decreased with time. This leads to the assumption that overflows from lake Titicaca lowered the threshold between the northern and the southern basin which resulted in an increased inflow into the central Altiplano (Risacher & Fritz 2000, Fig. 4). Thus, it must be assumed that the formation and duration of paleolakes in the Salar de Uyuni was not only controlled by local paleoclimatic variations but also by the input of waters from the northern Altiplano (Fornari et al. 2001).

2.5 Brine chemistry and origin of solutes

The pores of the salt and mud layers of the Salar de Uyuni are filled with an interstitial brine. This brine is mainly composed of sodium and chloride, with high amounts of lithium, magnesium, potassium and boron. Thereby, the content of solutes increases towards the delta of the Rio Grande, in this area up to 4.7 g/L Li and 4.3 g/L B are contained in the brine (Risacher & Fritz 1991b).

When discussing possible sources of the solutes that are occuring in the Salar de Uyuni, the annual cycle of weathering, leaching and precipitation of salts must be considered. According to Wolf (1988) the processes can be divided into four phases. The first phase begins at the end of the rainy season, when heavy precipitation has moistened the ground and filled the aquifers. Intensive chemical weathering leads to the dissolution of ions. The rapid desiccation of the soils by the sun results in a capillary ascension of the solution to the surface, where the solutes are precipitated in form of salts. These salts are composed of sulphates (mainly gypsum) or chlorides (mainly halite) (Wolf 1988). The second phase is characterised by the solution of the deposited salts with the beginning of the rainy season. Since large parts of the precipitation do not directly infiltrate due to still dry grounds, the solutes are transported with the surface run-off into rivers and ephemeral streams and finally to the basins of the Salars. Wolf (1988) estimates 14 billion m^3 of aboveground water per annum reaching the Salar de Uyuni. The third phase, which starts in the rainy season and lasts for weeks, is the flooding of the widespread areas situated in the delta regions of the inflows. This process is connected to a slowdown of the water masses transported from the river and stream systems and the sedimentation of detritus material. The delta area of the Rio Grande is such a plain region, comprising an area of approximately 300 km^2. The final phase starts with the beginning of the dry season, when the flooding decreases and is finally restricted to the central basin of the Salar de Uyuni. As long as the aboveground water is not saturated it dissolves parts of the upper crust, until the evaporation prevails and the crystallisation of halite starts, which results in the formation of a new salt crust. The evaporation of capillary risen brine from the upper centimetres results in the cementation of the surface. The formation of desiccation cracks leads to the further rising of brine, forming small elevations of precipitated salts along the

cracks, which are termed salt efflorescences (Risacher et al. 2006). These polygon shaped patterns give the Salar de Uyuni its typical appearance.

There are various assumptions to explain the source of the saline components and especially the amount of lithium accumulated in the Salar de Uyuni. Rhyolitic rocks from the central Andes contain high amounts of water soluble salts, the volcanism in that area provides the heat for the convective flow of groundwater, which results in a selective leaching of the rocks (Ericksen 1978). Another reported source is the abundance of mineral and hydrothermal springs on the Altiplano, whose mineralization are often characterised by high amounts of lithium. A probable main source of solutes is the leaching of salt formations associated to gypsum diapirs from ancient geologic systems (Fig. 2). These formations were dissolved in one of the first paleolakes, their amount of solutes since then was conserved in a circle of dissolution and precipitation in the different stages of paleolakes, until the present stage of complete precipitation was reached in the Salar de Uyuni (Risacher & Fritz 1991b).

3 Methods

The following chapter comprises two parts. First the field investigations are described, including the drilling procedure and field analyses. Then the analyses of the core and brine samples performed in the laboratory follow.

3.1 Drilling procedure

Two field campaigns were performed between July and September 2009. In the first attempt, lasting from the 22nd July to the 5th of August, a Bolivian drilling company was contracted, but failed due to improper equipment. The second campaign, lasting from 11th to 28th of September, conduced to the realization of the drilling, the installation of the wells, the sampling of salt cores and brines and finally the implementation of pumping tests.

Drilling in salt as well as working with highly saline brines require specific demands to the technical equipment. Furthermore the work in an isolated area far beyond any civilisation and technical support demands a thorough preparation of the materials and a realistic time management.

3.1.1 First attempt

The first drillings were done with a Bolivian drilling company. The drilling machine was based on rotation and driven by a diesel engine (Fig. 7). Sediment cores of 2” and 4” were able to be obtained. Two different diamond bits, one for hard rock, the other for sediments like clay were used. In the first trial it was drilled without a drilling fluid. That was done in order to avoid a mixing of brine and fresh water, a dissolution of salt structures and furthermore damages in form of corrosion of the drilling machine. After having drilled at highest engine power for two hours the drilling hole had a depth of only 40 cm. A look into the core sampler showed that the salt material was extremely compacted and stuck in the tube, therefore the progress of the drilling was far too low to continue. A second trial was done with the brine as drilling fluid.

Fig. 7: Drilling machine of the Bolivian drilling company (left), pump for drilling fluid (top right), core barrel for cores with a length of 1 m and a diameter of 4" (down right)

A hole with an area of 1 x 1 m and a depth of 40 cm was excavated and the brine that poured in from cavities was pumped in a cycle from the pool into the bore hole and over a narrow channel back to the pool.

Despite the removal of the detritus the drilling progress was extremely low, after several hours of drilling a depth of 1.60 m was reached. Reasons for the low progress of drilling, with and without fluid, with different drill bits and diameters may be various. The main reason probably is the inappropriate plane drill bit with diamonds. It abrades the surface of the salt aggregates, compacting but not destroying them. Possibly also the power of the drilling machine was too low, resulting in a low rotation velocity. Another reason is the low pressure of the pump for the flushing of the borehole, which leads to an aggregation of detritus in the bore hole.

3.1.2 Second attempt

The second drilling campaign in September 2009 was implemented with a German drilling machine. The machine was built by the company Diamasa Diamantbohrtechnik GmbH (Grimma, Saxony) and was modified especially for the application in salt. Technical details are given in Table 2. With a bore diameter of 76 mm core samples with a diameter of 64 mm were obtained. The used bore rods were made of carbon steel, boring bars of aluminium were tested as well, as they alleviate the work due to their low weight.

The electricity for the drilling machine was produced by a 5.5 kW gasoline generator. The auger was set into a drill rig with a height of altogether 1.70 m. The fixation of the construction to the surface of the ground was required for stability and the secure performance of the works. For that a massive wooden board was fixed with anchors to the upper 20 cm of the salt crust. Upon the board the drill rig was fixed to the anchors (Fig. 8). For further stability the board was fixed to the ground by a vehicle, whose wheel stood on the free end of the board.

Table 2: Properties of the drilling machine

Parameter		Diamasa DK32S
revolutions per minute		300/590/960
power supply		3 kW / 220 V
drill bit	type	plate drill bit with core retainer
	inner / outer diameter	64 / 76 mm
drill rig	type	D300 AMB
	total height	1.70 m
	working height	1 m
drilling rod		hexagonal, diameter 50 mm

For dragging out the drilling rods and the core sampler from the bore hole a tripod was used (Fig. 8). From a depth of about 7-8 m, as the weight was too high to be lifted by human power, the tripod was taken supportively.

Fig. 8: Diamasa drilling machine (left); fixation of the drill rig with anchors (middle); using the support of the tripod (right)

The brine as drilling fluid was taken from the aforementioned basin, filtered through a rough sieve, filled into a hand pump and was pumped through a hose into the drilling system.

3.1.3 Distribution of boreholes and drilling patterns

The drilling was planned to be performed on four distinct points, SLT-01 to SLT-04, distributed in all parts of the Salar de Uyuni. These locations were chosen after specific conditions. SLT-01 is situated in the central eastern part of the salt pan, with a distance of about 10 km to the eastern border (Fig. 9). According to the literature (Risacher & Fritz 1991b) the upper salt crust in that area reaches a thickness of more than 10 m. As it is estimated that the major part of the brine is situated in the salt pores of the upper crust, this location has high capacities for the storage of large amounts of brine.

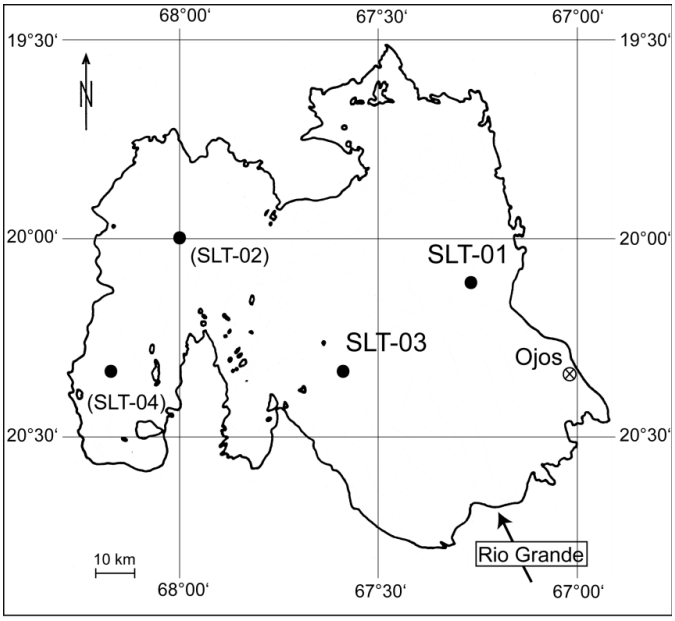

Fig. 9: Distribution of performed and planned drillings on the Salar de Uyuni (modified after Risacher & Fritz 2000)

SLT-03 is situated 10 km southeast from the island Inkahuasi, with a distance of about 40 km to the delta area of the Rio Grande de Lipez. At this point the concentrations of lithium in the brine are amongst the highest over the Salar, and the upper salt crust still has a thickness of 4-5 m (Risacher & Fritz 1991b). The locations SLT-02 and SLT-04 serve as contrast points to the regions in the east and for the verification of statements in the literature.

According to Risacher & Fritz (1991b) the thickness of the upper salt crust extends to no more than 2-3 m and the lithium concentrations are the lowest on the whole Salar. GPS positions of all drilling locations and sampling points are given in Table 3. An overview of performed drillings is comprised in Table A1 (Appendix).

Table 3: GPS-positions of important points (geographic coordinates converted from UTM, geodetic datum: Prov S Am'56)

Name	Description	Easting	Northing
SLT-01	drilling location 1	W67° 16' 48"	S20° 07' 03"
SLT-02	drilling location 2 (planned)	W68° 02' 45"	S19° 59' 13"
SLT-03	drilling location 3	W67° 33' 54"	S20° 20' 44"
SLT-04	drilling location 4 (planned)	W68° 11' 16"	S20° 20' 58"
SLT-S	"Eyes of the Salar", gas emanation from the subsurface, water sampling point	W66° 59' 50"	S20° 18' 43"

At location SLT-01 in total 5 drillings were performed after the pattern shown in Fig. 10. The depths of the wells varied from 3.30 m to 12.50 m. The filters are located in different depths in order to enable the taking of samples orientated upon the depth. Looking from the principal well A the observation wells B, C, F and E are distributed in several directions for a spatial evaluation. Distances between the wells vary from 2.50 m to 10 m.

At location SLT-03 altogether 4 drillings were performed (Fig. 11). Well C is located in the centre of the observation wells A, B and E. The distances between the wells range from 3 to 10 m, the depths from 2.70 m to 11.80 m.

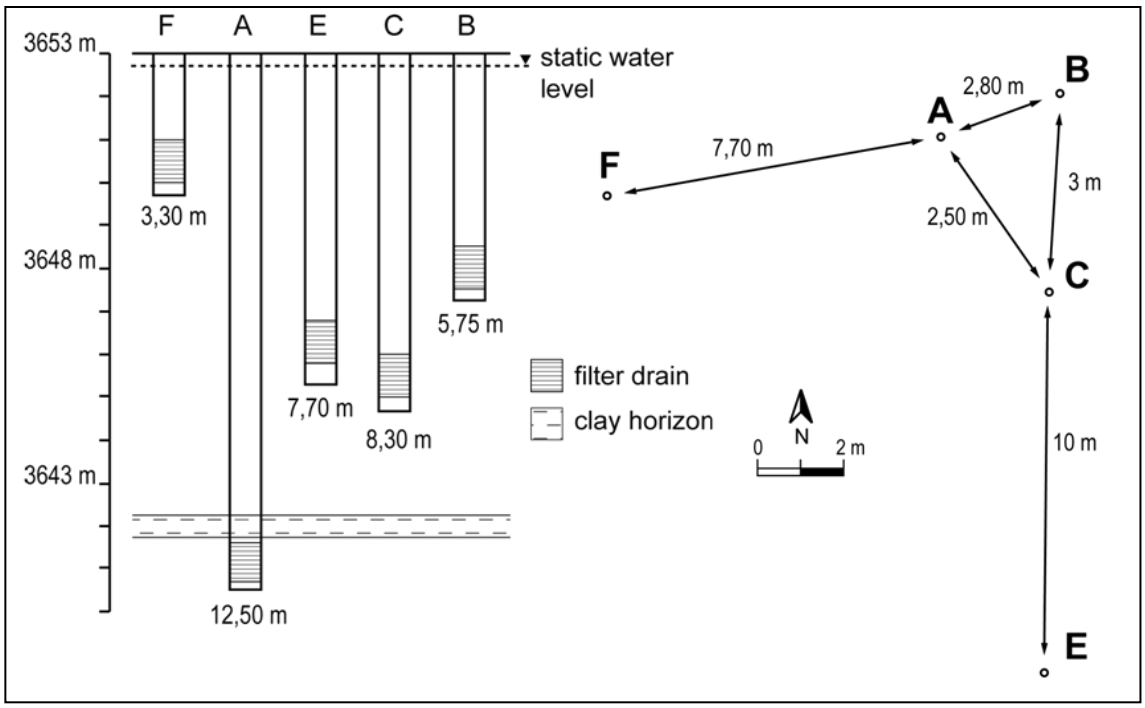

Fig. 10: Depths of the drillings in location SLT-01 (left) as well as arrangement of the boreholes (right)

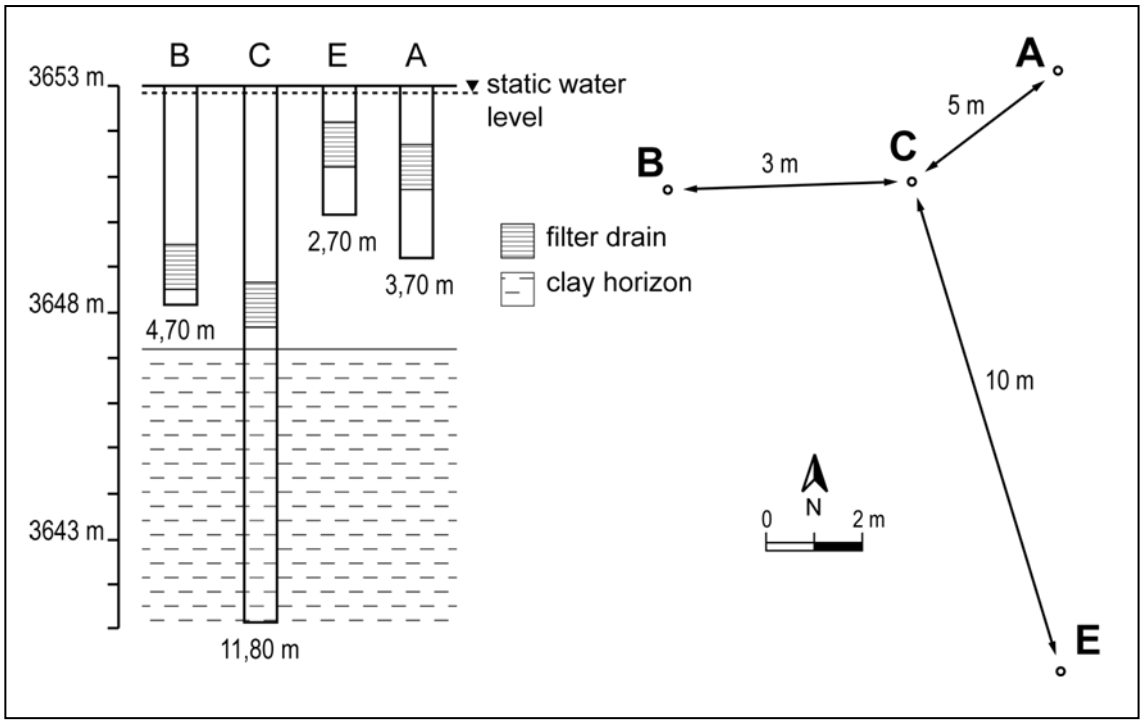

Fig. 11: Depths of the drillings in location SLT-03 (left) as well as arrangement of the boreholes (right)

3.1.4 Sampling of salt cores

The salt cores were carefully pushed out of the core tube with the help of a wooden stick. They were lain out onto the ground surface on large plastic tarps to be dried in the sun for a few days. At night the cores were covered with plastic film for protection. Written and photo documentation were done immediately after the extraction of the cores. Samples of salt detritus from the drilling fluid were gained, when the yield of salt cores was low, especially in the upper meters. They were collected in plastic bags and put in the sun for drying. When the cores were as dry as possible they were wrapped with plastic foils and fixed with tape in order to protect them from atmospheric humidity. Plastic tubes with a diameter of 7.6 mm and a length of 1 m were cut lengthwise with a hacksaw. The sealed salt cores were then shoved into the prepared tubes. The tubes were compressed to the diameter of the cores and fixed with wire.

Finally five tubes were put together into one wooden box, which was prepared for the transport of the damageable cores to Potosí. In Potosí a large box was taken to transport all the salt samples by plane to Freiberg.

3.2 Well casing

For a depth dependent brine sampling the bore holes were cased. The schema of a completely constructed well is shown in Fig. 12. PVC pipes with a length of each 6 m and a diameter of 2” were used as casing. The pipes were sticked together using PVC-adhesive and supplementary wire. The interstices were sealed with silicone to inhibit an infiltration of brine. The lowermost tube was sealed by a plastic cap. The slotted screens were prepared by a hacksaw on a length of 8 cm with a slot size of 1 mm and a gap of 1 cm between each other. Ten slots alternated with 10 cm of solid pipe for stability. The filter pipe had a length of 1 m. Before implementing the casings, the bore hole was flushed with brine by a water pump to eliminate sediment deposits. Gravel to fill the annulus was taken from an ancient riverbed south-eastern of the Salar near the city Uyuni. It was composed of very pure quartz. Grading with sieves of 1 and 5 mm provided a grain size between 2 and 4 mm, just enough to avoid a plugging of the filter pipe and to fill the space between the bore hole wall and the tube. The gravel was filled up around the whole filter pipe and additionally 10 cm to prevent a plugging of the filter. The annulus above the gravel up to the surface was filled with clay, which was obtained from a quarry near the village Colchani east of the Salar. The large clay blocks were crushed and sieved, the fine powder then was mixed with brine to produce a clay mud that could easily be filled into the annulus. The upper casing ended 50 cm above the surface to be visible and accessible even in the wet season and was cemented by a concrete cap to prevent surface water to enter the bore hole.

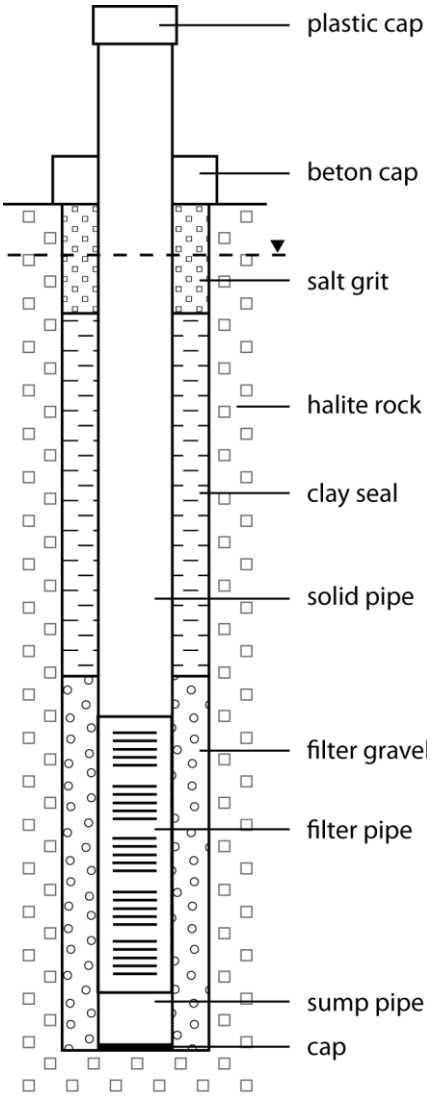

Fig. 12: Schema of the well casing (not to scale)

Glow stickers around the supernatant tubes cared for an improved visibility at night. The upper tube was sealed with a plastic cap.

3.3 Field analyses and brine sampling

Brine samples were taken from every well at the drilling points SLT-01 and SLT-03. From well SLT-01A no sample could be obtained because of technical difficulties with the suction pump. Furthermore one brine sample (SLT-S) was taken from a gas emanation spot at the eastern border of the Salar, near the village Colchani (see Table 3, Fig. 9). At this point the crust is broken up and pools with the size of a few square meters and a depth of few centimetres have formed. These spots are locally called “Ojos del Salar” (Eyes of the Salar). The apparent emanation of gas from the underground impedes the crystallisation of a halite crust.

On-site the parameters temperature, pH, oxygen content, electric conductivity and redox potential were measured. Furthermore the content of redox-sensitive species was obtained photometrically. The measurements were made in a self constructed flow through cell in order to avoid degassing of CO_2 and redox reactions in the brine by the contact with atmospheric oxygen. The values were obtained after the constancy of parameters.

Fig. 13: Determination of field parameters of the brine in a flow through cell

The **pH-value** was determined by a WTW Multiline P40. For the pH a two-point calibration (pH 4.01, pH 7) was done every day for assuring the accuracy of the instrument. The electrode was stored in a 3 mol KCl solution.

The **redox potential** was measured with an Ag/AgCl electrode, the values were displayed on the WTW Multiline P40. The obtained values were noted when being constant, which took no more than 2 min.

A standard solution of 228 mV (at 20°C) served for the verification of the instrument's accuracy. Measured values of 247 mV and 250 mV are within the tolerance area. The values shown on the display are the electromotive force (EMK), that still have to be corrected by means of adding the potential of the reference electrode and correcting for temperature dependency, which is dependent on temperature. The following relation transfers the EMK into the standard redox potential E_0 at 25°C:

$$E_0 = EMK - 0{,}198\ (T - 25\ °C)mV$$

In a second step, E_0 must be converted to the potential of a standard hydrogen electrode by a correction factor. This factor amounts to 207 mV for T = 25°C and the used Ag/AgCl electrode with an electrolyte of 3 mol KCl (Hölting & Coldewey 2009). It follows:

$$E_H = (E_0 + 207)mV$$

The finally obtained value E_H is the redox potential corresponding to standard temperature and the standard hydrogen electrode.

The **specific electric conductivity** was measured with an HQ40d MultiMeter from Hach. The measured conductivity of a 1000 µS/cm standard solution was in the tolerance area between 920 and 1081 µS/cm.

The content of **dissolved oxygen** was determined with an optical oxygen sensor with integrated temperature probe attached to an HQ40d instrument from Hach. A calibration as well as the verification with standards was not necessary. Contents of oxygen were displayed in mg/L and %.

The **water temperature** was obtained by the parallel measurement of the temperature probes of the pH, the oxygen and the conductivity sensors. A mean temperature was calculated from the three values.

Photometrical measurements were made within few hours after sampling with a DR/890 colorimeter from Hach. The concentrations of the redox-sensitive elements iron (Fe^{2+}, Fe^{3+}), sulphide ($H_2S_{(aq)}$, HS^-, S^{2-}), nitrite (NO_2^-) and ammonium (NH_4^+) were obtained by photometry, in order to avoid chemical and microbial redox processes by the contact with atmospheric oxygen. Previously, samples were filtrated through 200 nm cellulose acetate filters. The contents of the species were obtained according to the instructions. Important parameters for the different methods are shown in Table 4. When the concentration range was exceeded, the brine was diluted with deionized water and measured one more time.

Table 4: Parameters of the single methods used for photometry

Species	method nr. (after Hach)	concentration range [mg/L]	EDL [mg/L]	accuracy [mg/L]	interferences
Fe^{2+}	8146	0 – 3.00	0.03	0.017	-
Fe_{ges}	8008	0 – 3.00	0.03	0.017	Cl > 185 g/L, Ca > 10 g/L as $CaCO_3$, Mg > 100 g/L as $CaCO_3$
NH_4^+	8155	0 – 0.5	0.02	0.02	Ca > 1 g/L as $CaCO_3$, SO_4^{2-} > 0.3 g/L, NO_2^- > 12 mg/L, Fe, S^{2-}
NO_2-N	8507	0 – 0.350	0.005	0.001	Fe^{2+}
S^{2-}	8131	0 – 0.7	0.01	0.02	-

EDL = estimated detection limit

Sampling

For sampling the brine from the wells a small suction pump with a ½”-hose at the desired depth of the well was used. The SLT-S sample was taken from a brine pool in a depth of few centimetres. Samples were taken when all field parameters reached constant values. Samples for ICP-MS were filtered with 200 nm filters, acidified with ultra-pure 10 molar HNO_3 to a pH < 2 (3 drops on 30 mL sample) and stored in 30 mL acid-washed PE-bottles. Samples for IC and photometry were not treated and stored in 50 mL HDPE-bottles.

3.4 Laboratory analyses

3.4.1 Analyses of the core samples

Selected core samples were investigated in different laboratories. An overview of performed analyses is given in Table A1 (Appendix).

3.4.1.1 Geochemical and mineralogical composition

The analyses were performed at the Bundesanstalt für Geowissenschaften und Rohstoffe (BGR) in Hannover. The core of the drilling point SLT-01A was investigated for its elemental composition and the distribution of minerals. Therefore altogether 102 material samples were taken along the whole length of the core, always when the texture or the colour of the core changed visibly. The samples were dissolved in water, anions and cations were then determined by ICP-OES. The quantitative mineral content was then stoichiometrically calculated from these principal components. X-ray analyses were performed only with the samples that contained a high amount of water insoluble residues.

3.4.1.2 Computer tomography

The determination of the pore volume, the distribution of pores and their connectivity was done by computed tomography (CT). The measurement was made in the institute of Ceramic, Glass and Construction Materials (IKGB) at the TUBA Freiberg. The instrument was a CT-ALPHA from the ProCon X-Ray GmbH Garbsen. A digital X-ray XRD 1620 AN CS from PerkinElmer Optoelectronics (Canada) served as detector. Two core samples from SLT-01 were investigated by the method, one sample from the upper crust (depth between 0.20 and 0.25 m) and one sample from a depth between 3.00 and 3.05 m. Cores were cut to a length of about 5 cm. The sample was fixed on a column inside the instrument (Fig. 14). Technical parameters varied for the used samples, they are combined in Table A4 (Appendix).

Fig. 14: Fixation of the core sample in the instrument

Each core sample was scanned by the CT in X, Y and Z direction, taking a picture each time after an increment of 75 µm. From that raw data (2815 pictures for the first sample and 2880 pictures for the second sample) the software XRay Office compiled a 3-dimensional model of each sample displaying empty spaces in dark shades and material in different grey scales. The resolution of the instrument is defined by the size of the minimal detectable volume, a voxel, with an edge length of 75 µm. For the determination of the pore volume and the evaluation of their connectivity a number of transformations had to be applied to the 3-D models of the cores:

- The first step was the binarization, meaning the transformation of the grey-scale pictures into binary images, with white areas of salt and black pores.
- The next step was the virtual cutting-out of a cube out of each core sample. This had to be done, because the program does not recognize the transition from the core to its surrounding as the sample's boundary, but would treat the vicinity as a large pore. The cubes had side lengths of x = 530, y = 530 and z = 750 pixel, which corresponds to 4 x 4 x 5.6 cm.
- The following step was the labelling by reconstruction which serves for the identification of single pore objects. Here, every black area is treated as a single object, and each object is then assigned to a certain colour according to its volume.
- The last transformation of the images was the application of an object filter which eliminates all pores except for the largest pore. So, the final image does only show the system of connected pores in a green colour, which corresponds to the effective porosity of the respective sample.

3.4.2 Analyses of the brine samples

The analyses of the 9 brine samples were performed at the department of Hydrogeology at the TU Bergakademie Freiberg (TUBAF). Furthermore the brine samples from the drilling points SLT-01 and SLT-03 were analysed at the BGR in Hannover for the content of main anions and cations and the density. An overview of the performed analyses of the brine samples is given in Table A5 (Appendix).

3.4.2.1 Ion chromatography

Ion chromatography was used to obtain the concentrations of major anions and cations in the brine samples.

The concentration of the **anions** fluoride, sulphate and chloride were obtained with a Metrohm 881 Compact IC Pro. The instrument was driven with a pressure of 12 MPa and a column temperature of 45°C. A mixture of 3,0 mM $NaHCO_3$ and 3,5 mM Na_2CO_3 served as eluent with a flow rate of 0,7 mL/min. For the detection of chloride the samples had to be diluted 1:2500. For sulphate and fluoride a dilution of 1:100 was prepared.

The **cations** lithium, sodium, potassium, magnesium and calcium were measured with a 850 Professional ion chromatograph by Metrohm. Here the pressure was 7.8 MPa at a column temperature of 30°C. As eluent a solution of 2 mM HNO_3 and 0.7 mM Dipicolinic acid was used, which had a flow rate of 0.9 mL/min. Before utilisation the eluents for both cation and anion chromatography were aerated with nitrogen to remove dissolved gases and other disturbing substances. Samples had to be diluted 1:2000 for the determination of Na, 1:1000 for K and Mg and 1:250 for Ca and Li.

3.4.2.2 Total inorganic carbon

For the measurement of the contents of total inorganic carbon (TIC) the elemental analyzer “LiquiTOC” from Elementaranalysen Systeme GmbH was used. The samples were diluted between 1:20 and 1:50, in order to prevent damage of the instrument caused by the high salt contents.

For dilution deionized water was used, which was aerated with nitrogen. The samples were acidified with H_3PO_4 in order to transform all carbonate species into carbon dioxide. All samples were measured in the infrared range 1, because of the high sensitivity at low concentrations. The insert volume of diluted sample was 10 mL. The quantification of TIC contents was done by a calibration curve with standards. For TIC a parent solution of 1,000 mg/L Na_2CO_3 (1.0 g C_{anorg}/L) was used. The solutions were diluted into steps from 0.5 mg/L to 10 mg/L TIC.

3.4.2.3 Mass spectrometry with inductively coupled plasma

ICP-MS measurements were performed with a X Series 2 from Thermo Scientific. A pH test showed, that samples didn't have pH values < 2. About 15 drops of ultra-pure 10 mol HNO_3 had to be added to 30 mL sampling volume of each sample in order to obtain the acid conditions. For the determination of the major elements Li and B the samples were diluted with deionised water 1:2000. A dilution of 1:500 was needed for measuring the amounts of Br. A dilution of 1:100 was done for the quantification of the other elements. 10 mL of diluted sample was prepared in vials. For the recovery rate 100 µL of an internal standard containing 1 mg/L Rh, 5 mg/L Ge and 1 mg/L Re was added to every sample. Quantification was done by a standard calibration curve for each determined element. For that the peak area of samples with different known amounts of the desired elements were measured.

The elements were measured either in normal or in collision mode. The collision mode uses a different carrier gas mixture of 93% He and 7% H_2 compared to normal mode, where Argon is used. A summary of measured elements, detection limits and the applied modes are contained in Table A8 (Appendix).

The accuracy of measurements performed by ICP-MS can always be negatively influenced by matrix effects, especially when the samples are highly concentrated saline waters.

In order to verify the results of the lithium content quantified by the standard calibration, the calibration for two samples (SLT-01B, SLT-03A) was done by standard addition. Therefore, defined amounts of lithium standard were added to the samples, and measured by ICP-MS. The concentration in the original sample is then obtained by linear regression.

3.4.2.4 Determination of viscosity and density

The **viscosity** of two brine samples (SLT-01B, SLT-03A) was determined by a rotational viscometer in the laboratory of the IBZ-Salzchemie GmbH & Co. in Freiberg. The method is based on the principle that the dynamic viscosity of a solution is dependent on the torque that is needed to turn a cylinder in it. The required torque, the exact geometry of the rotating body and the rotational speed are combined to determine the viscosity. For the measurements a Model DV-II+ viscometer from Brookfield was used. An UL adapter was required to measure viscosities in a low range and to be able to take a small sample volume (16 mL). With this adapter the lower gaugeable limit is 1 mPa·s, which corresponds to the viscosity of water at 20°C. Preparative the samples were cooled to the average temperatures that were measured in the field (5°C for SLT-01B and 8°C for SLT-03A), as the dynamic viscosity is dependent on the temperature. The brine sample was filled into the test cell with the cylinder and the dynamic viscosity was obtained with adjusted rotational speeds of 30 and 60 rpm.

Fig. 15: Viscometer with UL adapter

The **density** of the brine samples from SLT-01 and SLT-03 was determined by the BGR in Hannover by means of a pycnometer, which functions according to the principle of displacement. Thereby the density is calculated from the relation between the mass of the empty flask, the mass of the flask filled with water and with the brine. The measurements were done at a room temperature of 20°C. As the density changes in dependency of the temperature, the obtained values must be corrected for the measured temperatures of the brines in the field.

3.4.3 Methods of evaluation

3.4.3.1 Check for plausibility

The brine water analyses contain a large number of parameters that were obtained by different methods under different conditions. Thus, it is likely that errors occur which can falsify the results. A number of plausibility analyses were performed in order to evaluate the data.

The **analysis error** was calculated for each brine sample with the help of PhreeqC (Parkhust & Appelo 1999). For the percentage deviation between the sum of the equivalent concentrations of anions and cations a value of 2% should not be exceeded.

Another method of validation is based on the **exclusion** principle. That means when a species in a solution exists in a certain concentration it is possible to exclude concentration ranges of other species caused by the specific redox condition of the solution.

3.4.3.2 Statistical data treatment

In a first step the data set was prepared by means of identifying values below and above detection limit and replacing missing values. In a second step multivariate statistics was applied in order to find relations between different samples and parameters.

Data processing

In a first step the detection limits were calculated and compared to the obtained data. A possibility to determine the lower detection limit LOD is to sum up the blank's signal and the threefold of the standard deviation of the blank value. For that reason the detection limit is specific for the measuring instrument and the measured element. Obtained values below the detection limits were replaced by values half of the LOD.

Values exceeding the upper detection limit did not occur in the data set, because in every measurement the samples were diluted at least 1:100. As there were no missing values in the data sheet no empty spaces had to be filled up.

Cluster analysis

Cluster analysis is a method to arrange different samples into groups according to the similarity of all parameters (Rudolf & Müller 2004). The goal is to find out, if the concentrations of elements are characteristic for samples from different drilling points and sampling locations. The applied hierarchical clustering is an iterative process. Starting with each object as a single cluster, in each step clusters are combined that are in a certain context closest to each other (Voß 1997). The similarity between objects is defined by their distance, here the squared Euclidean distance was used. The scale of the data has a high influence on the distance. In fact, the concentrations of different elements in the samples vary in several orders of magnitude, consequently the scale difference is very high. Therefore it is useful to perform a standardization (Stoyan 1997) by means of a **Z-transformation**. For that all data were transformed according to:

$$z_i = \frac{x_i - x}{s} \text{ for } i = 1,...,n$$

with z_i = standardised value; x_i = measured value x = mean; s = standard deviation

The distances between clusters were calculated according to the Ward-algorithm, which produces homogeneous clusters with small distances to the cluster centres (Stoyan 1997). The cluster analysis was performed for the classification of the objects into 2 and 3 clusters. The significance for each number of clusters was tested with the **Kruskal-Wallis-Test**. This test is checking the equality of different groups by comparing their medians. As it is a non-parametric method, normal distribution is not assumed. The null hypothesis saying that there is no difference between the groups is rejected, when the value of 5% for the error probability α is exceeded.

3.5 Pumping Tests

Pumping tests were performed in order to investigate the permeability of the sediment structures in different layers of the salt crust. Sedimentary salt inhibits very specific characteristics, which make it a challenge to accomplish a pumping test. Hence a solid preparation is indispensable. The pumping was done with a gasoline driven pump (Honda). Because of the limited diameter of the well, the 2” connection of the pump had to be reduced to 1.5”. The pumped brine was drained off by a 1” water hose to a spot that had a distance of about 30 m to the pumping well. The measurement of the flow rate was done with a 20 L bucket, regular measurements showed a flow rate of 1.3 L/s. The drawdown was registered by electric contact gauges. The sensors had to be rinsed with clear water after every contact with brine, because the salt quickly formed a crust on the surface, in consequence the device produced a permanent signal.

A pumping test was performed in location SLT-03. Therefore, brine was pumped over a time period of 160 min from the principal well SLT-03C. The drawdown was recorded in the observation wells SLT-03 B and SLT-03 E.

Due to technical problems, a pumping test over a period of several hours could not be performed in location SLT-01. Therefore, the brine was pumped from the well SLT-01A until the water table was below the maximum drawdown of the pump. Then the recovery in this well was measured until the water table reached the static water level.

4 Results and Evaluation

This chapter is divided into three parts. First, the investigations of the core samples in terms of stratigraphy, chemical and mineralogical characteristics as well as porosity are displayed. Second, the data obtained from the pumping tests are evaluated. The third part attends to the hydrochemical and physical properties of the brine samples.

4.1 Core samples

In total, 37.5 meters in location SLT-01 and 22.9 m in location SLT-03 were drilled which equals altogether slightly more than 60 m. Barely 37 m of it were transported to Germany for further investigation of geochemical, mineralogical, and physical properties.

4.1.1 Stratigraphy

The examination of the cores and the characterization of their geological qualities and properties were done in the field. The core documentation, shown in Fig. 17 for the upper 2.70 m of the core from bore hole SLT-01E, contains the photo profile on the left side with the lengths of each obtained core piece. Aside the schematic geological profile with the signature after DIN 4023 is arranged. On the right hand side a brief written description of the drilled segment is added, with particular observations that were made in the field. This documentation, which was created with the program Adobe Illustrator CS4, was done for all the core samples that were transported to Germany for further investigations and is attached in the Appendix (Figures B1 – B13). The following description of the stratigraphy first deals with the core samples from SLT-01, then the cores from SLT-03 follow. In order to avoid misunderstandings it should be admitted that the terms clay and clayey are always referred to the particle size, not to the mineral type.

4.1.1.1 Drilling location SLT-01

In the north eastern part of the Salar de Uyuni five bore holes were drilled with depths between 3.30 and 12.50 m. The very upper crust has a thickness of approximately 15 cm in all bore holes from SLT-01, which coincides with the depth of the brine table in that area. It differs significantly from the lower layers in terms of structure and porosity. The crust consists of clear white halite layers with a thickness of each 2 – 4 cm, separated by darker narrow halite layers with a thickness between 1 mm and 3 cm each (Fig. 16). Thereby the color changes from brown in the upper part over grey to almost black in the lower part of the upper crust. The crust is characterized by roundly shaped, elongate pores, which are mainly oriented vertically. Though there is a high porosity, the halite aggregates of the crust are densely cemented and very hard. This is caused by the evaporation of brine by capillary forces during the dry season, whereby the crust is cemented into a very compact and hard pavement. A macroscopic crystal structure is not in evidence.

Below the upper crust the structure of the core samples in SLT-01 visibly changes. It follows a layer of approximately 10 cm thickness of unconsolidated material of halite aggregates that marks the transition between the dry crust and the underlying halite, whose pores are saturated with brine. This layer is similar in all drilling points from SLT-01.

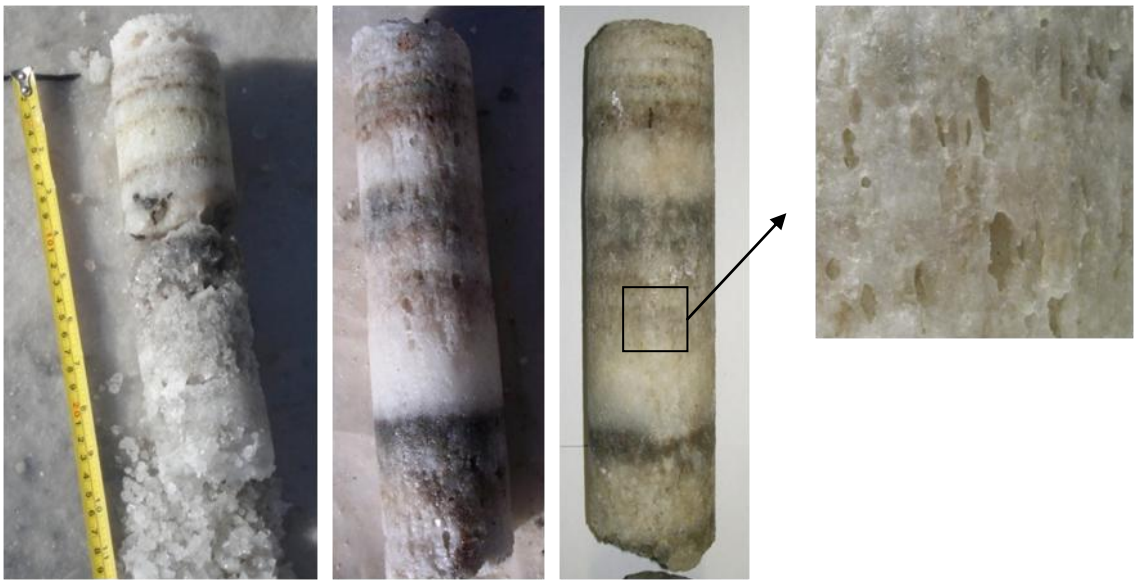

Fig. 16: Upper crust of SLT-01A (left) with a length of 10 cm, SLT-03C (middle) and SLT-03A (right) with a length of 25 cm each

Underneath this layer begins the zone, where pores are completely filled with interstitial brine. The core samples from the drilling holes A and F show a similar stratigraphic sequence, but differ a lot from B and C. Drilling hole E show a structure that differs from all other points of SLT-01. In general, the cores are composed of halite in form of crystals of varying sizes and salt aggregates without a definite structure. In SLT-01A the layer between a depth of 1.00 and 3.50 m is composed of very dark halite aggregates with a high brittleness and no observable changing stratigraphy. Beneath, the sediment structure changes by means of a lightening color and increasing solidity, until the halite is clear white with a high yield of complete cores from a depth of about 4.70 m. Between 5.00 and 9.50 m the halite layers are repeatedly interrupted by thin, few mm to cm thick, dark grayish to black layers. The core samples are broken in these zones and show rather smooth endings than irregular break edges, indicating that these thin layers must consist of fine-grained material that was removed by the process of drilling and flushing. In contrast, the structure and color of the cores do not change significantly in drilling holes B and C. From 1.50 m until the final depths the core samples are composed of bright halite with differing crystal sizes and few zones of unconsolidated material. Thin dark layers as in drill hole A were not observed. In a depth of 7.80 m a layer of black muddy clayey material with a thickness of 5 cm is located, which exists in the stratigraphy of drillings A and C. Between 10.30 and 10.40 m there is a thin (~ 2 cm) layer of almost white, very dense material, probably gypsum.

The mud layer in SLT-01A starts in a depth of 10.40 m and has a thickness of about 60 cm. It is composed of black clayey material without obvious halite substance. The drilling progress in this layer was slow, as the sticky mud constrained the rotation of the drill bit. The drilling was stopped in the next salt layer in a depth of 12.50 m, since the weight of the bore rods was too high to be lifted even with the help of the tripod.

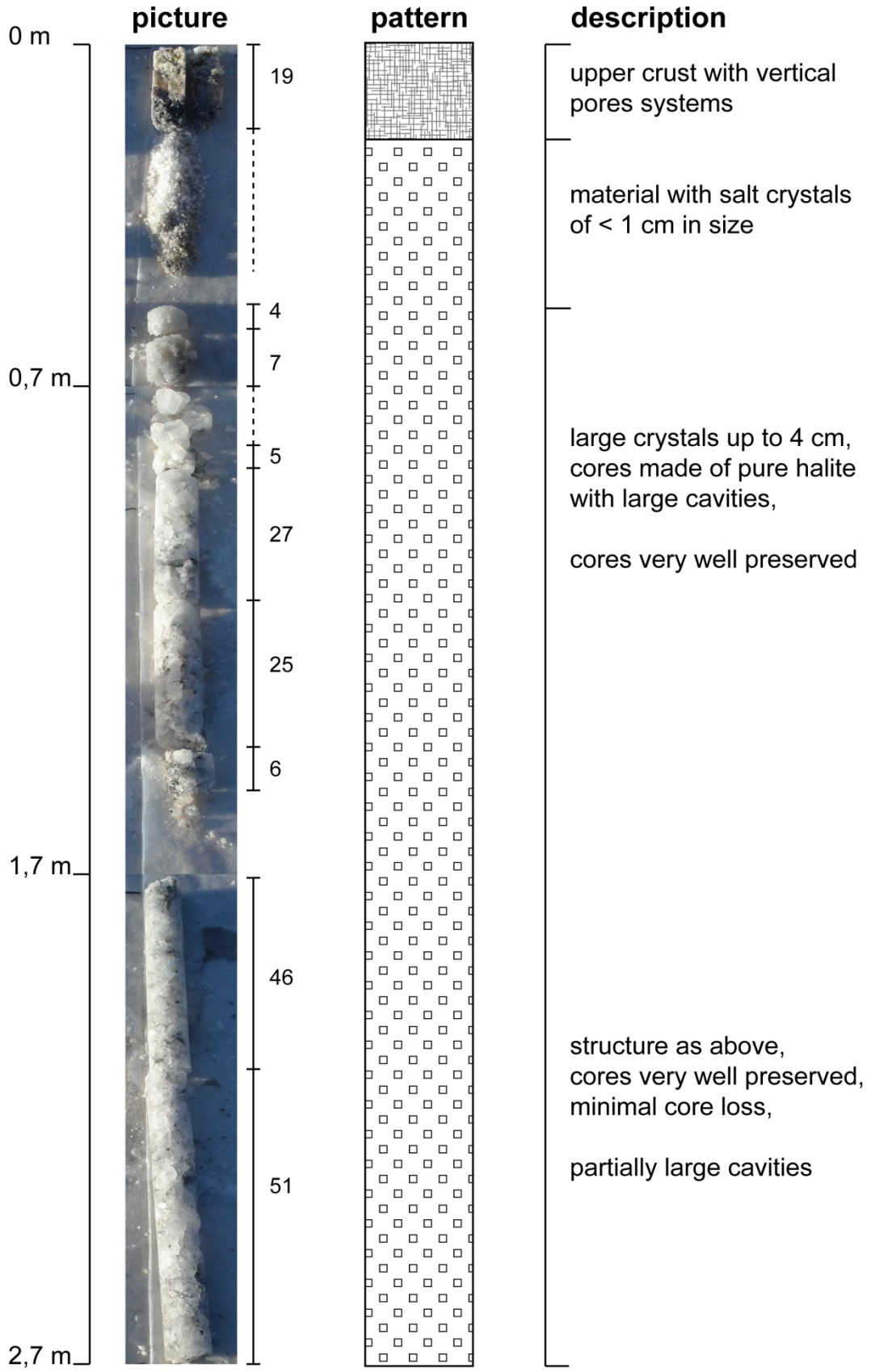

Fig. 17: Core documentation for drilling hole SLT-01E for the upper 2.70 m, the 1st column shows a picture and associated lengths of complete core samples, the 2nd column shows the pattern with signature after DIN 4023, the 3rd column shows a brief description of specific features of a segment

The drill core from SLT-01E shows a significantly different structure. Until a depth of about 6 m the core consists of clear halite with few clayey inclusions. In partially large cavities halite crystals with sizes up to 3 cm were formed. At a depth of 6 m the drilling machine suddenly subsided into the depth for 1.50 m without any resistance. It was not able to gain core material and detritus from the drilling fluid. Thus, it can be speculated that a large cavity in that locally very limited area exists, because a similar anomaly was not observed in the surrounding drilling points of SLT-01.

It could be observed that the drilling location in SLT-01 is characterized by large local heterogeneities in terms of structure, composition, and porosity of the sediments. The thin dark layers found in different depths in SLT-01A could only be partly observed in the other drillings.

Another observation made only in the surrounding of SLT-01 were small naturally formed holes in the upper salt crust with a diameter of approximately 10 cm and a depth of 20-30 cm. The apparent brine table in these holes was not covered by a thin salt crust, which indicates a permanent movement either by the rise of gas (which was not visible) or of lower concentrated brine from deeper zones. These holes developed during the progress of the dry season, as they could only be observed during the field campaign in September, but not in June.

4.1.1.2 Drilling location SLT-03

The four drilled boreholes in location SLT-03 show depths between 2.70 and 11.80 m. Here, the upper crust has a thickness of about 25 cm (Fig. 16), which is consistent with the brine table in the wells. The crust, similar to SLT-01, consists of an alternating layering of white and brown parts, whereby the dark layers are much more narrow than in the crust of SLT-01. These brownish layers are supposedly made up of material that has been transported to the Salar and deposited on the surface of the salt crust. That can be dust particles carried by atmospheric winds from the surrounding plain areas as well as suspended solids transported by streams and rivers during the rainy season.

A zone of unconsolidated material under the upper crust as in SLT-01 could not be observed, instead of that the upper layer directly passes into a zone of halite with a high content of black clay material.

In approximately 2 m depth a thin layer (~ 2 cm) of white fine-coarsed extremely dense material could be observed, which appears to be very similar to the assumed gypsum layer in SLT-01 in a depth of 10.40 m. Between 4.50 and 5.70 m the ends of the halite core samples are characterized by rests of a black clayey substance, which is in consistence to the observation made in SLT-01A between 5 and 10 m. The mud layer in SLT-03 starts in a depth of about 5.50 m and continues until the final profundity of drilling in 11.80 m depth, so that conclusions about its thickness cannot be made. In this layer the drilling progress, similar to SLT-01, was slow and samples of the mud layer could only be gained from the upper centimetres, because the underlying material was completely removed by the drilling fluid.

In general, the drilling location SLT-03 shows a much lower local heterogeneity than SLT-01, because the stratigraphy, the structure of the single layers as well as the porosity were similar in all four drilling holes. Compared to SLT-01, the salt was hard to drill over the whole length, which is confirmed by the higher visible density of the cores with less cavities over the most part of the depth.

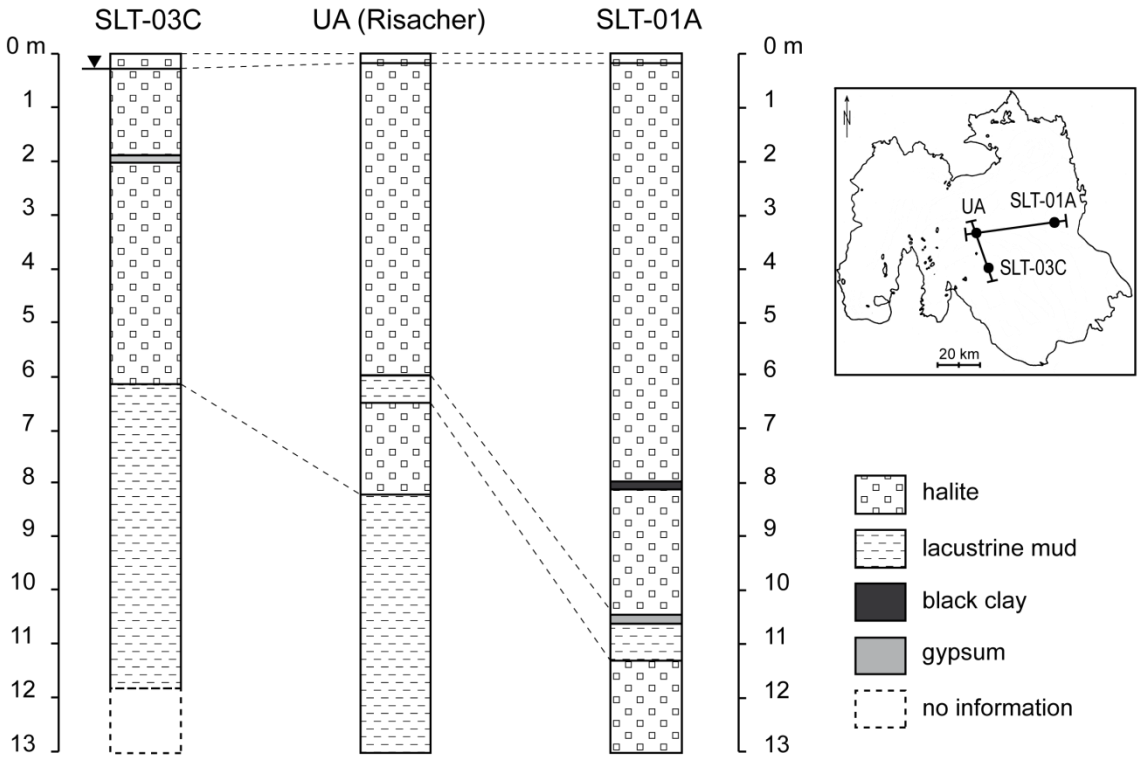

Fig. 18: Profile of the deepest drillings from SLT-01 and SLT-03 in comparison to the drilling UA in the central part of the Salar (Risacher & Fritz 1991b, Fornari et al. 2001); the layers of black clay and gypsum are vertically exaggerated, true thickness is 2 cm each

In 1986 a bore hole (named UA) was drilled in the central part of the Salar de Uyuni, 10 km north of the island Incahuasi (see chapter 2.4). The stratigraphy of that drilling was interpreted, amongst others, by Risacher & Fritz (1991b) and Fornari et al. (2001). When comparing the stratigraphy of both drilling locations SLT-01 and SLT-03 to the bore hole named UA, a concordance is partly observed. Fig. 18 shows a profile through the deepest wells of SLT-01 and SLT-03 as well as UA. In SLT-01A and UA a mud layer with a similar thickness of about 50 cm was reached in 10.50 and 6 m respectively.

That means that the first thick mud layer observed in drilling UA has not been reached yet in SLT-01, but should be expected in the following 1 – 2 m. The half meter thick mud layer does not exist in the stratigraphy of drilling location SLT-03, because the first mud layer, that was reached at about 6 m depth, has a thickness of at least 6 m. In conclusion, it could be shown that the expected depths of the first and second mud layer according to the literature were confirmed.

4.1.2 Rock quality and core loss

The evaluation of drilling cores requires the thorough recording of the distinguishable layers, the measurement of the core pieces' lengths and information about the quality and the state of preservation of the cores. In total 53 core meters were documented carefully and the size of the individual core pieces was measured. Only 21.6 m of the gained material were obtained as core pieces, which resulted in a total core loss of 59.2%. Thereby, unconsolidated and missing material is considered as core loss. A core piece must be unbroken and have a length of at least 1 cm.

Table 5: Core losses for the documented drilling profiles

	Drilling hole						
	SLT-01A	SLT-01B	SLT-01C	SLT-01E	SLT-01F	SLT-03A	SLT-03C
Depth of borehole [m]	12.50	5.70	8.30	7.70	3.30	3.70	11.70
Sum of core pieces [m]	6.06	2.68	2.54	4.78	0.45	2.70	2.40
Core loss [%]	51.5	53	69.5	37.9	86.4	27.2	79.5

Nevertheless, information about stratigraphy and composition can also be obtained from the sampled loose material. The core losses of the individual drilling locations are combined in Table 5.

A number of methods is known to classify the drilled rock according to its solidity. The L_M value is an adequate parameter for characterizing the rock quality (Meier 1999). In comparison to other parameters it considers areas of weakness in terms of fault zones and zones with low solidity. The L_M value is calculated as follows:

$$L_M\,[cm] = \frac{(\sum X_1)\cdot k_1 + (\sum X_2)\cdot k_2 + \ldots + (\sum X_{20})\cdot k_{20}}{\sum (X_1 + X_2 + \ldots + X_{20})}$$

with $\sum X_1$, $\sum X_2$ Sum of measured core pieces of each class

k_1,k_2 Average lengths of the classes (k_1 = 2,5 cm; k_2 = 7,5 cm…)

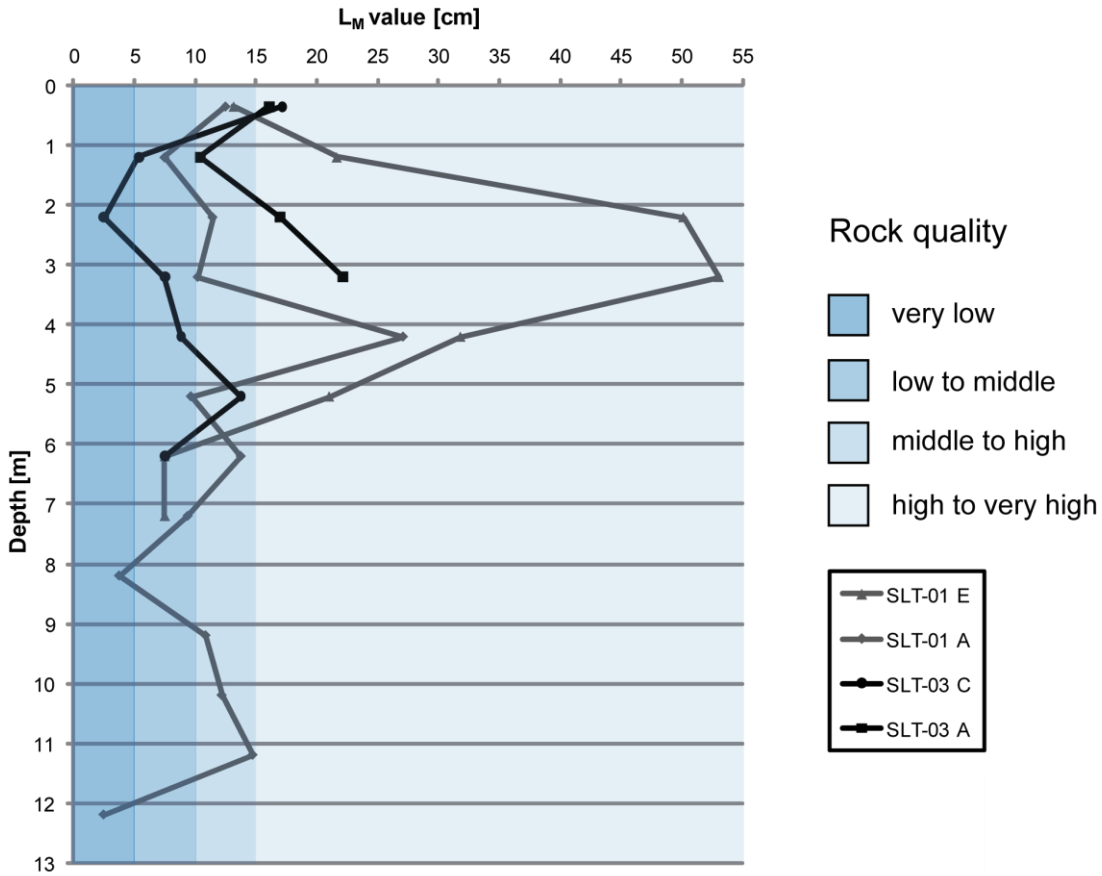

Fig. 19: Gradient of the rock quality after Meier (1999) with sampling depth for selected drilling points from SLT-01 and SLT-03

The core pieces are distributed into classes with a length of each 5 cm. As the parameter is calculated for every meter, a depth orientated evaluation is possible. It appears that the core sample from SLT-01E has a high solidity along its main length. The decreasing L_M-value between 6 and 8 m is explained by the missing of any kind of material, which leads to the conclusion of a large cavity in that area. Comparing the rock quality of the core samples from different drilling points at location SLT-01 large heterogeneities in a small regional scale are obvious. The core sample from SLT-01A has a much lower rock quality over the length of the core. In a depth of 3 – 4 m seems to be a halite layer with a significantly higher solidity compared to core samples from other depths. The high core losses in drilling points SLT-01C and F can be explained by the fact, that they were the first holes drilled with the new drilling machine. As it was drilled at highest rotation speed, the cores broke up under the obviously too high pressure. The following drillings were then performed at lowest and medium speed of rotation. Consequently, the risk of damaging the cores was lowered.

In location SLT-03 the situation was similar. As mentioned earlier, the sediment was hard to drill over the whole length, so that a high rotation speed had to be utilize. Hence, the cores of SLT-03C have a low solidity. The high core loss in that point is also explained by the removal of the mud layer by flushing the cuttings from a depth of 6 m and the lack of core sample caused by this procedure. With further experience of drilling the hard salt layers in SLT-03 the speed could be slowed down, and a high fraction of well preserved core samples from SLT-03A was reached.

In general, the fragility of the core depends on the fraction of dark muddy material, whose content could be estimated by the color of the core material. With increasing darkness of the aggregates the amount of clayey substance increases and the solidity of the core decreases. Further it could be observed that the partially fragile core samples cemented and hardened when put in the sun for drying. On the one hand this is caused by the content of clay, that works as an adhesive for sticking the aggregates of salt together. On the other hand the cementing is caused by the precipitation of salts from the evaporating of brine that is located in the pores of the sediment.

4.1.3 Chemical and mineralogical composition

Altogether 102 samples of the drilling core from SLT-01A were investigated for their chemical and mineralogical composition. The results in tabulary form are comprised in Tables A2 and A3 (Appendix). The quantitative distribution of mineral phases was stoichiometrically calculated from the geochemical main components Na, K, Ca, Mg, Cl and SO_4, that were obtained by ICP-OES from the dissolved samples, performed by the BGR.

Halite is the major mineral in the core samples. The average proportion for all samples is 92.2% of the whole mineral content (Fig. 20). This is in accordance with results from Risacher & Fritz (1991b) who reported 92.4% halite in the upper 6 m of the salt crust. When the samples with high contents of the water-insoluble fraction in a depth of 8 m, 9.8 m and 10.8 m are excluded, halite makes up 97% of the minerals in the other 94 samples. The second most common mineral in the samples is gypsum. Samples from depths of 5.5 m and 9.9 m have not been completely chemically decomposed, so that the portion of sulphate minerals is too low. Hence, the amount of especially gypsum should probably be higher in these samples.

Samples with high contents of the water insoluble fraction were further analysed by X-ray measurements, revealing that they consist of biotite and clay minerals such as muscovite, illite and cristobalite amongst others. The phases defined as other minerals comprise polyhalite, kieserite, carnallite and sylvite. Their fractions of the total mineral distribution and their contents in wt% are displayed in the lower diagram of Fig. 20. In depths of approximately 8, 10 and 10.50 m there are significant high peaks of non-halite minerals, and the content of halite totals less than 25%. These zones are associated to layers that differ in structure, mineral size and colour from halite layers, which is shown in Fig. 21. The layer between 10.50 m and 11.10 m refers to a lacustrine phase and is made up of lacustrine sediments. X-ray analyses of four samples from this depth showed that these sediments mainly consist of gypsum, calcite, and halite, with minor amounts of bassanite, quartzite, cristobalite, biotite and clay minerals such as muscovite and illite.

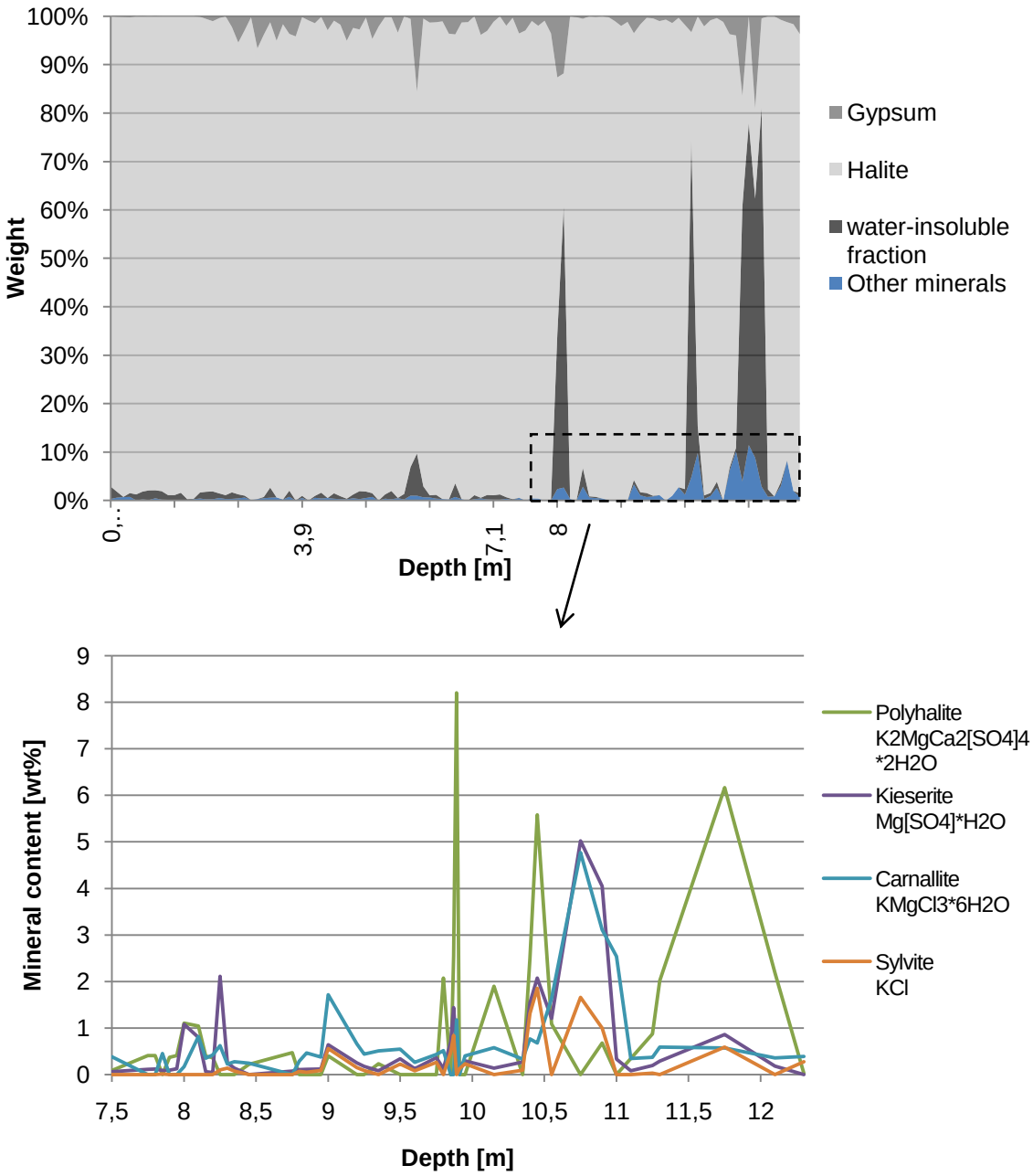

Fig. 20: Distribution of minerals determined in the core samples from SLT-01A in dependency of the depth and the splitting of the fraction summarized as other minerals

Sylvite, polyhalite and kieserite are typical evaporative minerals that occur in salinar sediments. These secondary salts are formed during the evaporation process by the interaction of the brine with earlier formed minerals such as gypsum. These processes, also called backreactions, occur at the sediment-brine interface as well as in places where more and less dense brines are mixed (Warren 2006).

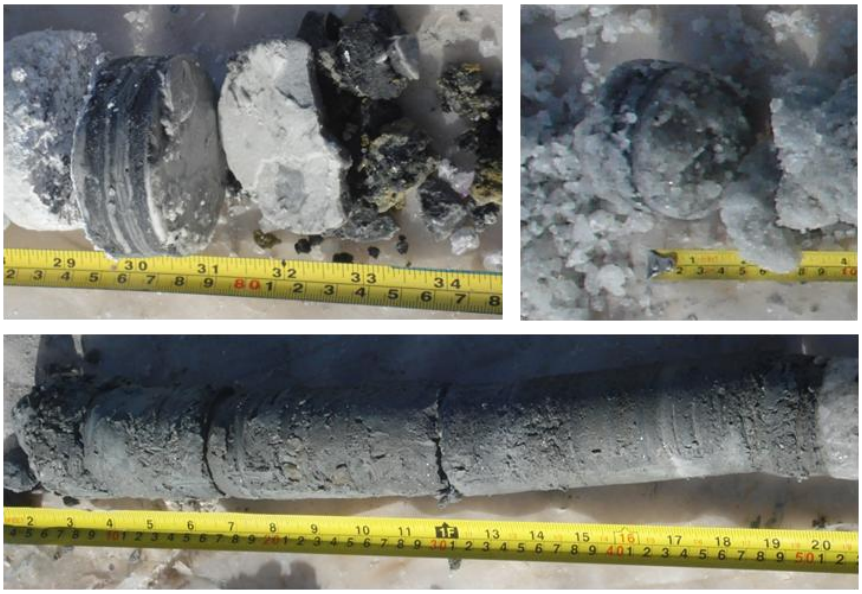

Fig. 21: Pictures of core samples associated to layers with low content of halite: layer of 5 cm with a different colored zoning from a depth of 8 m (top left); dark to black 5 mm layers in halite in a depth of 9.80 m (top right); 0.45 m of grey clayey layer in a depth from 10.50 m (below)

Sylvite (KCl) for example is formed by the incongruent dissolution of carnallite ($KMgCl_3 \cdot 6H_2O$) under the presence of undersaturated waters. Kieserite ($Mg[SO_4] \cdot H_2O$) is formed by the dehydration of hexahydrite ($Mg[SO_4] \cdot 6H_2O$) in the process of the brine evaporation (Warren 2006). Polyhalite ($K_2Ca_2Mg[SO_4]_4 \cdot 2H_2O$) is a common evaporate mineral containing amounts of potash and magnesium. It can precipitate as a primary mineral from the concentrated brine, but the by far largest part of polyhalite is formed by diagenetic alteration of other sulphate minerals, predominantly gypsum, under the influence of brines enriched in magnesium and potassium (Risacher & Fritz 2000). In the samples polyhalite occurs in depths from about 10 m in significant amounts of partly more than 5% of the total mineral content. This depth corresponds to the base of the upper salt crust, and thus conforms to the first masses of salt precipitated from the water masses of paleolake Tauca. When the waters of this lake evaporated, a highly saline brine was formed. When the brine was concentrated enough that potash-magnesia salts could precipitate, polyhalite was formed by the replacement of formerly precipitated gypsum (Holser 1966). This explains why gypsum contents in the salt cores are prevalently low when amounts of polyhalite occur (Fig. 20).

The dominance of halite in the core samples is affirmed by the amounts of sodium and chloride being the predominant elements with together averaged 97 wt% in the salt. The bromine content in halite varies between of < 5 and 28 mg/kg, whereby 5 mg/kg corresponds to the lower detection limit of the ICP-OES analysis (Fig. 22). Bromine has an ionic radius of 1.95 Å, which is similar to that of chlorine with 1.81 Å (Pauling 1927). Hence, it is able to substitute for chlorine in the crystal lattice of halite and other chloride minerals. Thereby the concentration of bromine in halite increases with increasing amounts of bromine in solution. The concentration in halite is also dependent on the temperature of the solution, the speed of crystallization and the amounts of other ions in the brine.

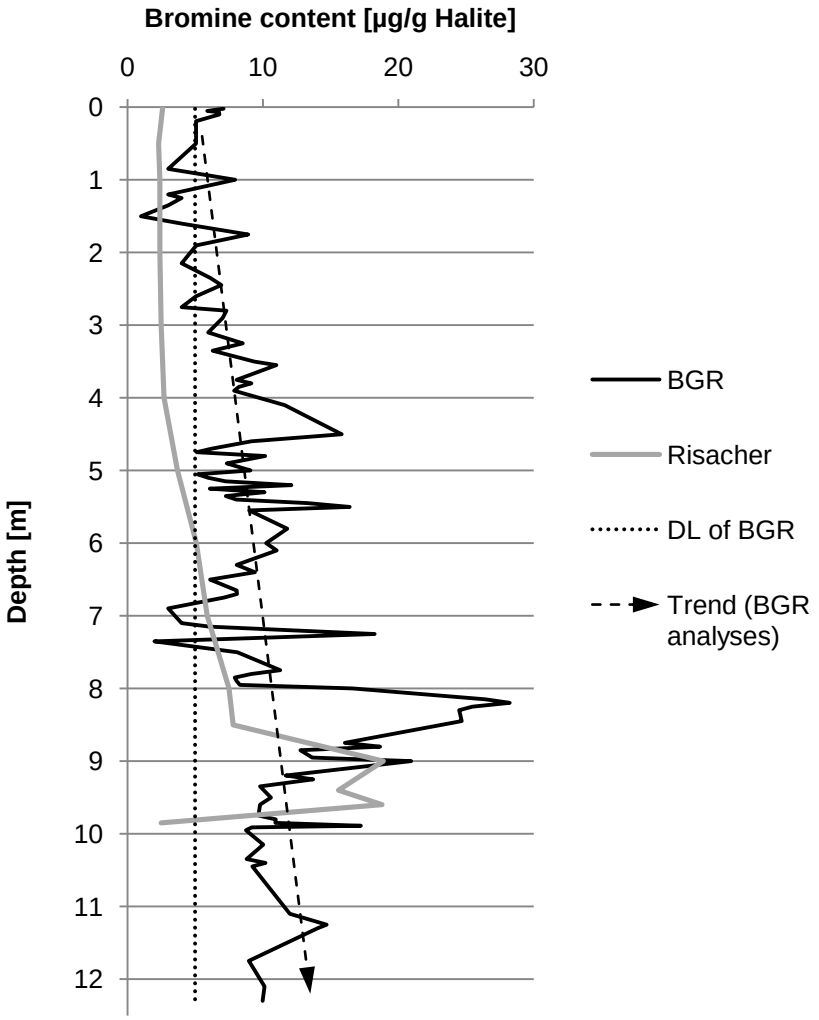

Fig. 22: Comparison of the bromine content in halite in core samples from SLT-01A analysed by the BGR (102 samples) and from a point with a low distance to SLT-01A according to Risacher & Fritz 2000 (15 samples); the dotted line refers to the lower detection limit (DL) of the BGR analyses, the dashed line means the trend in bromine content with depth at SLT-01A

The distribution of the bromine content in halite with depth can give information about the brine stability at the time when the salt was precipitated (Warren 2006). In general, a decreasing bromine content in halite with depth indicates an increasing annual salinity of the brine (Warren 2006). This is the case when the water of a saline lake is evaporated because of the lack of precipitation and a lowered entry of low salinity waters by streams as well as a higher solar insolation. In contrast, an increasing bromine content in halite with depth suggests a freshening by a higher annual water input (Warren 2006).

The core samples from SLT-01A show a slightly downward increasing trend of bromine in halite in the upper 12 m (Fig. 22). This suggests that the amount of water inflow and precipitation increased during the sedimentation of the upper crust. An increasing downward trend of the bromine content in the sediment cores was also observed by Risacher & Fritz (2000). A salt core taken from a sampling location near to SLT-01 revealed constant bromine contents in the upper 4 m and a peak of high concentrations between 9 and 10 m (Fig. 22). This observation supports the assumption of a severe drought that occurred during the Holocene. At this time, the brine level decreased resulting in the concentration of bittern solutes. As the drought ended, the brine level started to rise again caused by increasing rainfall and surface inflows.

4.1.4 Porosity

The porosity, the pore sizes and the distribution of pores in two selected halite core samples from SLT-03 were investigated by computer tomography (CT). The first sample is from a depth of 25-30 cm below the surface, the second sample from a depth between 3.00 and 3.10 m. Both samples had a length of approximately 5 cm.

The 3-D pictures of both core samples are significantly different. The core from 25-30 cm below the surface shows roundly shaped pores and aggregates. The pores seem to be uniformly distributed over the volume of the sample and are of rather small size and apparently connected (Fig. 23). In contrast, the structure of the core from a depth of 3 m shows significantly different features. Here, block-shaped halite crystals grow into connected, vertically extending cavities which determine the porosity of the sample (Fig. 24).

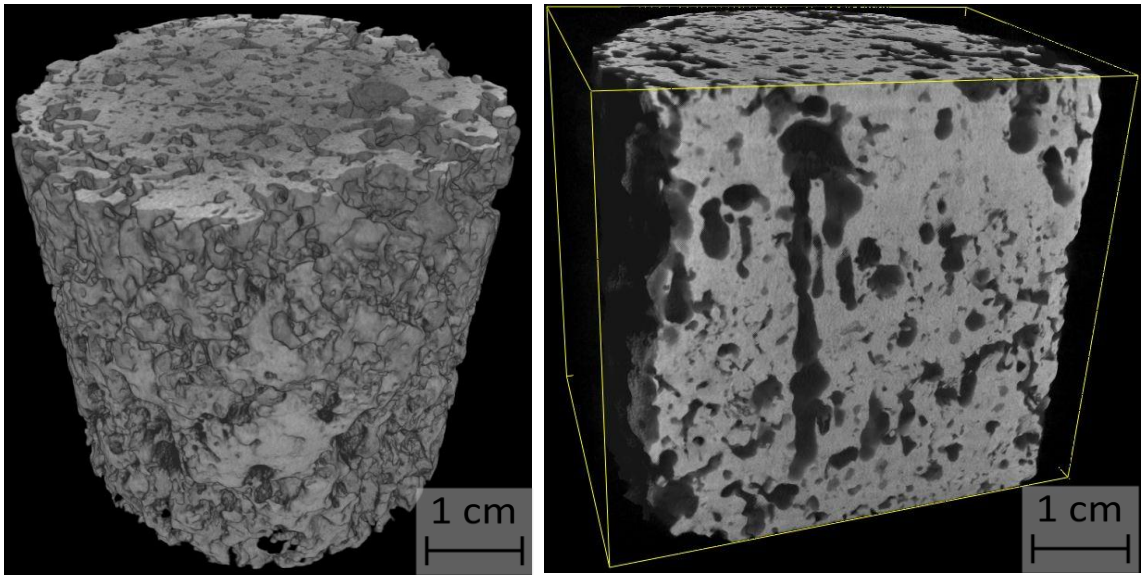

Fig. 23: 3-dimensional images of the upper crust sample from SLT-03: slant side view (left), the same core sample longitudinally cut to show connected pores (right)

A number of transformations on the raw data images was performed for the determination of the pore volume and the evaluation of their connectivity as explained in chapter 3.4.1.2. The grey-scale images of the core samples showed that beside white areas of halite and dark areas of pores also grey spots occurred. As these spots were often connected to pores, it is possible, that they consist of salt that precipitated from the interstitial brine, when the core samples

were dried in the sun. This salt has a lower density than the older halite and thus appears in a different grey scale. Thus, at the binarization step the threshold was modified in such an extent that these special grey values were allotted to a black value and therefore also treated as pores. Examples of the resulting images of the binarization are shown in Fig. 25.

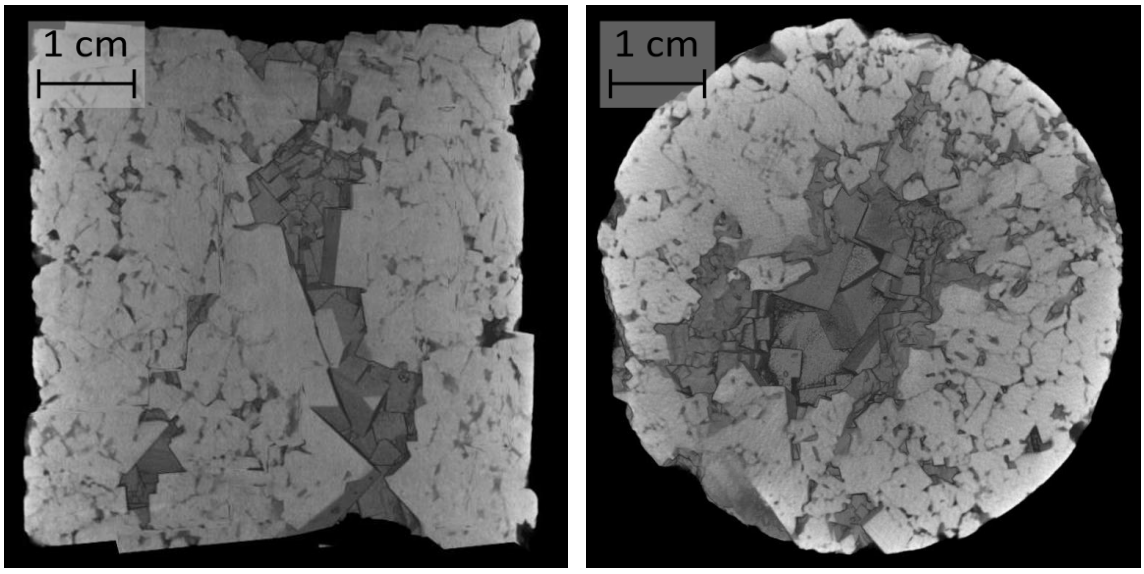

Fig. 24: 3-dimensional images of the sample from a depth of 3 m from SLT-03: side view showing vertical cavity (left); top view (right)

The step of labelling by reconstruction for the core samples showed, that the large part of the pores in both cores are of the same brown colour (Fig. 25). As each colour represents a single pore object, it can be assumed that these pores are in some way connected to each other and are therefore treated as one single large pore object. Table 6 shows the results of the computer tomography after the application of the explained transformations.

Table 6: Volume of the pores in both cores obtained by computer tomography

	SLT-03 (0.25-0.30 m)		SLT-03 (3.00-3.05 m)	
Total volume of the sample	92.978 cm³	100%	113.10 cm³	100%
Solid fraction	61.098 cm³	65.71%	91.157 cm³	80.59%
Connected pores	31.072 cm³	33.42%	21.025 cm³	18.6%
Closed pores	0.8076 cm³	0.87%	0.9187 cm³	0.81%

Comparing both core samples it is remarkable that the sample from the upper crust has a 1.5 times higher porosity than the sample originated from a greater depth. The distribution of the pore volume in the salt differs significantly between the samples. While the pores are uniformly distributed over the whole salt core from the upper crust, the pore volume in the deeper sampler is mainly made up of a large cavity located in the centre of the core, surrounded by a denser halite structure. This implies that the pores of the upper crust have developed from a former dense halite matrix where the circulation of less saline water lead to a solution of the mineral. Thereby, the dissolving water probably derives from the infiltration of precipitation and inflows from the Salar's tributaries during the wet season. The continuous circulation impedes the formation of larger halite crystals, so that salt aggregates in the upper crust above the brine table are of irregular shape.

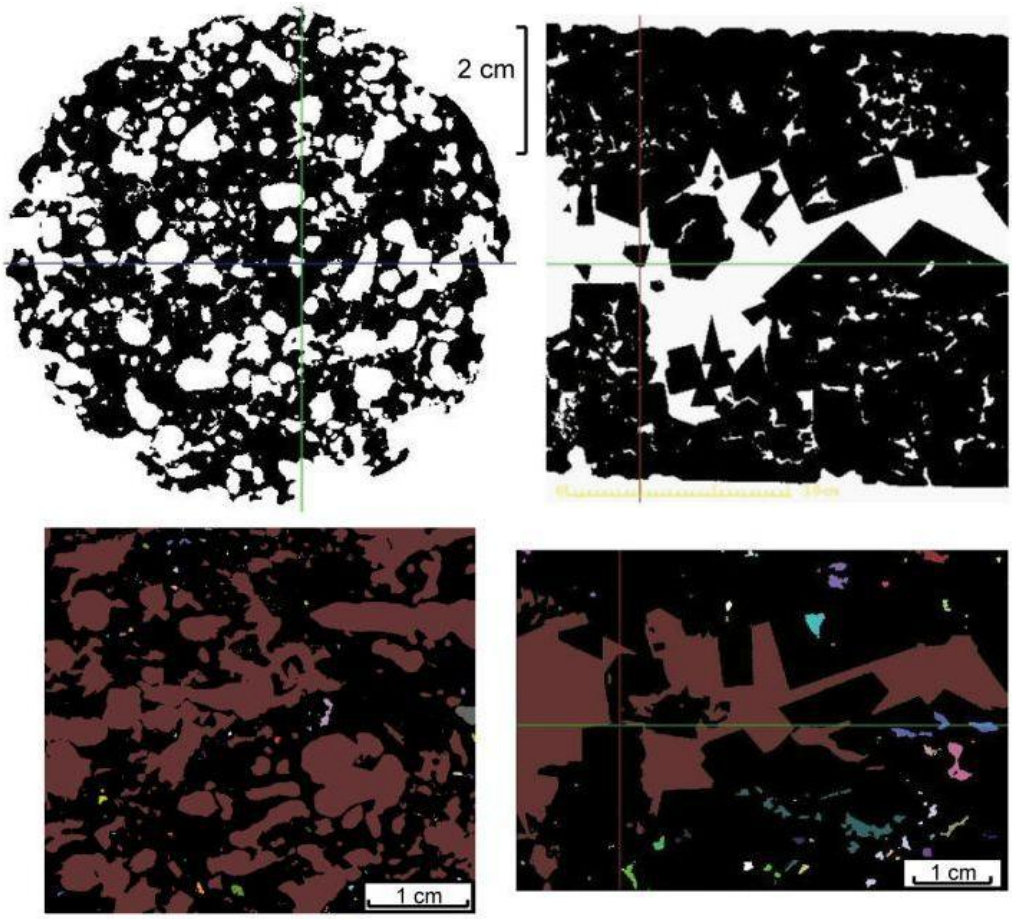

Fig. 25: Processing of the raw images derived from CT analyses: top view of the binarized image and longitudinal section of image processed by labelling from the crust sample (left); longitudinal section of binarized image and labelled image from the sample from a depth of 3 m (right)

In contrast, the core sample from a depth of 3 m shows crystals of halite with a typical cubic shape. These crystals are formed under the presence of a brine constantly oversaturated in NaCl.

During the core documentation performed in the field it could be observed that the presence and size of cubic halite crystals increased with the depth. This leads to the assumption that during the wet season raining water slowly infiltrating into the upper crust is rapidly enriched in solutes, by which the roundly shaped pores in the upper centimetres are formed. When reaching the brine table it is mixed with this highly saline water forming a transition between the infiltrating waters from the surface and the saturated brine from below. Halite layers in that area consist of small crystals with partly cubic shape, because the formation of larger crystals is stopped with the beginning of the wet season.

It was shown that the application of computer tomography is very appropriate for the determination of the porosity and the distribution of pore and pore sizes in a halite sample. The weakening of X-rays depends on the applied wave length, the ordinal numbers of the elements the sample consists of, the density as well as the thickness of the sample. As the halite weakens large parts of the X-rays it can be clearly differentiated from parts without material (pores) and parts consisting of other minerals (e.g. gypsum). A further advantage is the non-destructive of the sample and the exact determination of the volume of pores with a certain size and their connectivity. Another method for the experimental determination of the pore volume of a porous media is the mercury porosimetry, which works by the intrusion of mercury into a material at high pressures. Though, the disadvantage here is the small usable sampling volume, which would not reflect the real distribution of pore sizes. Another problem comprises the effects at the edges of the sample. The boundary of the sample has to be flush with the boundary of the surrounding vessel, which is not realizable for a core sample with an extremely irregular shaped edge because of heterogeneously distributed pores.

4.2 Hydraulic conductivity

Pumping tests were performed with the aim to gain insights into the hydrodynamic conditions and to determine important hydrogeological parameters such as hydraulic conductivity, transmissivity and storage capacity that characterize an aquifer (Bamberg & Eschner 1979). A pumping test was done at the 25th September 2009 in well SLT-03C. Wells SLT-03A and SLT-03E served as observation wells, where the changing in water levels was measured.

A decisive question that must be answered prior to the application of different methods for the evaluation of pumping tests is that, if the aquifer, where the water is pumped off, is confined or unconfined. The stratigraphy, which is obtained by the analysis of the sediment cores (see chapter 4.1.1), is the most effective source of information to answer the question. The core documentation showed that the halite aquifer is not overlain by an aquiclude, an impermeable layer, in the drilling locations SLT-01 and SLT-03. Thus, it can be assumed that unconfined conditions exist.

The methods applied for the evaluation of pumping test data are based on the requirement that a number of assumptions and conditions have to be met (Kruseman & de Ridder 2000):

- the aquifer is homogeneous and isotropic
- the aquifer has a constant thickness over the area influenced by the pumping
- the aquifer seems to be of an unlimited extent
- the discharge rate is constant over the duration of pumping
- the well is complete, meaning that it penetrates the whole thickness of the aquifer and thus water flows to the well only horizontally
- before pumping the piezometric height is (nearly) horizontal over the influenced area
- the aquifer doesn’t receive inflows from surface waters in the influenced area

When all mentioned conditions are met, the well discharge can be expressed in the well formula by Dupuit/Thiem (1906) as following:

$$Q = \frac{\pi \cdot k_f}{\ln\left(\frac{r_B}{r_E}\right)} \cdot (h_B^2 - h_E^2)$$

where

Q	discharge rate [m³/s]
k_f	hydraulic conductivity [m/s]
r_B, r_E	respective distances of the piezometers B and E from the pumping well C [m]
M	thickness of the aquifer (depth of well minus static water level) [m]
h_B, h_E	respective steady-state elevations of the water levels in the piezometers [m]

The pumping test in SLT-03 was performed as described in chapter 3.5. The obtained values for the drawdown in SLT-03B and SLT-03E over time are comprised in Table A13 (Appendix). After 160 min of pumping with a discharge rate of 1.3 L/s steady state conditions were reached, which is illustrated in Fig. 26.

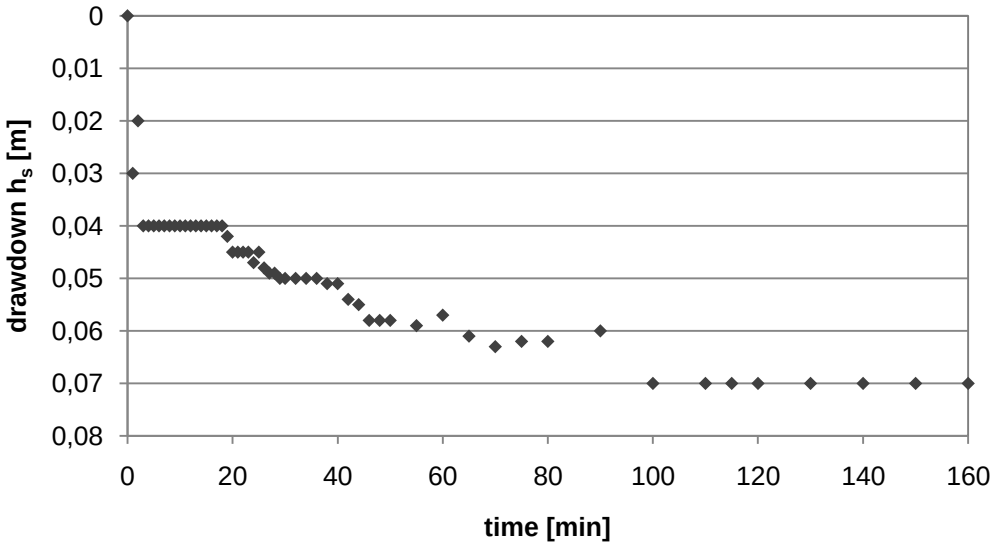

Fig. 26: Drawdown curve in observation well SLT-03B for a pumping duration of 160 min

When the well formula is rearranged to solve for k_f and values summarized in Table 7 are inserted it follows:

$$k_f = \frac{0.0013\ m^3 \cdot \ln\left(\frac{3.04\ m}{10.1\ m}\right)}{\pi \cdot (5.44^2 - 5.38^2)\ m^2} = 7.39 \cdot 10^{-4}\ m/s$$

According to DIN 18130-1 the obtained k_f value of $7.39 \cdot 10^{-4}$ m/s is in the range of a middle grained sand and indicates a high permeability for water.

The transmissivity T_M is a parameter for the characterization of the transport capability of an aquifer for water (Langguth & Voigt 1980). It includes the thickness of the aquifer and is calculated from the obtained k_f value as following:

$$T_M = k_f \cdot M = 4.032 \cdot 10^{-3}\ \frac{m^2}{s}$$

The porosity of a medium is reduced by retained water that is adhesively bound to the surface of rock particles and hold against gravity. The fraction of the total pore volume that is available for the transport of the fluid is referred to as the effective porosity n_{eff}. Marotz (1968) found a formula to describe the relation between the effective pore volume and the k_f value:

$$n_{eff} = [0.462 + 0.045 \cdot \ln(k_f)] \cdot 100\%$$

By inserting the former calculated k_f of $7.39 \cdot 10^{-4}$ m/s an effective pore volume of 13.76% is obtained. For comparison, middle grained sand has an n_{eff} in the range of 10–15%.

Table 7: Parameters for the determination of k_f

Pump well	Q	r_B	r_E	h_B	h_E	M
SLT-03C	0.0013 m³/s	3.04 m	10,1 m	5.38 m	5.44 m	5.45 m

The hydraulic conductivity k_f includes the resistance in form of friction caused by the rock that is flown through by the fluid. Further it depends on the properties of the fluid (temperature and viscosity) as well as the properties of the aquifer (pores).

As the groundwater brine has a higher density and viscosity than normal water (see chapter 4.3.9), the k_f cannot exactly describe the conditions of the aquifer regarding the transport of a fluid. Hence, another parameter, the intrinsic permeability K is introduced. It describes the transport qualities of a pore system independent from the properties of the fluid that fills the pores. Thus it is a parameter that is specific for a particular rock. The relation between the intrinsic permeability and the hydraulic conductivity is defined as following (Hölting & Coldewey 2009):

$$K = \frac{k_f \cdot \eta}{\rho \cdot g}$$

where
- K intrinsic permeability [m²]
- ρ density [kg/m³]
- η dynamic viscosity [kg/(m·s)]
- g gravitation [m/s²]

The determination of viscosity and density (results in chapter 4.3.9) of the brine from SLT-03 yielded values of 3.2 mPa·s and 1234.4 kg/m³ respectively. When these values are placed into the equation it follows:

$$K = \frac{7.39 \cdot 10^{-4} \frac{m}{s} \cdot 0.0032 \frac{kg}{m \cdot s}}{1234.4 \frac{kg}{m^3} \cdot 9.81 \frac{m}{s^2}} = 1.95 \cdot 10^{-10}\ m^2$$

The obtained values for hydraulic conductivity, transmissivity and permeability of the aquifer in SLT-03 indicate a high transport availability of the halite layers for the interstitial brine.

In well SLT-01A a recovery test was done at the 26th September 2009. The well is screened beneath the mud layer in the second aquifer, in a depth between 11.70 and 12.30 m. As the aquifer is covered by the mud, it is assumed that the groundwater table is confined. The well is not complete, because its profundity does not reach the lower base of the aquifer. For the recovery test the brine was pumped from the well tube with a discharge rate Q of 1.3 L/s until the suction limit of the pump was reached, then the rise of the water table in dependency of the time was measured, until the static water level was reached.

The results for the rise of the water table in dependency of time are combined in table A14 (Appendix). When the assumptions of confined aquifer and unsteady-state are made, the transmissivity conforms to the following relation (Hölting & Coldewey 2009):

$$T_M = \frac{2.3 \cdot Q}{4\pi \cdot \Delta h_s}$$

For the determination of Δh_s the rise of the water level is plotted against the time on semi-log paper (Fig. 27). Then the best-fit line between a logarithmic time decade is drawn and the value for the drawdown difference is calculated from a logarithmic decade (indicated by dashed lines in Fig. 27).

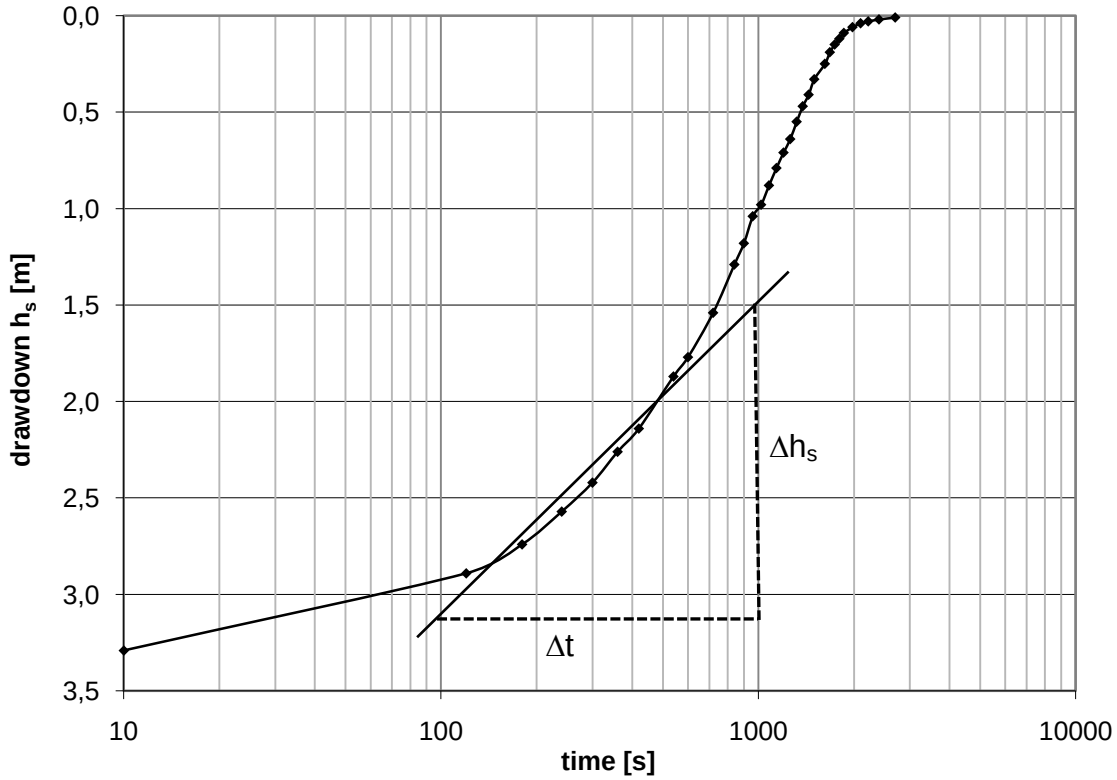

Fig. 27: Curve of drawdown versus time for the recovery test in well SLT-01A, the Δh_s for the determination of T_M is obtained from a logarithmic time decade

With a Δh_s of 1.61 m it follows:

$$T_M = 1.48 \cdot 10^{-4}\ m^2/s$$

The thickness of the aquifer M in SLT-01 is calculated as the difference between the well depth (12.50 m) and the depth of the lower limit of the mud layer (11 m). Hence, the k_f is calculated according to:

$$k_f = \frac{T_M}{M} = \frac{1.48 \cdot 10^{-4}\ m^2/s}{1.50\ m} = 9.87 \cdot 10^{-5}\ m/s$$

For the determination of the intrinsic permeability a viscosity of 2.6 mPa*s and a density of 1224.7 kg/m³ (average of the brine samples from SLT-01, see chapter 4.3.9) are assumed. It follows:

$$K = \frac{9.87 \cdot 10^{-5}\ \frac{m}{s} \cdot 0.0026\ \frac{kg}{m \cdot s}}{1224.7\ \frac{kg}{m^3} \cdot 9.81\ \frac{m}{s^2}} = 2.14 \cdot 10^{-11}\ m^2$$

According to Todd (1959) the obtained value for the intrinsic permeability is classified between highly permeable aquifer (> 10^{-10} m²) and weakly permeable aquifer (< 10^{-13} m²). When comparing the obtained results for k_f, T_M and K, the aquifer of the uppermost halite layer in SLT-03 shows an approximately 10 times higher overall permeability for the migration of brine in the pores. The transport capacity in the halite horizon beneath the mud layer in SLT-01 indicates a significantly lower potential for the migration of the interstitial brine.

The results of the aquifer tests in SLT-01 and SLT-03 must be regarded critically. The required assumption for the validity of the used formulas, that the pumping well must reach the base of the aquifer, was not fulfilled in SLT-01. Further, the velocity of the drawdown and recovery rates may not only be caused by the hydraulic conductivity itself. Also the quality of the filter tubes and the functionality of the filter gravel and the caulking clay have an effect on the replenishment of the brine. It is possible that salt crystallization processes occur when the filter slots come into contact with the highly saline brine. This would lead to clogging of the filters and thus to a hindered inflow of ground water. Further, it is thinkable that the clay mud was transported in larger pores and cavities into the width and depth. Hence, it does not fulfill its function as a sealant but contributes to the clogging of the pores.

Furthermore, the comparatively short length of the filter tube of only 60 cm in SLT-01A could result in lower obtained permeability parameters. Another critical point is the use of the water pump for pumping the brine. Three main reasons were responsible for the restricted functionality of the pump. First, the high altitude of more than 3500 m leads to a significant lowering of the pumping power due to lower air pressure for the burning process of the gasoline pump. Second, the high density of the brine resulted in a lower pumping capacity. Finally, the suction diameter of the pump had to be reduced from 2” to 1.5” because of the limited diameter of the well. Thus, the pumping power was further reduced.

4.3 Brine samples

In total, nine brine samples were taken at different locations of the Salar de Uyuni. Four samples each were obtained from bore holes of the drilling locations SLT-01 and SLT-03. Thereby from every well one brine sample was taken, thus the different samples origin from different depths. Another brine sample was taken from a brine pool at the border of the Salar, where brine is exposed at the surface of the salt crust. In the following chapter this sample is named SLT-S.

4.3.1 On-Site parameters

On-site parameters were determined during the field trip in September 2009 in the subsurface brine pumped from the installed wells. The results of the analysis of on-site parameters is combined in Table 8. The values from SLT-01 and SLT-03 are averaged for the n samples from different wells, the standard deviation indicates the variation between samples. The original data for each well are comprised in Table A6 (Appendix).

Table 8: Summary of parameters determined in the field including the standard deviation

Sampling location	n	pH	EC [mS/cm]	E_H [mV]	O_2 content [mg/L]
SLT-01	4	7.10 ± 0.015	235 ± 6.39	110 ± 28.5	4.28 ± 1.35
SLT-03	4	6.89 ± 0.044	204 ± 7.86	-61.9 ± 6.70	6.77 ± 0.32
SLT-S	1	5.84	230	210	0.38

n = number of samples from different depths

The measured **pH-values** are in the range between 5.84 and 7.12. The low standard deviations show, that differences exist mainly between the different sampling locations, but not between wells from one drilling location. Hence, a dependency on the sampling depth is not observed. pH values of brines from the drilling locations are in consistency with Rettig et al. (1980) who reported pH in the range of 7 and slightly above for several points all over the Salar.

In contrast, most other salars and playas in the southern part of the Altiplano have significant higher pH values between 8 and 9, as reported by Risacher & Fritz (1991a). The SLT-S sample with a pH of 5.8 generally shows a lower value than the samples from other points. At this point gas streams through cracks from the subsurface upwards. Former investigations showed, that this gas consists to 95% of CO_2 (Merkel, B., personal communication). When coming into contact with the brine, the gas is solved and thus the pH of the brine is lowered.

Redox potentials are in the range of -70 to 200 mV which corresponds to reducing and partly reducing conditions. When displaying the results in an E_H/pH diagram samples can be distinguished according to their location on the Salar (Fig. 28). The samples from SLT-03 exhibit reducing conditions which indicates that the brine might be influenced by the underlying thick mud layer, where anoxic conditions prevail. The SLT-S sample has the highest redox potential with more than 200 mV.

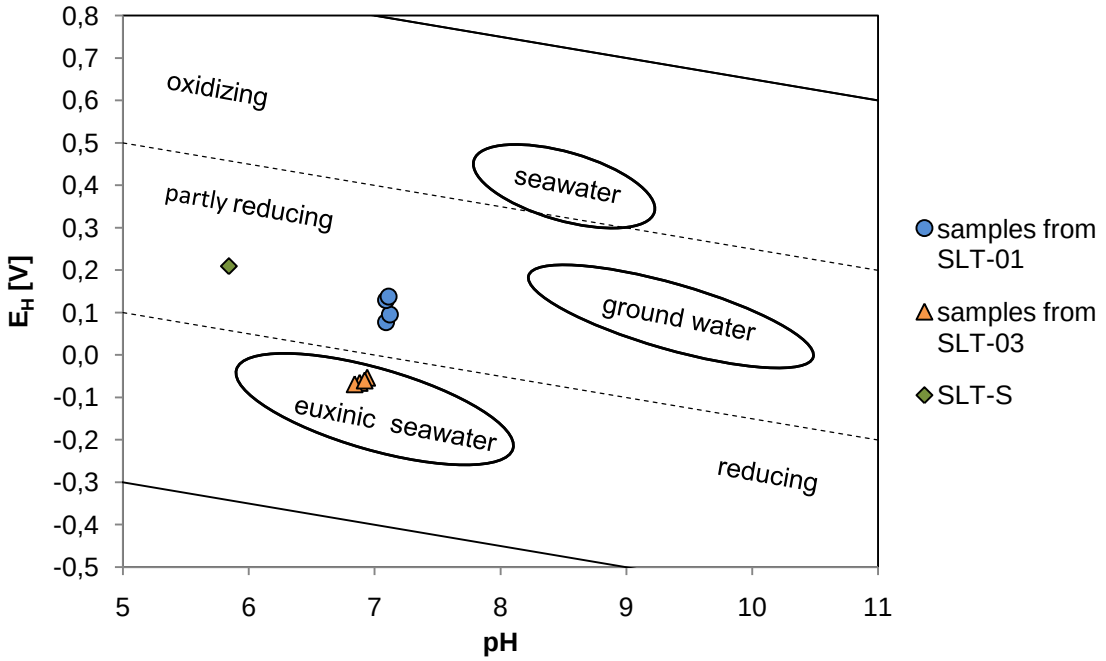

Fig. 28: E_H/pH-diagram with upper and lower stability limits of water (closed line), borders of E_H for oxidizing and reducing conditions (dashed line), the values of the brine samples and conditions of natural waters as comparison (after Hölting & Coldewey 2009)

Values between 194 and 242 mS/cm were obtained for the **electric conductivity (EC)**. Samples from SLT-03 with average 235 mS/cm have a 15% higher EC than samples from point SLT-01 with 204 mS/cm. The SLT-S sample from the surface has an EC of 230 mS/cm which is in the range of the subsurface brine.

The measured conductivities should be considered with caution, as the values are near and partly exceeding the upper range of the instrument's detection limit of 200 mS/cm. Hence, it is possible that they do not represent the real salinity of the brine.

The **content of oxygen** is in the range of 0.38 mg/L in the SLT-S sample up to 6.99 mg/L for a sample from SLT-03. The obtained values must be evaluated critically, as the extraction of the brine with a pump causes inevitable turbulences, which result in a mixture of the water with atmospheric oxygen and thus in higher oxygen contents. The high value of the sample from SLT-01 from a depth of 7 m may be due to that cause of error.

4.3.2 Photometry

Photometrical measurements were performed for the brine samples in order to determine the concentrations of Fe_{total}, Fe^{2+}, NO_2^-, NH_4^+ and sulphide as a sum parameter for S^{2-}, HS^- and H_2S (aq). Table 9 shows the average values for brines from different depths of one drilling location. The results for each brine sample are comprised in Table A6 (Appendix). Samples had to be diluted 1:10 for NH_4^+ (SLT-01, SLT-03) as well as 1: 10 for Fe^{2+} (SLT-S), 1:20 for Fe_{total} (SLT-S) and 1:100 for NH_4^+ (SLT-S).

Table 9: Results of photometrical analyses performed in the field: average values of the samples from each drilling location with standard deviation (all values in mg/L)

Sampling location	Fe_{total}	Fe^{2+}	S^{2-}, HS^-, H_2S	NO_2^-	NH_4^+
SLT-01	0.038 ± 0.009	< 0.03	< 0.01	0.021 ± 0.003	1.95 ± 0.34
SLT-03	< 0.03	< 0.03	0.03 ± 0.02	0.115 ± 0.039	2.03 ± 0.61
SLT-S	31.4	28.0	< 0.01	0.019	75.0

In general, the values obtained for SLT-01 and SLT-03 are very low, mainly below or in the range of the estimated detection limit for all measured species except for NH_4^+.

Except for NO_2^-, the results do not differ significantly between both drilling locations according to the Kruskal-Wallis-Test using an error probability α of 5% (statistical values calculated with the program SPSS, results in chapter 4.3.7).

In contrast, the SLT-S sample is significantly enriched in iron, whereby the major amount occurs in the reduced form. Also nitrogen occurs predominantly in the reduced form with high contents of NH_4^+. Reducing conditions in the SLT-S sample are also indicated by the low measured oxygen content.

4.3.3 Total dissolved solids

The content of total dissolved solids (TDS) was calculated as the sum of the four most frequent cation species (Na, Mg, K, Li) and the four most frequent anion species (Cl, SO_4, HCO_3, Br) in the samples. TDS values are in the range between 270 and 330 g/L. In comparison to normal seawater, which has a TDS of average 35 g/L (Hölting & Coldewey 2009), the brine samples are enriched to almost the tenfold. Three groups of TDS values can be distinguished according to the sampling locations of the brines (Fig. 29). Thereby, samples from different depths in one location show very similar values, hence, it could not be observed, that the salinity of the brine does change with depth.

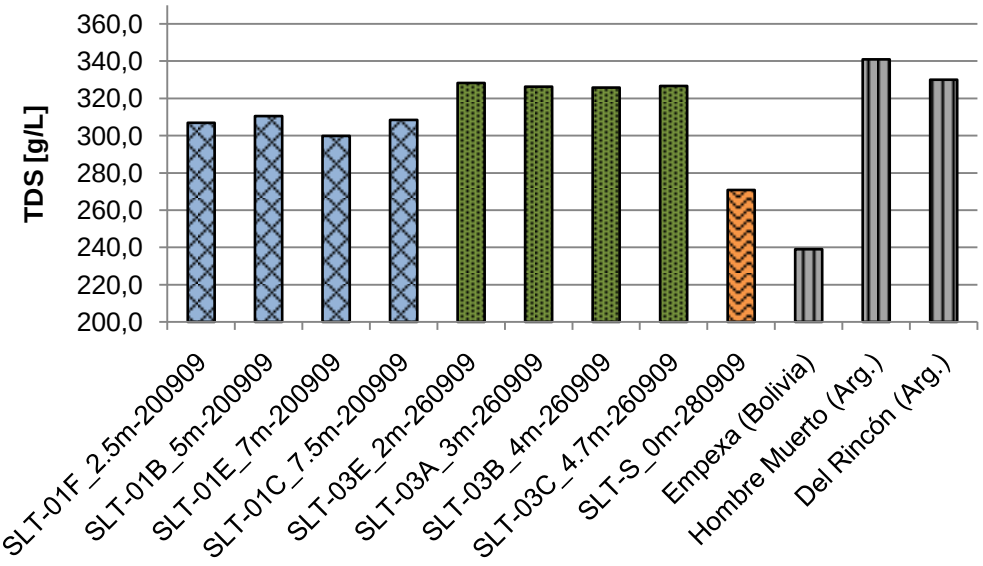

Fig. 29: Contents of total dissolved solids in the samples and comparative values of brines from other saline pans in South America (after Warren 2006)

Obtained values are comparable to TDS contents of brines in other salt pans in South America, for example the Salar del Rincón in Argentina, where the salinity is similar with average 330 g/L (Warren 2006). The waters of the Rio Grande shortly before entering the Salar de Uyuni have a TDS of roughly 2 g/L (Risacher & Fritz 1991b), which means an enrichment of about 150 times in the brines from SLT-01 and SLT-03 compared to the main tributary. The brine in the SLT-S sample has a significantly lower salinity. Samples from SLT-03 show a higher content of TDS and are therefore enriched in solutes compared to samples from SLT-01.

4.3.4 Main anions and cations

By ion chromatography the contents of cations Na^+, Mg^{2+}, K^+, Ca^{2+} and Li^+ were determined in the brine samples as well as the concentrations of anions Cl^-, SO_4^{2-}, HCO_3^- and Br^-. The obtained concentration ranges in the nine brine samples are shown for every species in Fig. 30. The individual results for every brine sample are combined in Table A7 (Appendix).

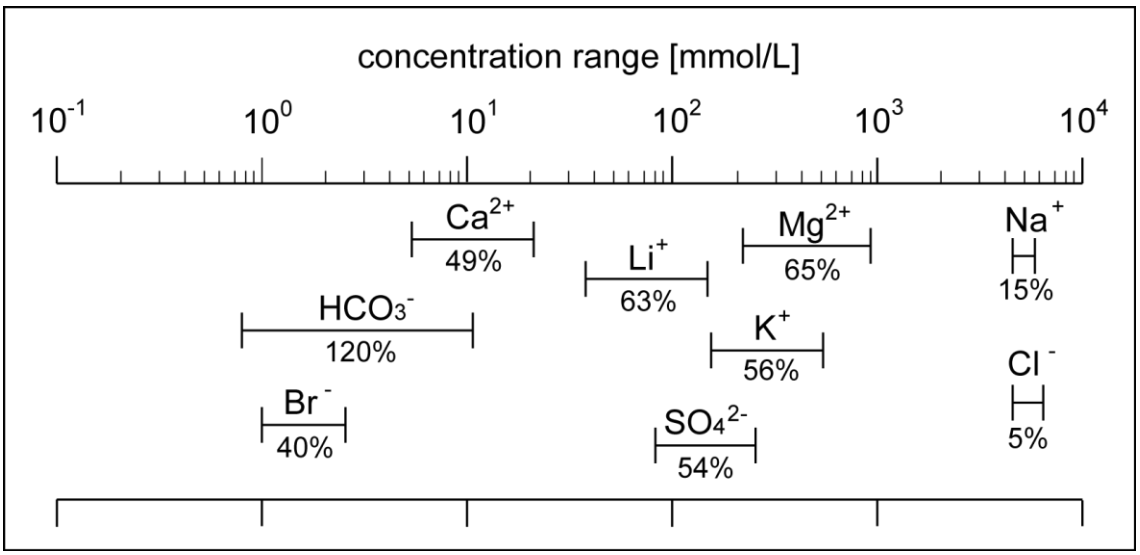

Fig. 30: Concentration ranges in mmol/L of main cations and anions in the nine brine samples (numbers below elements are the standard deviations of the data in % of the mean)

When classifying the brine samples according to water types by means of major ions, samples from SLT-01 and the SLT-S sample are of Na-Cl type and samples from SLT-03 are of Na-(Mg)-Cl type.

Thereby, components without parentheses exist in concentrations above 25 eq%, components shown in parentheses occur between 5 – 25 eq% (Eugster & Hardie 1978). Both identified water types in the samples show a large excess of Na and Cl. The concentration ranges in the brine samples are lowest for Na and Cl, which is supported by the lowest percent standard deviations of 15% and 5% respectively (Fig. 30). This implies that contents of these ions are less dependent on the concentration factor by means of total salinity of a solution, at least in the salinity range of the investigated brines.

In order to compare the ionic composition between the samples, the individual components must be evaluated by reference to a conservative solute. A conservative solute is characterized in that its concentration in a solution increases directly with increasing total content of solutes (TDS), which means that this component stays in solution until a high grade of salinity of the brine. Chloride behaves conservative, but only until the point of halite precipitation, which makes it useless for that purpose in view of the halite predominance in the Salar de Uyuni (Risacher et al. 2006). Another appropriate species would be bromide. Although a small fraction of bromide replaces chloride in halite, the major part stays in solution and its use as reference element has been suggested in marine evaporites (Braitsch 1971). However, there is evidence that bromine could be released into the atmosphere, which results in a depletion of bromine relative to lithium (Risacher & Fritz 2000). Other components in a solution, as magnesium and potassium, are as well inappropriate for the use as geochemical tracer, as they are bound in mineral phases as in sylvite (KCl), carnallite ($KMgCL_3 \cdot 6H_2O$) and polyhalite ($K_2Ca_2Mg(SO_4)_4 \cdot 2H_2O$) by precipitation processes in higher concentrated solutions. Lithium is most suitable, as it behaves conservative over the whole salinity range of brines from the Salar de Uyuni. Naturally occurring Li-bearing minerals are not known to exist in the Salar and the incorporation of lithium in clay minerals is low, because this process predominantly occurs in brines with high alkalinity and pH, which is not given in Uyuni brines (Starkey & Blackmon 1979, Weaver & Pollard 1975). Therefore the relation between lithium and other main ions in the brines will be displayed.

Fig. 31 shows the distribution of sodium and calcium in the brine samples plotted against the lithium concentration. Sodium shows a constant decrease with increasing contents of lithium. This is explained by the precipitation of halite at high TDS concentrations. Because of the predominance of chloride over sodium in the solution, sodium content decreases with further concentration of the brine and sodium is replaced by magnesium and potassium as the major cation, while chloride concentrations stay nearly constant (Rettig et al. 1980).

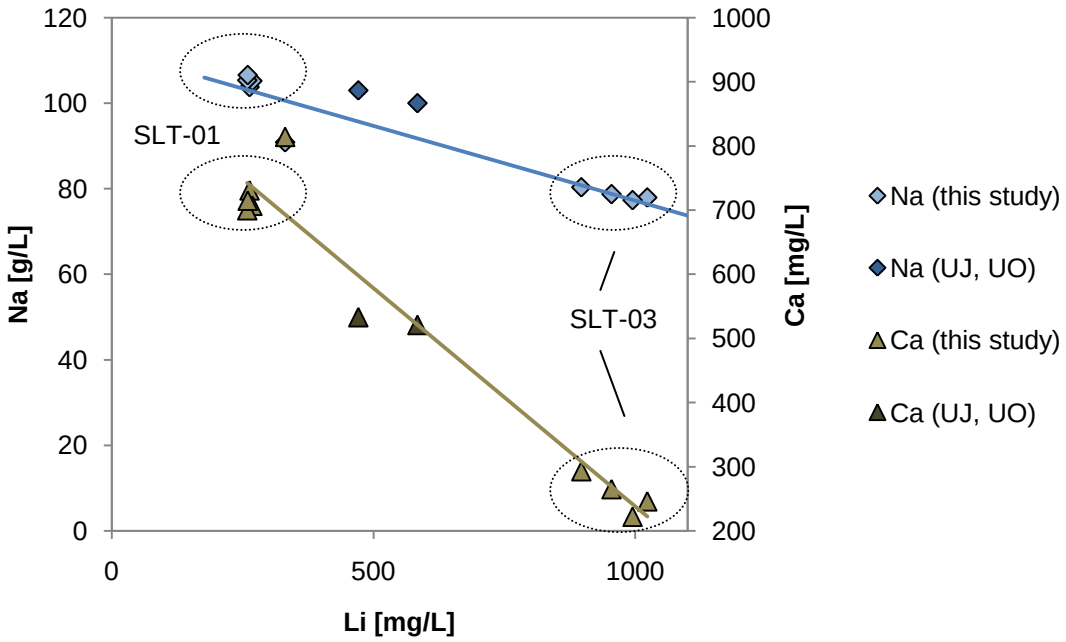

Fig. 31: Concentrations of sodium and calcium plotted against lithium contents in the brine samples, points in dashed circles indicate the sampling location (values UJ and UO serve as reference values and are obtained from two brine samples of Risacher & Fritz 1991b)

Calcium concentrations decrease strongly with increasing contents of lithium in the brines. This is caused by the precipitation of gypsum, which is reported to begin at salinities of 13 to 16% for seawater (Warren 2006). The dependency of calcium concentrations on the TDS content in the brines is also confirmed in the SLT-S sample, where the highest measured value for calcium goes along with the lowest obtained TDS value.

Magnesium, potassium and sulphate show a direct proportional trend to lithium for the entire concentration range of lithium in the examined brine samples (Fig. 32).

The linear equation of simple evaporative concentration was obtained by combining the relation between bromine and magnesium, sulphate and potassium and the relation between bromine and lithium with increasing concentration of a brine (Rettig et al. 1980):

$$Br\ [g/L] = 0.004 \cdot X\ [g/L] \qquad \text{with } X = Mg;\ K;\ SO_4$$

$$Br\ [g/L] = 0.1 \cdot Li\ [g/L]$$

Hence, for the relation of simple evaporative concentration between lithium and other ions follows:

$$Li\ [g/L] = 0.04 \cdot X\ [g/L] \qquad \text{with } X = Mg;\ K;\ SO_4$$

The relation between magnesium and lithium shows a slight departure from the line of simple evaporation, which indicates a loss of magnesium with further concentration of the brine (Fig. 32). This could be explained by the precipitation of minor amounts of magnesium in minerals as carbonates and silicates (Rettig et. al 1980).

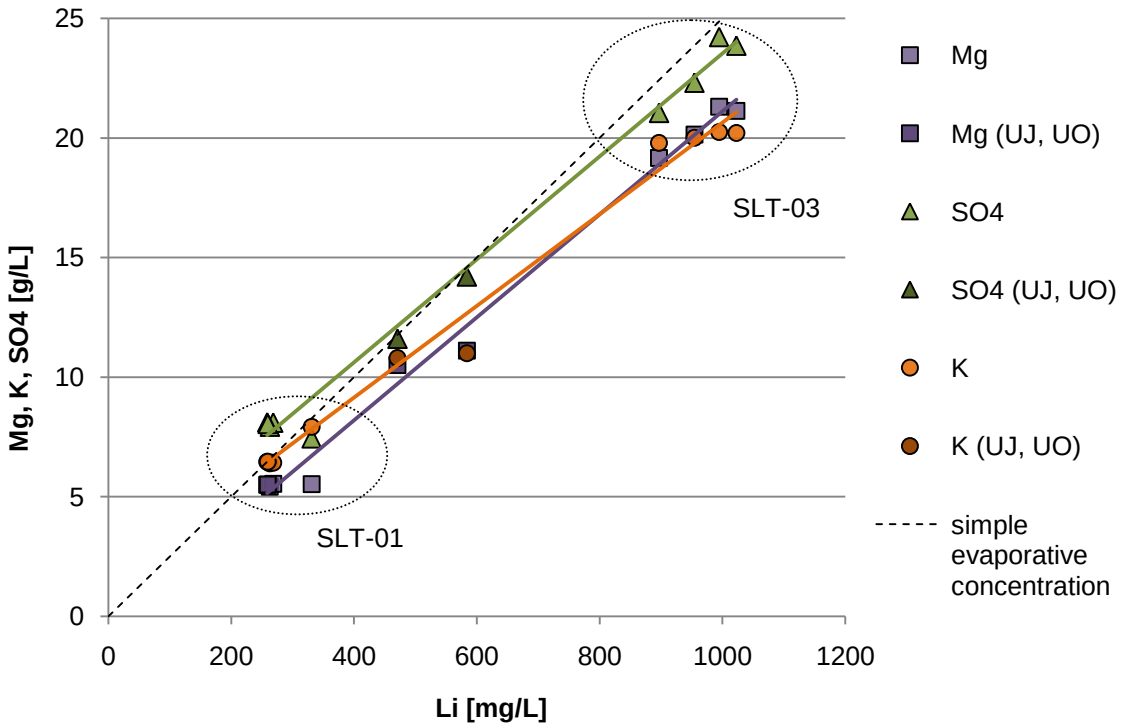

Fig. 32: Concentrations of Mg, K and SO_4 plotted against the content of lithium in the brine samples (values UJ and UO serve as reference values and are obtained from two brine samples of Risacher & Fritz 1991b); the dashed line represents the simple evaporative concentration for Mg, K and SO_4 in relation to lithium, the dotted circles indicate the sampling location

During the evaporation of seawater brines magnesium increases conservatively until an evaporation degree of about 70 times of the original brine salinity (McCaffrey et al. 1987). At this point the precipitation of magnesium sulphate begins to prevail, which inhibits a further increase of the ion in solution. This point of saturation is not reached for the investigated brine samples from both drilling locations, hence, the magnesium concentrations are still increasing with increasing salinity.

Sulphate concentrations behave similar to magnesium. They rise with increasing concentration of the brine until the point of saturation is reached, where magnesium and potassium sulphates precipitate. The lowered slope of sulphate increase in the brine samples compared to the straightforward evaporative concentration (Fig. 32) is probably due to the precipitation of gypsum, by which small amounts of sulphate are removed from solution.

Potassium shows, similar to magnesium and sulphate, an increase with rising lithium contents, but a slight departure from the line of simple evaporative concentration. An explanation could be the uptake of potassium in clay minerals and thus the removal of a minor amount from the solution. Clay minerals were detected in the mud layers of the drilling core SLT-01A by X-Ray analyses (see chapter 4.1.3) and presumably occur in the mud layers in SLT-03 as well. The precipitation of potassium sulphates and chlorides begins at a concentration degree of 80% of the original solution for seawater (McCaffrey et al. 1987). As this point is not reached in the Uyuni brines, the concentration of potassium in the Uyuni brine samples still rises with increasing amounts of lithium.

The plot of boron against the lithium content in the investigated brine samples almost perfectly fits the curve of the direct evaporative concentration (Fig. 33). This implies that a process of depletion of boron, as observed for the other solutes, is not in evidence or occurs only to a very low extent. As the boron concentrations rise with increasing amounts of lithium, it is estimated, that the brines are undersaturated with respect to borate, and this mineral does not precipitate. The good correlation between lithium and boron leads to the assumption that deposits of borax ($Na_2[B_4O_5(OH)_4]\cdot 8H_2O$) could be a good indicator for the occurrence of lithium-rich brines (Rettig et al. 1980).

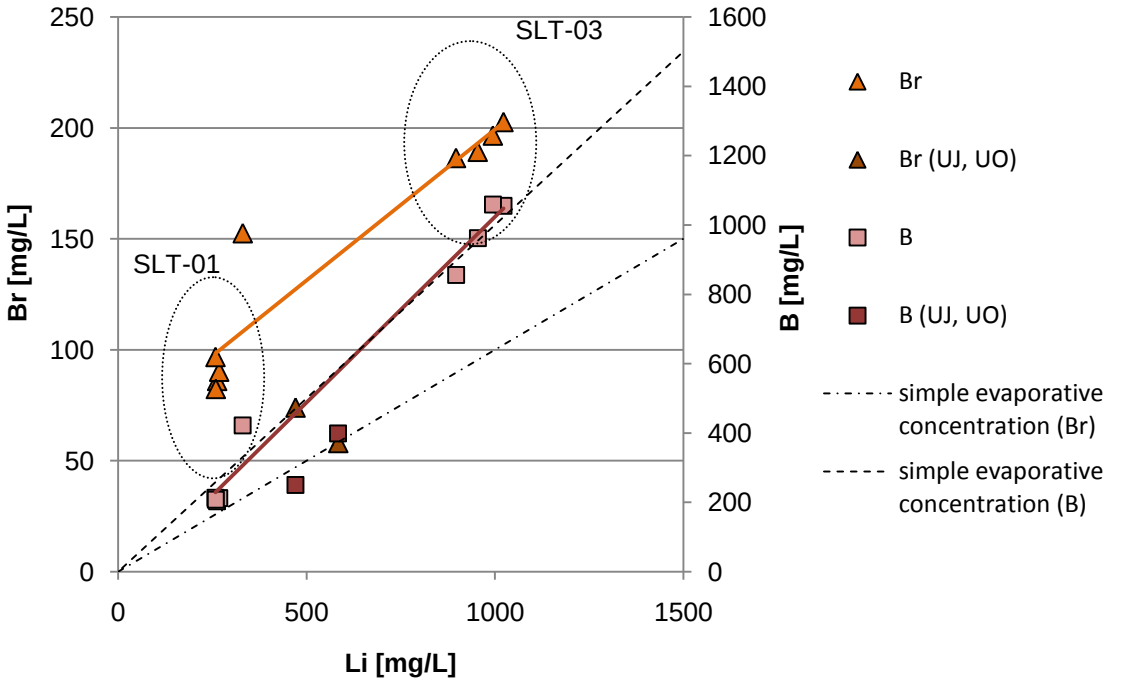

Fig. 33: Concentrations of Br and B plotted against the content of lithium in the brine samples (values UJ and UO serve as reference values and are obtained from two brine samples of Risacher & Fritz 1991b); dashed lines represent the simple evaporative concentration for Br and B in relation to lithium; dotted circles indicate the sampling location

Bromine contents in solution vary between average 90 mg/L for SLT-01 and 194 mg/L for SLT-03, which makes up 0.03 and 0.05% respectively of the total content of solutes. In comparison to normal seawater, where bromine occurs in a fraction of 0.0065% (Warren 2006), this is an enrichment with a factor of approximately 6. The distribution coefficient D_{Br} describes the partition of bromine between halite and the surrounding solution (Braitsch & Herrmann 1963):

$$D_{Br} = \frac{\text{wt\% Br (halite)}}{\text{wt\% Br (solution)}}$$

For the calculation the averaged values for Br contents in solution of brine samples from SLT-01 were taken. The contents in halite were provided by the results of the SLT-01A core analysis. The bromine distribution coefficient for the core and brine samples from SLT-01 varies between 0.0034 and 0.097.

The bromine content in the samples increases with increasing concentration of lithium (Fig. 33). That means that bromine is not precipitated in a mineral phase in the salinity range of the investigated brine samples.

4.3.5 Minor and trace elements

Altogether 34 elements were determined by ICP-MS measurements. Because of their high salinity the samples had to be diluted 1:100, by what the detection limit of every element calculated from the blank value is downgraded by a factor of 100. According to their concentration in the brine samples elements obtained by ICP-MS were classified arbitrarily as shown in Table 10. The obtained concentrations of elements as well as detection limits are contained in Table A8 (Appendix).

Table 10: Classification of determined species according to their concentration

Classification	Elements by ICP-MS
major elements (> 5 mg/L)	B, Br, Li, Rb, Si, Sr
minor elements (0.1 – 5 mg/L)	Al, As, Cs, Fe, I, Mn, Mo, P, Se
trace elements (< 0.1 mg/L)	Ag, Ba, Be, Bi, Cd, Co, Cr, Cu, Ga, In, Ni, Pb, Sb, Sn, Te, Tl, U, V, Zn

Fig. 34 illustrates the comparison of element concentrations between the samples from SLT-01, samples from SLT-03 and the SLT-S sample. The y-axis shows the enrichment (y > 1) and depletion (y < 1) of elements at SLT-03 and the SLT-S sample in reference to brines from SLT-01. Values were calculated as the quotient of the concentration in SLT-03 (SLT-S, respectively) and the-concentration in SLT-01. Thereby the concentrations in different samples from the drilling points were averaged, because significant differences with depth could not be observed. Be and Sn are not included in the graphic, as their contents were below the detection limit of 0.65 and 0.8 µg/L respectively in all nine samples. All elements, except V, Cr, Co, Ni, Ag, Cd, Tl, Pb and U, show significant differences between the three sampling groups according to the Kruskal-Wallis-Test (chapter 4.3.7). Most elements are enriched in SLT-03, only Sr, Ba and U occur in higher amounts in SLT-01. Compared to the brines from the drilling locations, the SLT-S sample is strongly (more than 10fold) enriched in Fe, Co, I, Cs, and Zn.

Reference values for uncharged components in brines of the Salar de Uyuni as well as brines of other salt pans are rare in the literature. Strontium contents reported by Rettig et al. (1978) are with 20 mg/L for a point near SLT-01 similar to the measured average value of 17.8 mg/L for SLT-01.

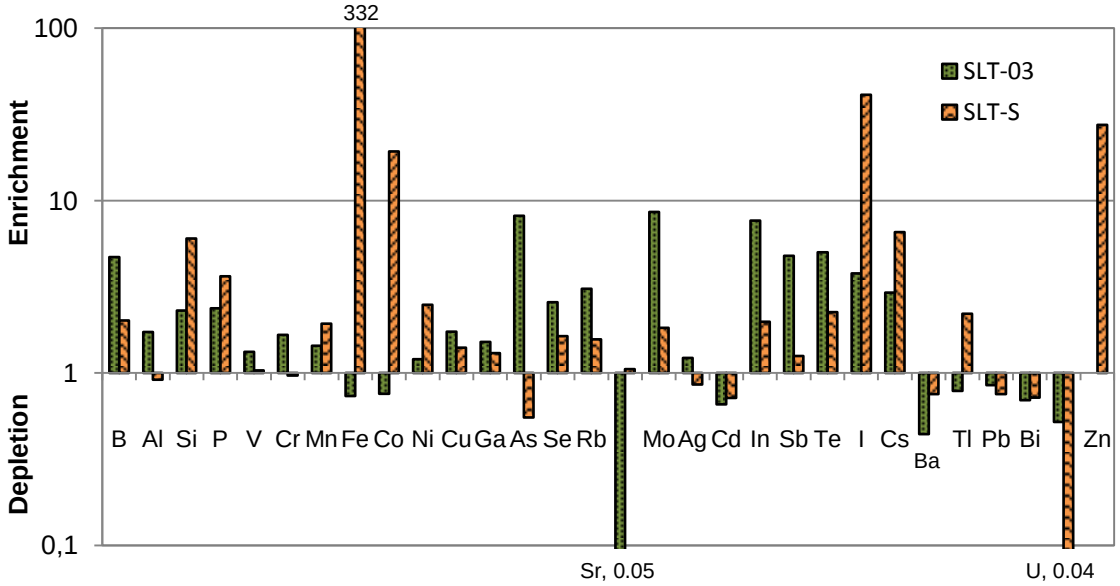

Fig. 34: Enrichment and depletion of elements at SLT-03 and SLT-S compared to SLT-01 (concentrations of samples from one drilling location are averaged; values > 1 mean an y-fold enrichment, values < 1 an y-fold depletion)

It is conspicuous that strontium shows an opposite trend compared to other elements, as its concentration in SLT-01 is about 20 times higher than in SLT-03. This could be due to the precipitation of a Sr-containing mineral as celestite ($SrSO_4$) caused by the higher overall mineralisation and therefore higher density in SLT-03, by which Sr is removed from the solution.

4.3.6 Evaluation of errors and check for plausibility

The percent charge balance errors of the brine analyses are in the range of -1.18 to 1.95% (Fig. 35). Thus, the analytical accuracy is sufficient (chapter 3.4.3). All four analyses of the brines from drilling location SLT-03 show a positive error, which is caused by an excess of positive charged cations. The analysis of the brine from drilling hole SLT-01E exhibits a clearly higher percent error than the other samples.

This might be explained by a lower content of chloride compared to brines from the same drilling location, which could be due to an inaccuracy during dilution. However, this conclusion cannot be verified as the other main ions were measured with lower dilution factors compared to Cl^-.

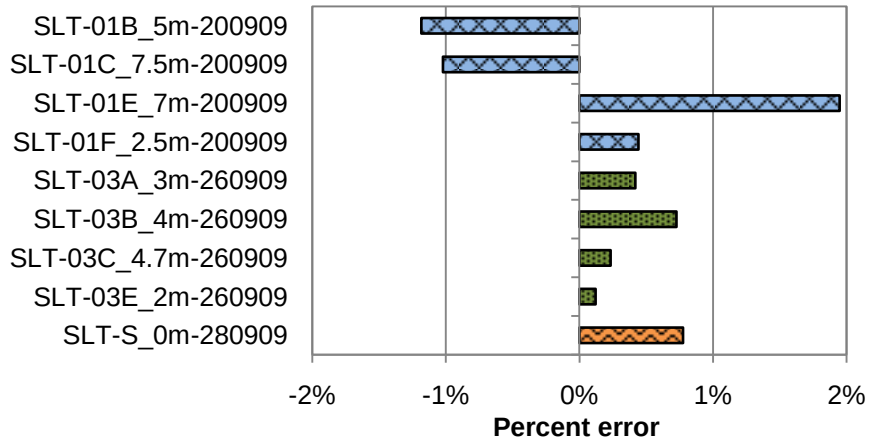

Fig. 35: Percent charge errors of the brine analyses computed with PhreeqC (Pitzer database)

For the verification of the accuracy of chemical analyses of the brine samples selected parameters were measured by the BGR. The results are comprised in Table A9 (Appendix). Especially the concentrations of Ca, HCO_3, Ba and B differ from the results of the own measurements. A reason could be different analysing methods (main anions and cations obtained by ICP-OES, HCO_3 obtained by titration). The contents of Ca measured by the BGR show a much lower variation between samples from different depths of one drilling location than the contents obtained by ion chromatography. Thus, the Ca values from the BGR were used for evaluation.

Another method for the check of plausibility is the “principle of exclusion”. In Table 11 a number of mutually exclusive elements are shown. When comparing to the obtained data it is obvious that the species Fe^{2+}, Mn^{2+}, NO_2^-, NH_4^+ and S_2^- exist in theoretically impossible concentrations in the samples (chapter 4.3.2). Since it is unlikely that all photometrical measurements (Table 9) and the ICP-MS result (Appendix A8) for Mn are defective, it is more plausible that the obtained concentrations of oxygen are faulty (Table 8). This is supported by the fact that the measured oxygen content in the SLT-S sample, where the brine is in contact with the atmosphere, is much lower than in the borehole samples,

where the brine origins from a depth, where conditions with low amounts of oxygen are expected. When applying the exclusion of species according to Table 11 it must be considered that these rules are valid for solutions with a mineralisation in the range of groundwater, which constrains their validity for the Uyuni brines.

Table 11: Exclusion of species based on the measured concentration of opposite species (source: DVWK rules 128, 1992)

Parameter	Exclusion of
O_2 > 5 mg/L	Fe^{2+} > 0.05 mg/L
	Mn^{2+} > 0.05 mg/L
	NO_2^- > 0.05 mg/L
	NH_4^+ > 0.1 mg/L
	H_2S > 0.01mg/L
Fe^{2+} > 1.0 mg/L	H_2S > 0.1 mg/L
Mn^{2+} > 0.2 mg/L	H_2S > 0.1 mg/L

The results for the electric conductivity obtained during on-site analyses must be regarded critically, as they are in the range of the instrument's upper detection limit of 200 mS/cm. The comparison with reference values from a standard solution of NaCl shows, that the measured conductivities of the Uyuni brine samples are generally too low as they do not fit the estimated curve (Fig. 36).

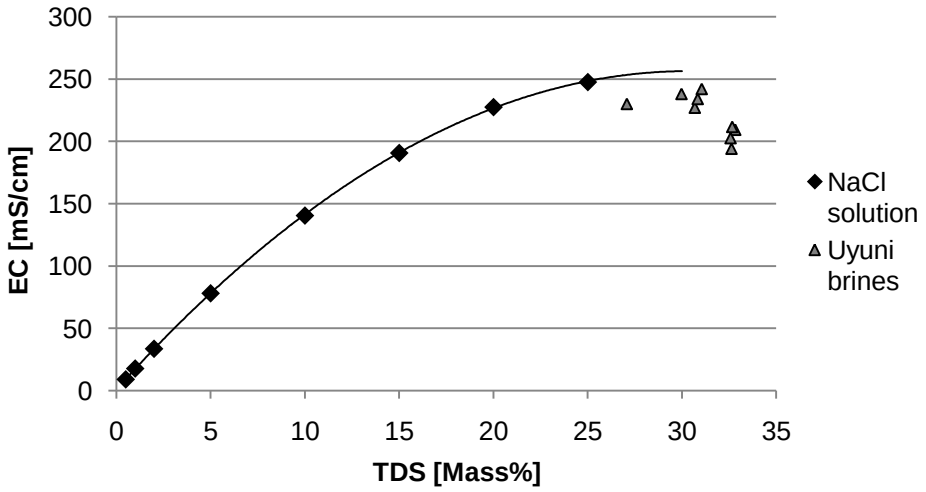

Fig. 36: Electric conductivity (at 25°C) of a standard solution of NaCl in dependency of salt concentration and comparison to measured values of the Uyuni brine samples (data from: Lide 2008)

A reason, beside the instrument's uncertainty, could be the composition of the Uyuni brines. In contrast to the standard solution, which is composed of only sodium and chloride, the sampled brines are a mixture of different ions in high concentrations, which interact and interfere each other.

Against the background of a possible future extraction of lithium from the brine it is essential that the determined lithium concentrations in the samples are as exact as possible. For that purpose a calibration by standard addition was performed (see chapter 3.4.2). In a diagram the obtained peak areas for the addition of different amounts of lithium are connected by linear regression (Fig. C1, Appendix). Table 12 shows the results for both samples SLT-01B and SLT-03A.

Table 12: Comparison of lithium contents for different calibration methods

	Li concentration [mg/L]	
	calibration line	standard addition
SLT-01B	263	269
SLT-03A	1023	1007

The variation of the lithium contents between the different calibration methods is about 2% for both samples and implies that matrix effects at a sample dilution of 1:1000 can be neglected for the determination of lithium.

4.3.7 Statistical evaluation

Cluster analysis was performed in order to test, if the brines can be significantly differentiated by means of hydrochemical parameters according to their sampling location. In the hierarchical clustering 45 parameters measured for nine brine samples were included (results of chemical analyses are comprised in Appendix A). The results of the cluster analysis are presented in a dendrogram (Fig. 37).

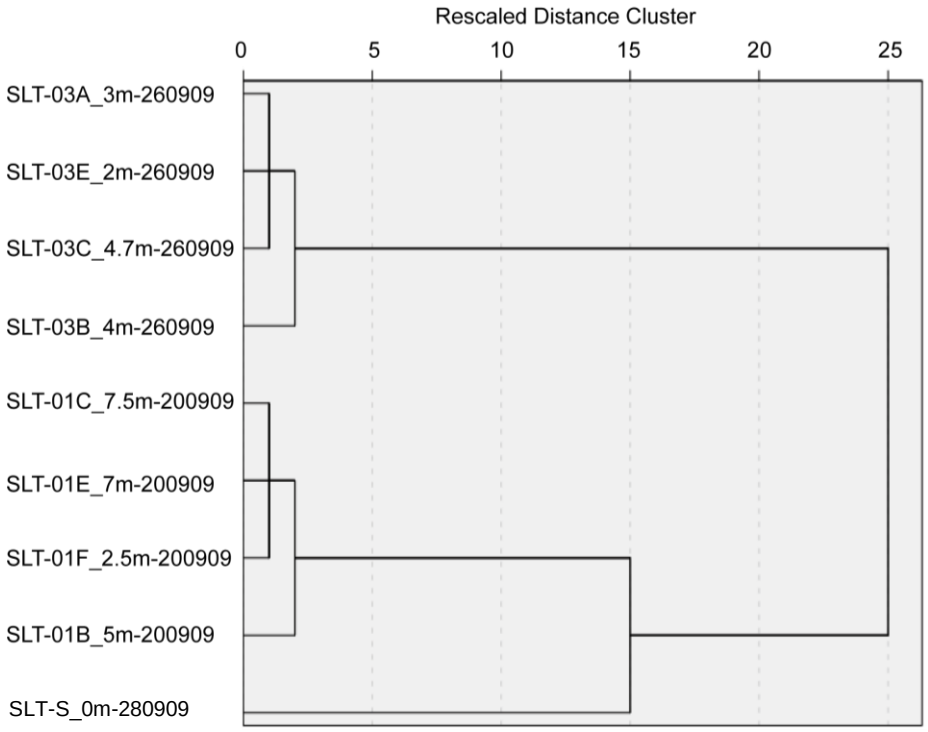

Fig. 37: Dendrogram resulting from clustering with 45 parameters obtained from chemical analyses of all nine brine samples

With the Kruskal-Wallis-Test it was tested for every parameter, if the cluster's medians differ significantly. The test was performed for the possibility of the formation of three clusters. When the data are clustered into three groups, 31 out of 45 parameters show a significant difference. Hence, for further evaluation the clustering with three groups is used, whereby each of the clusters comprises all samples from one (drilling) location on the Salar.

Table 13: Results of the Kruskal-Wallis-Test for clustering the data into three clusters

	medians are not significantly equal	**medians are equal**
3 clusters:	pH, pe	T
SLT-01 (n=4),	Ca, HCO_3^-, K, Li^+, Mg, Na, NO_3^-, SO_4^{2-}	Cl^-, NH_4^+, S^{2-}
SLT-03 (n=4),	B, Al, Si, P, Mn, Fe, Cu, Zn, Ga, As,	V, Cr, Co, Ni, Ag, Cd, Tl,
SLT-S (n=1)	Se, Br, Rb, Sr, Mo, In, Sb, Te, I, Cs, Ba, Bi	Pb, U

n = number of samples

4.3.8 Modelling with PhreeqC

For the calculation of geochemical reactions, the evaluation of saturation indices and ionic strengths the program PhreeqC Version 2.17.1 (Parkhust & Appelo 1999) was used. Therefore, data prepared for statistical evaluation were imported into the program. The calculations performed in PhreeqC are based either on the ion association theory or the specific Ion Interaction Theory (SIT). In the ion association approach the activity coefficient depends only on the ionic strength of a solution, and is calculated according to the “WATEQ” DEBYE-HÜCKEL limiting-law equation (Merkel & Planer-Friedrich 2002a). As the activity coefficient increases only until an ionic strength of about 1 mol/kg, this value is the upper limit for the validity of the ion association theory. At higher ionic strengths the theory of ionic interaction is more convenient. Here the PITZER equations describe best the interionic forces in a solution. Therefore, the in PhreeqC included Pitzer database was used for modelling. As this database comprehends a much lower number of species less information will be provided. Thus, a calculation showed that the species contained in the Pitzer database make up 99.99% of the dissolved substances in the samples, which is sufficient for preventing a loss of information.

4.3.8.1 Ionic strength

The ionic strength in mol/L of a solution is a measure for the ionic interactions and is defined by the amount and charge of the contained ions (Hölting & Coldewey 2009).

$$I = 0.5 \cdot \sum m_i \cdot z_i^2$$

Thereby, m_i means the molar concentration of an ion, z_i is the valency of the same ion. The ionic strength of the brine samples shows values between 6.85 and 10.21 mol/kg. Fig. 38 clarifies that the values do not show a depth dependent trend and are very similar within a drilling location, but the ionic strengths between the sampling locations differ significantly. Thereby, the ionic strength increases from the eastern border of the Salar to the centre and from north to south in direction of the Rio Grande delta. The upper limit of 1 mol/kg for the ion association theory is strongly exceeded for all brine samples.

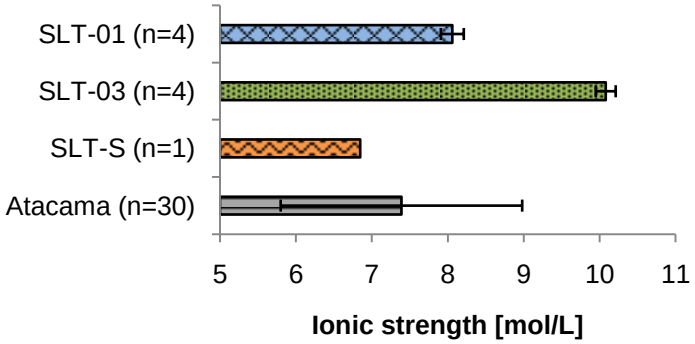

Fig. 38: Ionic strengths of the sampled brines calculated by PhreeqC using the database based on the Pitzer equation (values for Atacama obtained from data of Boschetti et al. 2007)

4.3.8.2 Saturation index

The saturation index SI describes the tendency of a solution to either dissolve or precipitate a particular mineral phase. It is calculated from the comparison of the chemical activity of a mineral's dissolved ions (I_{AP}) with the solubility product of the mineral phase K_{SP}:

$$SI = \log \frac{I_{AP}}{K_{SP}}$$

SI values between +0.05 and -0.05 indicate that the solution is saturated with regard to the ions of a mineral phase, it is in equilibrium to the corresponding solid phase. SI values higher than 0.05 show the oversaturation of a mineral phase in the solution, values below -0.05 show undersaturation of a solution with regard to a mineral phase. However, SI values exceeding 0 do not automatically result in the precipitation of a mineral phase, because precipitation kinetics can be very slow.

The calculation of SI in PhreeqC using the Pitzer database revealed 43 different mineral phases, which can be classified into chlorides, carbonates, sulphates and borates according to their main anion (Table 14). The exact SI values for all minerals are combined in Table A12 (Appendix).

Table 14: Comparison of the number of under- and oversaturated mineral phases for the three sample groups

		SLT-01	SLT-03	SLT-S
Chlorides	SI > 0.05	1	1	0
	0.05 > SI > -0.05	0	1	1
	SI < -0.05	4	3	4
Sulphates	SI > 0.05	4	6	3
	0.05 > SI > -0.05	0	0	0
	SI < -0.05	17	15	18
Carbonates	SI > 0.05	4	3	4
	0.05 > SI > -0.05	0	1	0
	SI < -0.05	7	7	7
Borates	SI > 0.05	0	0	0
	0.05 > SI > -0.05	0	0	0
	SI < -0.05	6	6	6

oversaturation	equlibrium	undersaturation

In general, there are only minor differences between the sampling groups in the number of over- and undersaturated solutions with respect to certain mineral phases (Fig. 39). All samples are prevalently undersaturated with regard to chlorides and borates. Brines from SLT-01 and SLT-03 have an SI for halite of 0.33 and 0.44 respectively, which means a two- to threefold oversaturation. In contrast, the sample SLT-S is in equilibrium with respect to halite.

All brine samples are clearly undersaturated with respect to magnesium sulphates and chlorides. Thereby the SI is lower in SLT-03 compared to SLT-01. The same is observed for potassium sulphates and chlorides. This means that these minerals do not precipitate from the solution at the present concentration of solutes in the brines of both drilling locations. Celestite ($SrSO_4$), a strontium bearing mineral, is oversaturated in samples from SLT-01, but undersaturated in samples from SLT-03. This is in contradiction to the formerly made assumption (see chapter 4.3.5), that in SLT-03 strontium could have precipitated as celestite. Here, the precipitation of another strontium mineral as Strontianite ($SrCO_3$) is supposable, which could explain that concentrations of strontium in solution are significantly lower in SLT-03 compared to SLT-01 and SLT-S.

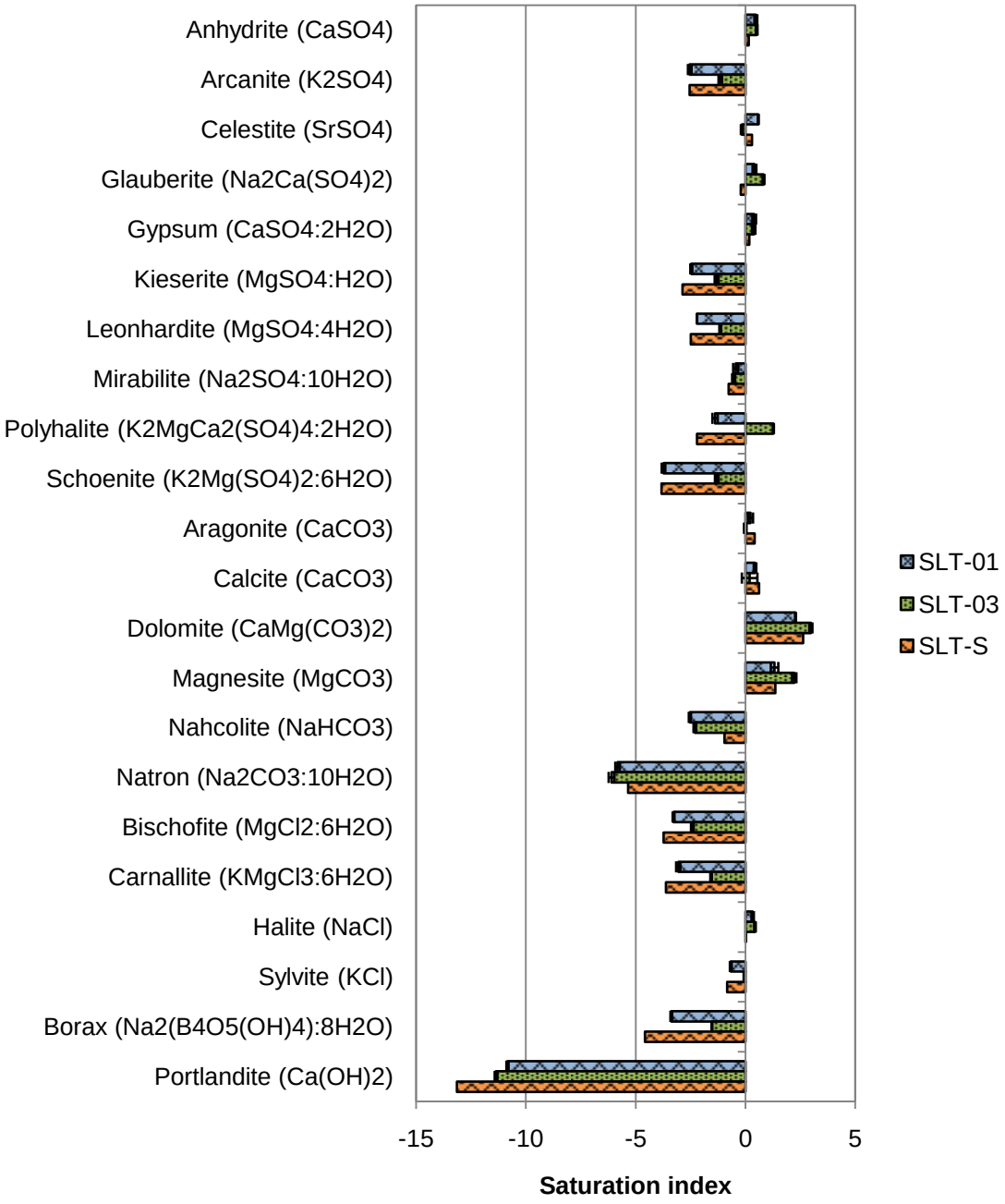

Fig. 39: Averaged saturation indices for selected sulphate, carbonate and chloride mineral phases; samples are grouped together according to their location on the Salar, standard deviations for samples from SLT-01 and SLT-03 are also shown

The results of the modelling of mineral phases in PhreeqC can be compared to the results of the mineralogical analyses of the core from SLT-01A (chapter 4.1.3). The brines are mainly undersaturated with regard to the obtained mineral phases carnallite, kieserite, and sylvite (Fig. 39). The only exception here is polyhalite, for which the SI value of the brine in SLT-03 is about 1.3, meaning that the solution is 20fold oversaturated with respect to that mineral phase.

An explanation could be the higher concentration of solutes in the brine, by which the ion activity product exceeds the solubility product of polyhalite. The strongly negative saturation indices of carnallite, kieserite, polyhalite and sylvite do not reflect the mineralogic composition evaluated in chapter 4.1.3. A reason might be uncertainty of the stoichiometric calculation of the mineral phases from the geochemical element concentrations.

All borates that were considered in the modelling, are undersaturated in all samples. That explains, why borate minerals were not identified in the mineralogy of the core from SLT-01. Borates occur in dissolved state in the brines, as the solutions are not concentrated enough that the required conditions for the precipitation of borax, the main borate mineral, are reached.

An analysis of the mineralogical composition of a drilling core from SLT-03 could verify the assumptions made from the data that were obtained from hydrochemical analyses of the brines and the geochemical analyses of the sediment core from SLT-01.

4.3.9 Physical parameters

4.3.9.1 Viscosity

The dynamic viscosity of the samples was determined by rotational viscometry (see chapter 3.4.2). The initial temperatures of the brines were 3.5°C for the sample from SLT-01 and 8°C for the sample from SLT-03. As the arbor of the instrument heats up by the rotation the final temperature of both brines was 17.5°C. Distilled water was measured as a control of the viscometer's accuracy.

Table 15: Dynamic viscosity of the samples (each sample was analyzed twice, values coincided exactly), of deionized water (dH_2O) and of a reference value with a defined composition (from Lide 2008)

	SLT-01B_5m-200909	SLT-03A_3m-260909	dH_2O	brine (26% NaCl)
T [°C]	3.5 – 17.5	8 – 17.5	23	20
dyn. viscosity [mPa·s]	2.6	3.2	1.0	1.99

The viscosity of the brine from SLT-03 is approximately 25% higher than that of the brine from SLT-01. (Table 15). In comparison to normal water the viscosities of the brines are about three times as high. As the chemical composition of brines from one drilling location is very similar, it can be assumed that the determined viscosities of the two single samples are representative for the viscosity of all brines in the respective location. Although the brines heated up during the measurement, the values for the viscosity stayed constant right from the beginning. That leads to the assumption that the temperature dependency at least in the measured temperature range is low for the brines. In contrast, Fig. 40 shows that especially between 5 and 20°C the dynamic viscosity of a standard solution with a salt concentration of 324 g/L is lowered by a factor of 50% (Holldorf & Baumbach 1987). The obtained viscosity for SLT-03 fits exactly in the curve of the standard solution, caused by the similar mineralisation of both brines. In contrast, the sample from SLT-01 has a lower viscosity because of the lower concentration of salts. It follows that the viscosity of a solution is a function of it's salinity.

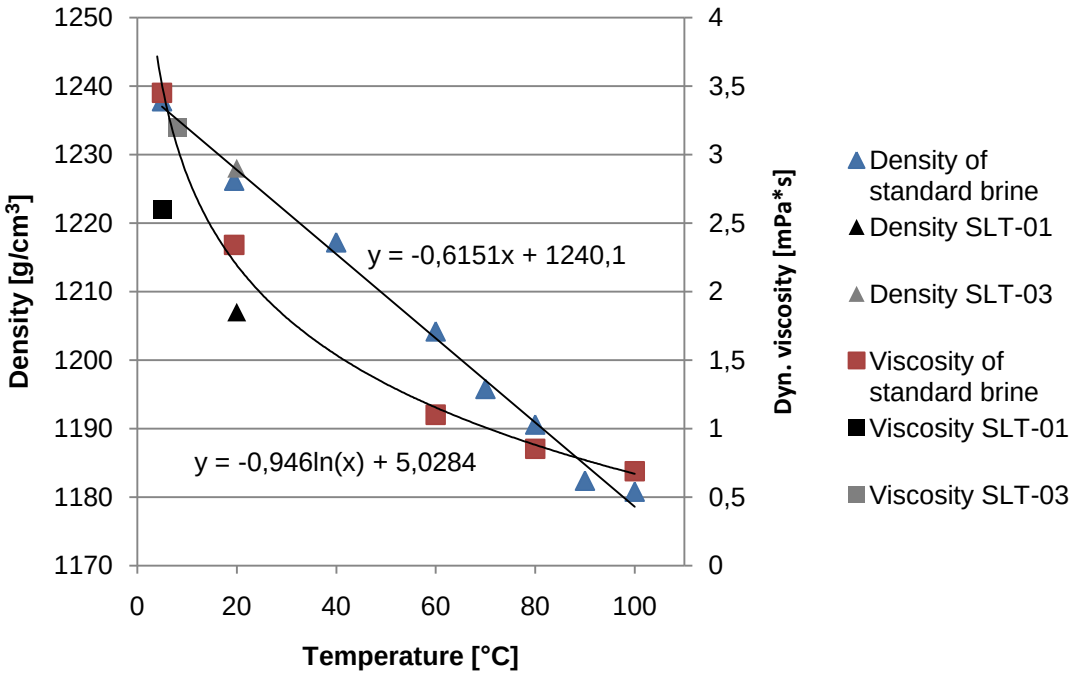

Fig. 40: Temperature – density and temperature – viscosity relation for a standard solution (Holldorf & Baumbach 1987) and the brine samples

The viscosity and density of a solution are important parameters for the determination of the permeability of a porous medium for that fluid. Thereby, the permeability coefficient increases with increasing density and decreasing viscosity (Hölting & Coldewey 2009). The viscosity is indirectly proportional to the flow rate of a fluid, meaning that a threefold increase of the dynamic viscosity of a fluid results in a threefold lower flow rate of this fluid in the porous medium.

4.3.9.2 Density

Densities of the brine samples from SLT-1 and SLT-03 were determined pycnometrically by the BGR in Hannover. The results are on average 1,207 kg/m³ for SLT-01 and 1,228 kg/m³ for SLT-03. Standard deviations of 0.03 and 0.11%, respectively, show that samples from different depths but the same drilling location exhibit similar densities. In total, samples from SLT-03 have a slightly higher density than samples from SLT-01, which is explained by the higher mineralisation (compare chapter 4.3.3). Risacher & Fritz (1991b) reported slightly higher TDS contents for samples with comparable densities (Fig. 41). There is a directly proportional relation between the density of a solution and its TDS concentration as shown in Fig. 41.

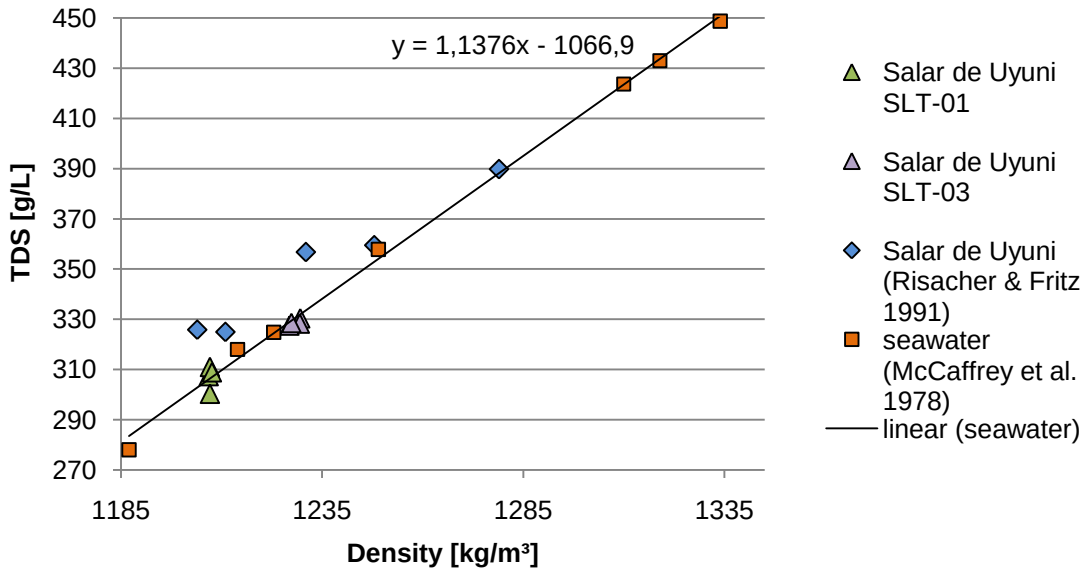

Fig. 41: Relation between TDS content and density of brines from the Salar de Uyuni and concentrated seawater

This diagram shows, beside the samples from the drilling locations and values obtained from Risacher & Fritz (1991b), the evaporation path of seawater (McCaffrey et al. 1987). When the TDS of a solution is increased by evaporation, the density rises linear. The point of maximum density and TDS in the evaporation path of seawater is reached at approximately 1,335 kg/m³ and just less than 450 g/L. Beyond this point sulphate precipitates as $MgSO_4$ and the decrease in TDS goes along with a decrease in density.

The density of the SLT-S sample was not determined in the laboratory. Nevertheless, it can be estimated from the linear equation obtained from plotting seawater samples in different evaporation stages. Fig. 41 shows that the brine samples from SLT-01 and SLT-03 fit well into this relation. Thus, the calculated density of the SLT-S sample (with a TDS content of 270.8 g/L) is 1,179.5 kg/m³.

The density of the samples was determined in the laboratory at a temperature of 20°C. When using it for the evaluation of pumping tests, the temperatures measured in the field must be used. Since the density is strongly dependent on temperature, the results must be corrected for the brine temperatures measured in the field. The temperature – density relation for a saturated solution is displayed in Fig. 40. Again, the averaged density of the samples from SLT-03 fits the curve very good. Brine densities were corrected by using the linear equation displayed in the diagram.

5 Discussion and conclusions

The drilling locations SLT-01 and SLT-03, situated in the north eastern and in the central part of the Salar de Uyuni, exhibit significant differences regarding stratigraphy of the sediment layers and chemistry of the interstitial brine. The obtained data are in accordance with former investigations by Risacher & Fritz (1991b) who observed an increasing trend with respect to the concentrations of elements from north to south towards the delta of the Rio Grande. This trend applies for most cations, all anions and the majority of other elements. Ca, Na and Sr show an opposite trend, as their concentrations are significantly higher in SLT-01. This is probably due to the precipitation of minerals as halite, gypsum, and celestite, by which Ca, Na, and Sr are removed from the solution and are depleted in relation to other elements. This process is caused by the higher overall mineralisation of the brines towards the Rio Grande inflow. A number of metals as Fe, Cd, Ba, and U are as well enriched in the northern point and in the surface sample of SLT-S. A reason could be the rise of deep groundwaters through fracture zones in the halite into layers near the surface. These groundwaters formerly were in contact with the underlying volcanic bedrock and are therefore enriched especially in metals. This assumption is supported by the permanent rise and emanation of mainly CO_2 in SLT-S, which indicates a present volcanic activity in that area. Also in SLT-01 small holes (about 10 cm in diameter) could be observed in the halite crust during the field work (see chapter 4.1.1). Although the emanation of gas could not be observed, the holes must have formed by the rise of gas or lower concentrated waters from deeper zones. These holes were not observed in SLT-03.

Differences regarding hydrochemical parameters could not be observed in brines from different wells in varying depths from the same drilling location. This is partly in contradiction to former investigations by Risacher & Fritz (1991b) where the concentrations of anions and cations prevalently rise with depth. Though, these results are comparable to only a limited extent to the results of the present study, as the samples were extracted from pores in the halite cores, in contrast to pumping the brine from installed wells as performed in this study.

Computer tomographic analyses showed the high variation between the uppermost cemented crust and the underlying halite layer in terms of size and distribution of pores and the structure of halite crystals and aggregates. This heterogeneity is explained by the annual cycle of dissolution and precipitation, caused by the climatic cycle of wet and dry seasons. At the beginning of the rainy season, the precipitations infiltrate through the upper crust until they reach the water level and mix with the highly saline brine. By this process halite aggregates and crystals are dissolved, which results in the formation of solution cavities, (karstification of rock salt). With the beginning of the dry season, when the surface is covered by the inflow waters from rain and tributaries, the strong solar insolation leads to the evaporation of the surface water and the concentration of the residual brine. When this brine is oversaturated with respect to NaCl, small halite lenses are formed on the surface of the water, which sink to the ground and are rapidly covered by new precipitates. As soon as the surface dries, it is cemented to a hard pavement by the evaporation of capillary rising waters from the brine table. By this process the underlying brine becomes oversaturated in halite. This favours the formation of cubic halite crystals with sizes up to 3-4 cm, which grow into the earlier formed cavities. This annual cycle is responsible for the different appearance of halite cores from the uppermost centimetres and deeper situated halite layers.

5.1 Review of salt deposits

The extraction of sediment cores revealed a heterogeneous distribution of halite and mud layers in the two drilling locations. Thereby the thickness of the uppermost halite layer increases to the northeast of the Salar to more than ten meters, before it is interrupted by a half meter thick mud layer. In contrast, the upper halite crust in SLT-03 exceeds to no more than 5 meters and the underlying mud layer has a thickness of more than 6 m. The uppermost halite crust of the Salar de Uyuni is assumed to have formed from the complete evaporation of Lake Tauca. Since then the salt layers have been covered by the annual input of solutes, that comes with the rain and the inflow of rivers and streams. Thereby, the main contribution can be assigned to the Rio Grande in the southeast of the Salar.

Assuming a certain composition of the rain- and Rio Grande water (Table 16), a rough estimation of the growth of the halite crust should be possible.

Table 16: Estimated concentrations c of solutes in precipitation and surface inflow from the Rio Grande, and contributions M of solutes per year to the Salar (see text for explanations)

Element	$c_{rainwater}$ [mg/L]	$M_{rainwater}$ / a [10^6 kg]	$c_{Rio\ Grande}$ [mg/L]	$M_{Rio\ Grande}$ / a [10^6 kg]	Totals / a [10^6 kg]
Cl	0.71	1.05	1580	94.8	95.9
SO_4	2.21	3.27	313	18.8	22.1
Na	0.51	0.75	908	54.5	55.3
K	0.29	0.43	41.9	2.51	2.94
Ca	1.08	1.59	202	12.1	13.7
Mg	0.17	0.25	56	3.36	3.61
Li	?	?	4	0.24	~ 0.24
Sum	~ 5	~ 7.3	3105	186	194

Concentrations of ions in rain water are taken from Risacher & Fritz (1991a). When relating the assumed annual precipitation of 141 mm to the surface area of the Salar de Uyuni of 10,500 km², it yields an amount of $1.4805*10^9$ m³/a. The average concentrations in the main tributary, the Rio Grande, are taken from Lebrun et al. (2002). Assuming an annual amount of inflow from the river of $60 \cdot 10^6$ m³ (Risacher & Fritz 1991b), the mass of total input of solutes per year can be calculated (Table 16). When the inflows from streams and precipitation evaporate after the wet season, the remaining brine is concentrated until finally no water is left, and all contained solutes are precipitated in mineral phases. The main ions are chloride and sodium, which results in halite being the major precipitating mineral. Halite has a density of 2.1 g/cm³ (Rösler 1984), other minerals of the evaporation path have densities in a similar range. Taking this density and the area of 10,500 km² into account, an amount of $2.21 \cdot 10^7$ t of salt would be needed for the formation of a 1 mm thick layer on the whole surface of the Salar. Assuming a porosity of roughly 34%, obtained by the CT analyses of the upper crust (chapter 4.1.4), an amount of $1.46 \cdot 10^{10}$ kg would be needed for the 1 mm thick layer.

When comparing to the total input of solutes of $193.74 \cdot 10^6$ kg/a, the salt crust would increase 0.0146 mm/a, which conforms to 1.5 mm in 100 years or 150 mm for the last 10,000 years (Holocene). This appears to be very low, considering the massive upper halite crust of several meters. When searching for a source of error, it is conspicuous that the annual inflow from the main tributary seems to be very low. It must be assumed that the discharge rate in the Rio Grande was estimated by Risacher & Fritz (1991b) in the dry season, where the river carries only small amounts of water. During the rainy season, the amount of inflow must be considered to be several orders of magnitude higher because of the large catchment area south of the Salar. Furthermore, ephemeral streams that reach the Salar from other directions than the south east, can carry large amounts of waters and solutes during and after the rainy season and therefore probably significantly contribute to the annual input of solutes. Hence, the value of total surface inflow (except for precipitation) into the Salar should be estimated much higher. About 240 t of lithium reach the Salar every year, when an average concentration of 4 mg/L Li in the Rio Grande waters is assumed. This number is, as explained above, supposed to be strongly underestimated.

5.2 Factors concerning brine evaporation

When considering the recovery of lithium from the brine, the first step is the evaporation of the solution with the help of evaporation cones, whereby different salts precipitate step by step according to their solubility product. Therefore, a rough understanding of the processes that occur during the evaporation of the brine is required. Thereby the type of the initial solution plays an important role. The analysed brines from SLT-01, SLT-03 and SLT-S are characterized by an Na-Cl type with high contents of magnesium and sulphate. Brines of this kind generally form under the condition that the mole ratio of SO_4/Ca is >> 1 (Herczeg & Lyons 1991), which is given for the Uyuni brines. By this requirement the content of sulphate increases with further concentration in the brine, while the content of calcium decreases by gypsum precipitation.

The concentration process of the brine can be simulated using PhreeqC and the Pitzer.dat database. Thereby, an increasing amount of water is removed from the solution in a number of steps, by which the content of solutes increases constantly. Every step is followed by a mixing step, where the resulting solution is mixed with itself. For the simulation the brine from drilling location SLT-01 is used. At first, the development of the saturation indices for the most important mineral phases was modeled in order to show, which mineral phases dominate in the solution and to estimate the point, at which the precipitation of a certain mineral begins. The results are shown in Fig. 42. The point where the solution is in equilibrium with a mineral (SI = 0) is indicated by the horizontal line.

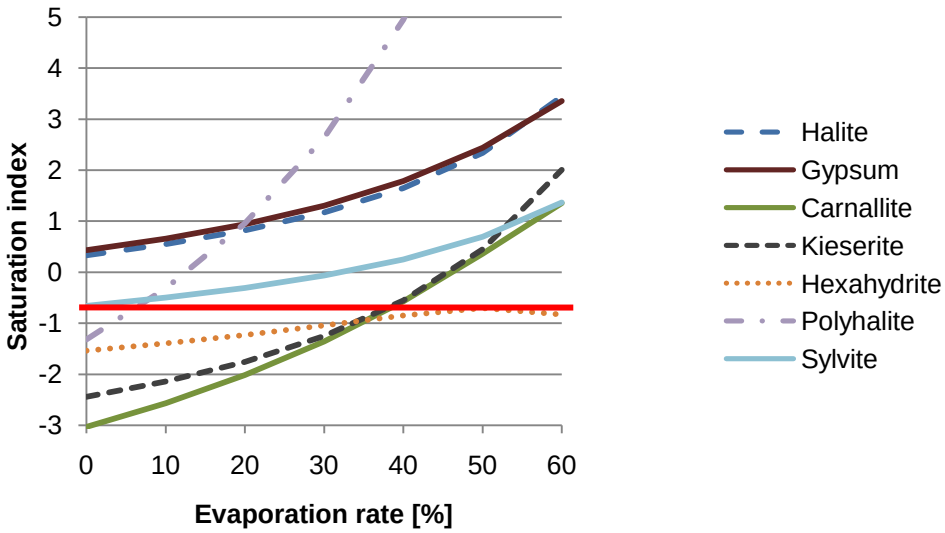

Fig. 42: Development of the saturation indices for important mineral phases with increasing evaporation rate of the brine from SLT-01 (modeled by PhreeqC); the highlighted horizontal line indicates the equilibrium of the solution regarding a certain mineral phase (SI = 0)

Halite and gypsum are already oversaturated in the original solution, which explains the dominance of these minerals in the salt layers. This confirms the results of geochemical analyses of the sediment cores from SLT-01 (see chapter 4.1.3). A positive saturation index is not necessarily an indicator for the precipitation of a mineral. As the precipitation of halite and gypsum is dominant in the whole range of the evaporation rate, chloride and sulphate are consequently removed from solution and are therefore only to a minor extent available for the formation of other chloride and sulphate minerals. Thus, the point of brine concentration, when a certain mineral starts to precipitate, is moved towards a point of higher concentration.

In a second step, the distribution of solutes was modeled at different evaporation rates under the assumption, that the considered mineral phases precipitate from the solution as soon as a positive SI indicates oversaturation (Fig. 43).

Sodium shows a constant slight decrease with further concentration of the brine, as it is removed by the precipitation in halite. Until an evaporation rate of 20% calcium shows a strong decrease by the removal in gypsum, then the evaporation rate is in equilibrium with the amount of precipitation and the calcium content stays constant. Lithium and bromine show a steady increase in concentration with a constant slope. The reason is the non-existence of lithium- and bromine-bearing mineral phases, by which these elements stay in solution until a high grade of evaporation.

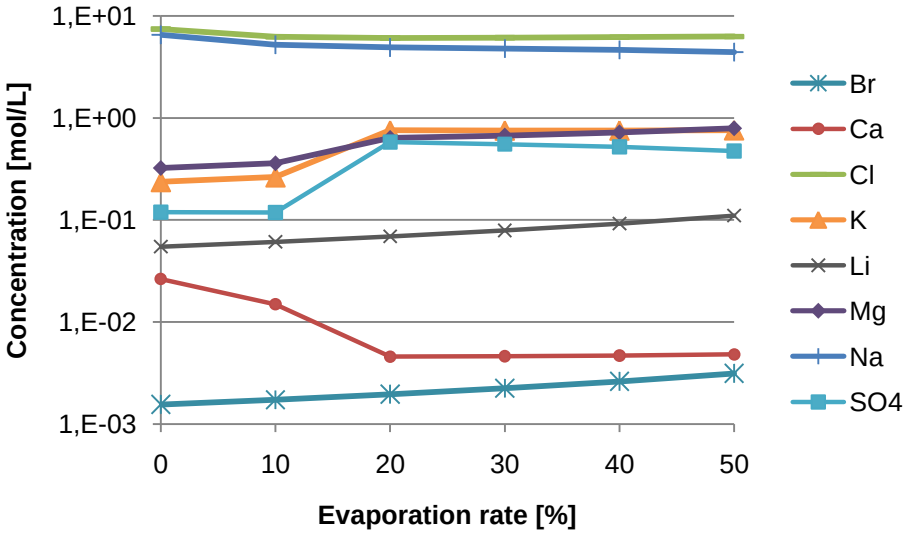

Fig. 43: Development of the concentration of solved components with increasing evaporation rate of the brine under the assumption that oversaturated mineral phases are removed from the solution by precipitation (modeled by PhreeqC)

The evaporation path has been extensively studied for seawater, which is in a rough approximation a 10 times diluted Uyuni brine. With a salinity up to 300-330 g/L the brine is mainly composed of Na-Cl (Warren 2006). When this value is exceeded by further concentration, the brine progressively transcends into the Mg-Cl type, because Na is removed from the brine due to the precipitation of halite. With further concentration Mg is replaced by K as the main cation caused by the precipitation of magnesium sulphates as kieserite.

Until this point of concentration the density in the brine has risen continuously, up to a maximum value of about 1.35 g/cm³. From that point the density of the brine decreases again with further evaporation, as the precipitation of minerals prevails. Cl is the dominant ion in the solution during the whole process of concentration, its concentration in the brine is more or less constant from the point of halite precipitation.

The position of the evaporation cones on the Salar de Uyuni, which are being developed by the cooperation between the TUBA Freiberg and the UATF in Potosí, is decisive for the efficiency of the brine evaporation. High solar insolation, strong winds and a lack of precipitation are ideal conditions required for an effective and rapid concentration process of the brine by evaporation. It should be expected, that these conditions are similar over the whole area of the Salar. Indeed, it could be observed during the field work in summer 2009, that wind speed is apparently increased in the drilling location SLT-03 compared to SLT-01 at similar air temperatures. Hence, it can be assumed, that the evaporation rate should be higher in the central part of the Salar. However, in order to make generalizations for the ideal position of the evaporation cones with regard to the wind conditions, the number of two investigated locations on the Salar is too low and observation time has to be extended as well. The potential evaporation E_{pot} is expected to be very high under the climatic conditions prevailing during the dry season in the Salar de Uyuni. Though, it must be considered, that the value of E_{pot} is negatively correlated to the altitude and temperature (Houston 2006). With each 1000 m rise in altitude, the E_{pot} is reduced for an amount of 600 mm/a, which means a significant decrease in evaporation at a height of 3650 m asl.

5.3 Chemical aspects of lithium recovery

The challenge of lithium recovery in the Salar de Uyuni is not only caused by the high altitude and the low temperatures during the dry season. Another important factor is the composition of the brine itself, which is characterized by a high ratio of magnesium and potassium to lithium. The brine analyses revealed that values of Mg/Li and K/Li ratios are average 20.5 and 22.8 respectively, which is in accordance with Ericksen (1978), who reported values of 20 for Mg/Li and K/Li for brines from the Salar de Uyuni. Compared to other brines in salt pans in the world the Mg/Li ratios are extraordinary high in the Salar de Uyuni, which is shown in Fig. 44.

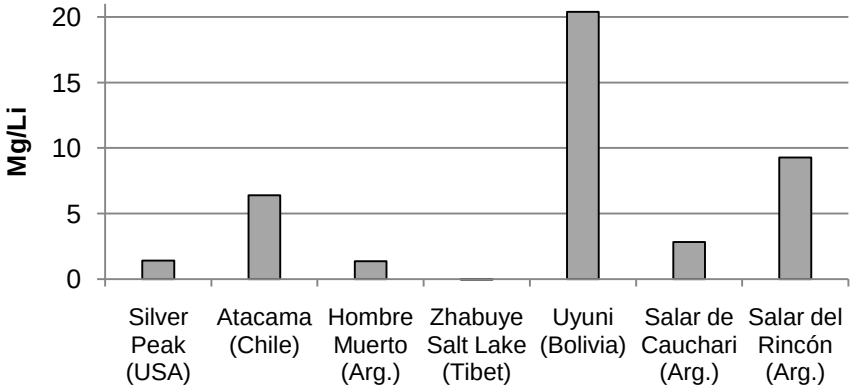

Fig. 44: Ratios of magnesium to lithium in brines from different salt pans (values for the Salar de Uyuni are from this study, other data are taken from King 2010)

The chemical similarity between Mg and Li is the reason for the similar solubility of magnesium and lithium salts. This is problematic for the recovery of lithium from the brine, as the Mg/Li separation is challenging and requires the development of new methods.

5.4 Environmental considerations

Another prerequisite is that the exploitation of lithium from the Salar de Uyuni must take place with regard to environmental aspects. The Salar de Uyuni is situated in the Bolivian ecoregion of the western cordillera's desert Puna (López & Zambrana-Torrelio 2006). The surrounding of the salt flat is characterized by a high number of endemic plant and animal species (López 2003). Small water pools on the surface at the border of the Salar serve as breeding areas for rare species of andean flamingos. Further, the Salar de Uyuni is an all-season touristic attraction, that provides a main subsistence for the surrounding communes. Thereby the tourism strongly depends on the grade of the landscape's naturalness. The development of techniques for the extraction of lithium carbonate must therefore always be considered under the aspect of compatibility with environmental interests. Not only for this reason the application of evaporation basins as used in the Atacama desert must be excluded, as they would irreversibly destroy the appearance of the salt flat. A sustainable management of the depleting resource lithium and a concept for its recovery must be developed, whereby the environmental impact should be kept as low as possible.

6 Perspectives and recommendations

The goal of the present work was to gain a first survey about the hydrogeological conditions of the Salar de Uyuni. There are various questions that arose from this thesis and that could be subject to investigations in future field campaigns.

One approach is the use of geophysical well logging. This technique could help to localize the occurrence of larger cavities and of local zones with differing characteristics by means of stratification and sediment structure compared to the surrounding (as it was observed in SLT-01E). Another approach is the analysis of isotopes in the brines from different locations. The knowledge of the distribution of lithium isotopes could help to understand the sources of this element and the processes that lead to its enrichment in the salt flat.

Computer tomographic analyses of core samples from the mud layers could give insights about the distribution and the volume of pores in these zones. With that knowledge it could be estimated if the mud layers are impermeable for the brine and therefore act as aquicludes, or if a migration of brine between separated halite layers is possible. This has consequences for the extraction of brine for the evaporation cones. Thus, the location and the depth of the planned pumping wells must be adapted to the conditions. Computer tomographic measurements of a larger number of halite core samples, especially from different depths and locations, should help to better understand the heterogeneity of pore structures and cavities, as well as the storage capacities of the halite for the interstitial brine.

The analytical detection of mineral phases in the solid core samples, for example by scanning electron microscopy and polarisation microscopy, could verify the obtained contents of salts (as carnallite, kieserite or sylvite).

The detection of strontium containing minerals by X-ray diffractometry of the solid salt sample could help to explain the removal of this element in brine samples with a higher mineralisation.

The drilling must be extended to more locations on the Salar de Uyuni in order to gain a better knowledge of the horizontal and vertical distribution of hydrochemical parameters of the brine as well as hydraulic properties of the salt crust.

The analysis of brine samples from the naturally occurring holes in the salt crust in the surrounding of SLT-01 could give information about their genesis and about the processes that keep them growing during the dry season.

For future field campaigns with a hydrogeological background in the investigation area an improvement could be achieved by a number of recommendations:

- enlargement of the deepest bore hole at every drilling location to a diameter of 4” for improving the performance of pumping tests by using 4” submersible pumps
- the use of a multi parameter probe for the measurement of on-site parameters directly in the borehole to avoid a contact with atmospheric oxygen
- avoiding the use of electric contact gauges because of the dysfunction by the extremely high conductivities of the brine, better: pressure sensor, well whistle, ultrasonic sensor
- on-site analysis of HCO_3^--content by titration or special sample conservation techniques in order to avoid consecutive reactions
- the extraction and analysis of pore water from the halite and the mud layers

7 Literature

ABELL, L., OPPENHEIMER, P. (2008) World Lithium Resource Impact on Electric Vehicles. Report, 18 pp.

ANGERER, G., MARSCHEIDER-WEIDEMANN, F., WENDL, M., WIETSCHEL, M. (2009) Lithium für Zukunftstechnologien - Nachfrage und Angebot unter besonderer Berücksichtigung der Elektromobilität. Fraunhofer Institute, 69 pp.

ARGOLLO, J. & MOURGUIART, P. (2000) Late Quaternary climate history of the Bolivian Altiplano. *Quaternary International* 72: 37-51

BAKER, P.A., RIGSBY, C.A., SELTZER, G.O., FRITZ, S.C., LOWENSTEIN, T.K., BACHER, N.P., VELIZ, C. (2001) Tropical climate changes at millennial and orbital timescales on the Bolivian Altiplano. *Nature* 409: 698–701

BALLIVIAN, O., RISACHER, F. (1981) Los Salares del Altiplano boliviano - Metodos de Estudio y Estimación economica. O.R.S.T.O.M. Paris, 253 pp.

BAMBERG, H.F. & ESCHNER, J. (1979) Pumpversuche. VEB Deutscher Verlag für Grundstoffindustrie Leipzig, 1st edition, 64 pp.

BOSCHETTI, T., CORTECCI, G., BARBIERI, M., MUSSI, M. (2007) New and past geochemical data on fresh to brine waters of the Salar de Atacama and Andean Altiplano, northern Chile. *Geofluids* 7: 33-50

BRAITSCH, O. (1971) Salt Deposits, their Origin and Composition. Springer New York, 297 pp.

BRAITSCH, O. & HERRMANN, A.G. (1963) Zur Geochemie des Broms in salinaren Sedimenten: Teil I: Experimentelle Bestimmung der Br-Verteilung in verschiedenen natürlichen Salzsystemen. *Geochimica et Cosmochimica Acta* 27: 361-391

CARMOUZE, J.P., ARCE, C. AND QUINTANILLA, J. (1978) Circulacion de materia (agua-sales disueltas) atraves del sistema fluvic-lacustre del Altiplano: la regulacion hidrica e hidroquimica de los lagos Titicaca y Poopo. *Cahiers O.R.S.T.O.M., Série Géologie* 10: 4-68

CLAPPERTON, C.M., CLAYTON, J.D., BENN, D.I., MARDEN, C.J., ARGOLLO, J. (1997) Late quaternary Glacier advances and Palaeolake highstands in the Bolivian Altiplano. *Quaternary International* 38-39: 49-59

DIN 18130-1 (2003) Baugrund; Untersuchung von Bodenproben; Bestimmung des Wasserdurchlässigkeitsbeiwertes – Teil 2: Feldversuche. Beuth-Verlag Berlin

DIN 4023 (2006) Geotechnische Erkundung und Untersuchung - Zeichnerische Darstellung der Ergebnisse von Bohrungen und sonstigen direkten Aufschlüssen. Beuth-Verlag Berlin

ERICKSEN, G.E., VINE, J.D., RAUL BALLÓN, A. (1978) Chemical composition and distribution of lithium-rich brines in salar de Uyuni and nearby salars in southwestern Bolivia. *Energy* 3: 355-363

EUGSTER, H.P. & HARDIE, L.A. (1978) Saline lakes. In: Lerman, A. (1978) Lakes – Chemistry, Geology, Physics, Springer-Verlag New York, pp. 237-293

EVANS, R.K. (2008) An Abundance of Lithium. Report, 17 pp.

FORNARI, M., RISACHER, F., FÉRAUD, G. (2001) Dating of paleolakes in the central Altiplano of Bolivia. *Palaeogeography, Palaeoclimatology, Palaeoecology* 172: 269-282

GARRETT, D.E. (2004) Handbook of Lithium and Natural Calcium Chloride - Their Deposits, Processing, Uses and Properties. Elsevier Academic Press Oxford, 1st edition, 235 pp.

GUYOT, J.L., ROCHE, M.A., NORIEGA, L., CALLE, H., QUINTANILLA, J. (1990) Salinities and Sediment Transport in the Bolivian Highlands. *Journal of Hydrology* 113: 147-162

HERCZEG, A.L., LYONS, W.B. (1991) A chemical model for the evolution of Australian sodium chloride lake brines. *Palaeogeography, Palaeoclimatology, Palaeoecology* 84: 43-53

HOLLDORF, H. & BAUMBACH, U. (1987) Bilanzierung der Totaleindampfung der Erdgasbegleitwässer bei Siedetemperatur. In: Lithiumgewinnung aus Erdgasbegleitwässern, Laborbericht 25, TU Bergakademie Freiberg

HOLSER, W.T. (1966) Diagenetic polyhalite in recent salt from Baja California. *The American Mineralogist* 51: 99-109

HÖLTING, B. & COLDEWEY, W.G. (2009) Hydrogeologie - Einführung in die Allgemeine und Angewandte Hydrogeologie. Spektrum Akademischer Verlag Heidelberg, vol. 7

HOUSTON, J. (2006) Evaporation in the Atacama Desert: An empirical study of spatio-temporal variations and their causes. *Journal of Hydrology* 330: 402-412

KING, M. (2010) Amended inferred resource estimation of lithium and potassium at the Cauchari and Olaroz Salars, Jujuy province, Argentina. Report, 126 pp.

KUSSMAUL, S., HÖRMANN, P.K., PLOSKONKA, E., SUBIETA, T. (1977) Volcanism and structure of southwestern Bolivia *Journal of Volcanology and Geothermal Research* 2: 73-74

KRUSEMAN, G.P. & DE RIDDER, N.A. (2000) Analysis and Evaluation of Pumping Test Data. *ILRI publication* 47, Wageningen, 377 pp.

LANGGUTH, H.R., VOIGT, R. (1980) Hydrogeologische Methoden. Springer-Verlag Berlin, 486 pp.

LEBRUN, V., PACOSILLO, P., GUTIERREZ, J., CACERES, F., POOL, E., PIRARD, E. (2002) Geochemistry of bitter brines in the Salar de Coipasa – Bolivia. *Aardkundige Mededelingen* 12: 185-188

LIDE, D.R. (2008) Handbook of Chemistry and Physics. CRC Press Taylor & Francis, 88th edition, 2640 pp.

LÓPEZ, R.P. (2003) Phytogeographical relations of the Andean dry valleys of Bolivia. *Journal of Biogeography* 30: 1659-1668

LÓPEZ, R.P., ZAMBRANA-TORRELIO, C. (2006) Representation of Andean dry ecoregions in the protected areas of Bolivia: the situation in relation to the new phytogeographical findings. *Biodiversity and Conservation* 15: 2163–2175

MAROTZ, G. (1968) Technische Grundlagen einer Wasserspeicherung im natürlichen Untergrund. *Schriftenreihe des KWK 18*, Hamburg, 228 pp.

MCCAFFREY, M.A., LAZAR, B. & HOLLAND, H.D. (1987) The evaporation path of seawater and the coprecipitation of Br^- and K^+ with halite. *Journal of Sedimentary Petrology* 57: 928-937

MEIER, G. (1999) Ein repräsentatives Verfahren zur ingenieurgeologischen Bohrkernauswertung im Fels in Altbergbaugebieten. *Berichte 12. Nat. Tag. f. Ing.-Geol.* Halle, pp. 192-199

MERKEL, B.J. & PLANER-FRIEDRICH, B. (2002) Integrierte Datenauswertung Hydrogeologie. *Freiberg Online Geology* 7, 61 pp.

NASA VISIBLE EARTH: Lake Titicaca, Lake Poopo, and Salar de Uyuni, Bolivia. *Catalog of NASA images and animations of our home planet*, www.visibleearth.nasa.gov, 12.03.2010

PARKHUST, D.L. & APPELO, C.A.J. (1999) PHREEQC for Windows. A Computer Program for Speciation, Batch-reaction, One-dimensional Transport and Inverse Geochemical Calculations. *U.S. Geological Survey Water Resources Investigations Report* 99-4259, 312 pp.

PAULING, L. (1927) The Sizes of Ions and the Structure of Ionic Crystals. *Journal of the American Chemical Society* 49: 765-790

RETTIG, S. L., JONES, B. F. & RISACHER, F. (1980) Geochemical Evolution of Brines in the Salar of Uyuni, Bolivia. *Chemical Geology* 30: 57-79

RISACHER, F. & FRITZ, B. (1991a) Geochemistry of Bolivian salars, Lipez, southern Altiplano: Origin of solutes and brine evolution. *Geochimica et Cosmochimica Acta* 55 : 687-705

RISACHER, F. & FRITZ, B. (1991b) Quaternary geochemical evolution of the salars of Uyuni and Coipasa, Central Altiplano, Bolivia. *Chemical Geology* 90: 211-231

RISACHER, F. & FRITZ, B. (1992) Paleoclimatic Significance of the Occurrence of Polyhalite in the Salar of Uyuni (Bolivia) - Detection of an Extremely Severe Drought in the Central Altiplano. *Comptes Rendus de l' Academie des Sciences Serie II* 314: 1371-1377

RISACHER, F. & FRITZ, B. (2000) Bromine geochemistry of salar de Uyuni and deeper salt crusts, Central Altiplano, Bolivia. *Chemical Geology* 167: 373-392

RISACHER, F., FRITZ, B. & ALONSO, H. (2006) Non-conservative behavior of bromide in surface waters and brines of Central Andes: A release into the atmosphere? *Geochimica et Cosmochimica Acta* 70: 2143-2152

ROSKILL (2009) The Economics of Lithium. *Roskill Information Services Ltd.*, 11th edition, 324 pp.

RÖSLER, H.J. (1984) Lehrbuch der Mineralogie. VEB Verlag Leipzig, 3th edition, 833 pp.

RUDOLF, M., MÜLLER, J. (2004) Multivariate Verfahren. Hogrefe-Verlag Göttingen, 331 pp.

Scientists extract lithium from sea. *The Japan Times Online* 18.04.2004, unknown author

STARKEY, H.C., BLACKMON, P.D. (1979). Clay mineralogy of Pleistocene Lake Tecopa, Inyo County, California. *USGS Prof. Paper* vol. 1061, 34pp.

STOYAN, D., STOYAN, H. & JANSEN, U. (1997) Umweltstatistik - Statistische Verarbeitung und Analyse von Umweltdaten. B.G. Teubner Verlagsgesellschaft Stuttgart, Leipzig, 348 pp.

SVENDSEN, J.B. (2002) Parabolic halite dunes on the Salar de Uyuni, Bolivia. *Sedimentary Geology* 155: 147-156

TAHIL, W. (2008) The Trouble with Lithium 2 – Under the Microscope. *Meridian International Research*, Report, 58 pp.

THIEM, G. (1906) Hydrologische Methoden. Gebhardt Leipzig, 56 pp.

TODD, D.K. (1959) Ground Water Hydrology. Wiley New York, 336 pp.

VINE, J.D. (1980) Where on Earth is all of the Lithium. *U.S. Geol. Survey*, Open-File Report 80-1234, 107 pp.

VOß, W. (1997) Praktische Statistik mit SPSS. Carl Hanser Verlag München, Wien, 361 pp.

WARREN, J.K. (2006) Evaporites – Sediments, Resources and Hydrocarbons. Springer Berlin, Heidelberg, 1035 pp.

WEAVER, C.E., POLLARD, L.D. (1975) The Chemistry of Clay Minerals. Elsevier Amsterdam, 213 pp.

WOLF, M. (1988) Salare des Altiplanos: Ihre Entstehung und wirtschaftliche Bedeutung. Veröffentlichung Nr. 2305 der Sektion Geowissenschaften, TU Bergakademie Freiberg, 39 pp.

HOARE, R.: Worldclimate - worldwide range of climate data, www.worldclimate.com, 03.05.2010

YAKSIC, A. & TILTON, J.E. (2009) Using the cumulative availability curve to assess the threat of mineral depletion: The case of lithium. *Resources Policy* 34: 185-194

Appendix

Appendix A: Tables

Table A1: Overview of the drilling locations and bore holes, the core sampling and performed field and laboratory investigations 105

Table A2: Geochemical composition of samples from drilling core SLT-01A with percent charge error of the analysis and distribution coefficient of bromine D_{Br} 106

Table A3: Mineralogic composition of samples from drilling core SLT-01A in weight% (samples in grey colour were not completely decomposed and serve only as a rough estimation); w.i.r. = water insoluble rest 108

Table A4: Technical parameters used for the computer tomographic analyses of two core samples 110

Table A5: Overview of the sampled brines and performed laboratory analyses .. 111

Table A6: On-site parameters of the brine samples obtained in September 2009 (EMF is the electromotive force measured in the field, E_h shows the redox potentials corrected with regard to a temperature of 25°C and the potential of a standard hydrogen electrode) 112

Table A7: Main and cations and anions in brine samples obtained by ion chromatography (contents of HCO_3^- obtained by calculation from TIC values) 112

Table A8: Concentrations of elements obtained by ICP-MS measurements (alphabetical order) with lower detection limit (DL), dilution factor and the measure mode of the instrument for every element (S = standard mode, C = collision mode) 113

Table A9: Results of hydrochemical analyses of the brine samples from SLT-01 and SLT-03 performed by the BGR (values are in mg/L) 114

Table A10: Densities of the brine samples obtained with pyknometry performed by the BGR and calculated densities at the temperatures measured in the field 115

Table A11: Reference values of density and TDS content of concentrated seawater samples from Mc Caffrey et al. (1987) and brines from the Salar de Uyuni by Risacher & Fritz (1991b) 115

Table A12: Mean saturation indices of the brines from different locations modelled by PhreeqC using PITZER 116

Table A13: Results of the pumping test in well SLT-03C at the 26th September 2009, the drawdown h_s was measured in the observation wells SLT-03F and SLT-03B in differing time intervals after starting the pump 117

Table A14: Results of the recovery test in SLT-01A at the 26th September 2009, the decreasing drawdown h_s was measured in SLT-01A in differing time intervals after switching off the pump 117

Appendix B: Drilling profiles

Fig. B1: Drilling profile for SLT-01A between a depth of 0 and 1.70 m and legend for the schematic illustration of the stratigraphy.....118
Fig. B2: Drilling profile for SLT-01A between a depth of 1.70 and 4.70 m 119
Fig. B3: Drilling profile for SLT-01A between a depth of 4.70 and 7.70 m 120
Fig. B4: Drilling profile for SLT-01A between a depth of 7.70 and 10.70 m 121
Fig. B5: Drilling profile for SLT-01A between a depth of 10.70 and 12.50 m 122
Fig. B6: Drilling profile for SLT-01E between a depth of 0 and 2.70 m 123
Fig. B7: Drilling profile for SLT-01E between a depth of 2.70 and 5.70 m 124
Fig. B8 : Drilling profile for SLT-01E between a depth of 5.70 and 7.70 m 124
Fig. B9: Drilling profile for SLT-03A between a depth of 0 and 1.70 m 125
Fig. B10: Drilling profile for SLT-03A between a depth of 1.70 and 3.70 m 126
Fig. B11: Drilling profile for SLT-03C between a depth of 0 and 2.70 m.....127
Fig. B12: Drilling profile for SLT-03C between a depth of 2.70 and 5.70 m 128
Fig. B13: Drilling profile for SLT-03C between a depth of 5.70 and 11.80 m 129

Appendix C: Others

Fig. C1: Results of the standard addition for two samples (the Y-intercept corresponds to the amount of lithium in the original solution).....130

Appendix A: Tables

Table A1: Overview of the drilling locations and bore holes, the core sampling and performed field and laboratory investigations

Drilling location	Bore hole	Depth of bore hole	Core documentation	Depth of core samples[1] [m]	Laboratory core analyses			Aquifer tests	
					mineralogy	chemistry	porosity	Pumping test	Recovery
SLT-01	A	12.5 m	x	0 – 12.50	x	x	-	-	x
	B	5.75 m	x	-	-	-	-	-	-
	C	8.30 m	x	7.70 – 8.70	-	-	-	-	-
	E	7.70 m	x	0 – 7.70	-	-	-	-	-
	F	3.30 m	x	-	-	-	-	-	-
SLT-03	A	3.70 m	x	0 – 3.70	-	-	x	-	-
	B	4.70 m	-	-	-	-	-	-	-
	C	11.80 m	x	0 – 11.80	-	-	-	x	-
	E	2.70 m	-	-	-	-	x	-	-

[1]core samples transported to Germany for further investigation

Table A2: Geochemical composition of samples from drilling core SLT-01A with percent charge error of the analysis and distribution coefficient of bromine D_{Br}

Sample	Depth [m]	Na	K	Ca	Mg	Cl	SO_4	Br	Error	D_{Br}
		%	%	%	%	%	%	‰	%	
SLT-01A-1.1	0.02	38.2	0.084	0.045	0.0562	59.1	0.111	0.007	0.12	0.024
SLT01A-1.2	0.05	38.6	0.083	0.034	0.0549	60.0	0.089	0.006	-0.35	0.021
SLT-01A-1.3	0.07	39.0	0.092	0.036	0.0643	60.5	0.106	0.007	-0.18	0.024
SLT-01A-1.4	0.1	38.7	0.099	0.043	0.0718	59.9	0.136	0.007	0.06	0.024
SLT-01A-2	0.19	39.1	0.032	0.027	0.0157	59.9	0.026	0.005	0.77	0.017
SLT-01A-3	0.5	38.6	0.043	0.059	0.0248	59.6	0.119	0.005	0.12	0.017
SLT-01A-4	0.85	38.9	0.046	0.032	0.0295	59.4	0.062	0.003	1.25	0.010
SLT-01A-5	1	38.5	0.061	0.032	0.0443	60.1	0.068	0.008	-0.77	0.028
SLT-01A-6	1.2	38.7	0.039	0.056	0.0278	59.5	0.110	0.003	0.53	0.010
SLT-01A-7	1.25	38.9	0.035	0.035	0.0174	60.6	0.051	0.004	-0.82	0.014
SLT-01A-8	1.35	38.9	0.035	0.029	0.0188	60.9	0.036	0.003	-1.35	0.010
SLT-01A-9	1.5	39.0	0.045	0.031	0.0274	59.7	0.050	0.001	0.95	0.003
SLT-01A-10	1.6	39.3	0.045	0.029	0.0267	60.5	0.048	0.004	0.35	0.014
SLT-01A-11	1.75	39.2	0.061	0.040	0.0428	61.1	0.096	0.009	-0.70	0.031
SLT-01A-12	1.9	39.0	0.051	0.132	0.0281	59.6	0.322	0.005	1.06	0.017
SLT-01A-13	2.15	38.4	0.042	0.177	0.0269	59.8	0.431	0.004	-0.83	0.014
SLT-01A-14	2.35	38.2	0.045	0.279	0.0301	59.2	0.694	0.006	-0.30	0.021
SLT-01A-15.1	2.45	38.6	0.071	0.112	0.0480	60.3	0.287	0.007	-0.94	0.024
SLT-01A-15.2	2.6	39.1	0.051	0.087	0.0306	60.0	0.202	0.005	0.76	0.017
SLT-01A-16	2.75	37.8	0.059	0.553	0.0388	58.6	1.40	0.004	-0.30	0.014
SLT-01A-17	2.8	36.7	0.060	1.27	0.0424	57.0	3.26	0.007	-0.72	0.024
SLT-01A-18	2.9	37.8	0.078	0.679	0.0609	58.7	1.76	0.007	-0.47	0.024
SLT-01A-19	3.1	39.2	0.054	0.119	0.0341	60.8	0.265	0.006	-0.35	0.021
SLT-01A-20	3.25	36.6	0.051	1.55	0.0328	57.3	3.96	0.008	-1.48	0.028
SLT-01A-21	3.35	37.6	0.056	0.965	0.0332	57.9	2.44	0.006	0.24	0.021
SLT-01A-22.1	3.5	38.2	0.061	0.427	0.0376	58.3	1.07	0.009	1.31	0.031
SLT-01A-22.2	3.55	37.1	0.128	1.18	0.0881	58.3	3.11	0.011	-1.53	0.038
SLT-01A-23.1	3.75	38.6	0.050	0.425	0.0333	60.0	1.06	0.008	-0.59	0.028
SLT-01A-23.2	3.8	37.1	0.090	0.853	0.0796	57.8	2.20	0.009	-0.60	0.031
SLT-01A-24	3.85	37.9	0.050	0.978	0.0276	58.8	2.47	0.008	-0.53	0.028
SLT-01A-25	3.9	39.1	0.065	0.082	0.0453	60.1	0.201	0.008	0.70	0.028
SLT-01A-26	4.1	39.2	0.076	0.207	0.0575	61.5	0.531	0.012	-1.38	0.042
SLT-01A-27	4.5	38.4	0.078	0.338	0.0509	59.6	0.867	0.016	-0.35	0.055
SLT-01A-28	4.6	38.9	0.052	0.142	0.0291	59.6	0.351	0.009	0.83	0.031
SLT-01A-29.1	4.7	38.2	0.061	0.769	0.0390	58.6	1.99	0.006	0.65	0.021
SLT-01A-29.2	4.75	38.5	0.048	0.301	0.0242	59.2	0.753	0.005	0.41	0.017
SLT-01A-30	4.8	38.3	0.054	0.439	0.0300	59.8	1.10	0.01	-1.12	0.035
SLT-01A-31	4.9	37.2	0.049	1.18	0.0242	58.3	3.02	0.007	-1.59	0.024
SLT-01A-32	5	37.9	0.069	0.564	0.0420	58.6	1.44	0.009	-0.06	0.031
SLT-01A-33	5.05	37.5	0.058	0.650	0.0317	58.4	1.66	0.005	-0.90	0.017
SLT-01A-34	5.1	38.5	0.076	0.113	0.0490	59.9	0.236	0.006	-0.47	0.021
SLT-01A-35.1	5.15	36.9	0.081	1.099	0.0874	57.3	2.85	0.007	-0.36	0.024
SLT-01A-35.2	5.2	38.5	0.066	0.540	0.0362	59.6	1.33	0.012	-0.12	0.042
SLT-01A-35.3	5.25	38.8	0.051	0.148	0.0230	59.8	0.341	0.006	0.24	0.021
SLT-01A-35.4	5.3	38.5	0.051	0.095	0.0271	60.1	0.207	0.01	-0.95	0.035
SLT-01A-36.1	5.35	37.8	0.064	0.845	0.0320	58.3	2.18	0.007	0.12	0.024
SLT-01A-36.2	5.4	38.8	0.050	0.053	0.0278	60.4	0.090	0.008	-0.71	0.028
SLT-01A-36.3	5.45	36.4	0.109	0.258	0.120	57.2	0.467	0.013	-0.87	0.045
SLT-01A-37.1	5.5	29.4	0.114	3.63	0.111	45.6	9.50	0.013	-0.81	0.045
SLT-01A-37.2	5.55	38.0	0.080	0.195	0.0691	60.0	0.392	0.009	-1.72	0.031
SLT-01A-38	5.8	38.4	0.093	0.310	0.0554	59.8	0.813	0.012	-0.71	0.042

Sample	Depth [m]	Na	K	Ca	Mg	Cl	SO_4	Br	Error	D_{Br}
		%	%	%	%	%	%	‰	%	
SLT-01A-39	6	38.4	0.054	0.378	0.0203	59.2	0.940	0.01	0.12	0.035
SLT-01A-40	6.1	38.8	0.063	0.297	0.0346	60.0	0.730	0.011	0.06	0.038
SLT-01A-41.1	6.3	37.9	0.071	0.852	0.0461	58.5	2.19	0.008	0.12	0.028
SLT-01A-41.2	6.4	36.9	0.083	0.912	0.0648	56.4	2.30	0.009	1.15	0.031
SLT-01A-42	6.5	38.8	0.055	0.431	0.0433	59.7	1.10	0.006	0.47	0.021
SLT-01A-43	6.65	39.1	0.046	0.401	0.0328	60.1	0.988	0.008	0.52	0.028
SLT-01A-44	6.7	39.1	0.046	0.078	0.0283	60.0	0.170	0.008	0.71	0.028
SLT-01A-45	6.75	37.6	0.056	0.899	0.0407	58.8	2.29	0.007	-1.30	0.024
SLT-01A-46	6.9	37.7	0.041	0.708	0.0252	58.4	1.79	0.003	-0.36	0.010
SLT-01A-47	7.1	38.6	0.027	0.320	0.0126	59.3	0.765	0.004	0.47	0.014
SLT-01A-48	7.15	38.9	0.028	0.064	0.0108	59.9	0.118	0.006	0.30	0.021
SLT-01A-49	7.25	38.3	0.067	0.493	0.0382	59.9	1.25	0.018	-1.17	0.062
SLT-01A-50.1	7.35	39.1	0.026	0.108	0.0114	60.6	0.235	0.002	-0.35	0.007
SLT-01A-50.2	7.5	37.9	0.065	0.845	0.0485	58.3	2.10	0.008	0.53	0.028
SLT-01A-51	7.75	38.7	0.053	0.794	0.0363	59.1	1.99	0.011	1.11	0.038
SLT-01A-52	7.8	39.1	0.053	0.375	0.0379	59.8	0.899	0.009	1.05	0.031
SLT-01A-53	7.85	38.4	0.069	0.473	0.0546	59.8	1.17	0.008	-0.64	0.028
SLT-01A-54	7.9	39.0	0.048	0.337	0.0314	60.1	0.819	0.008	0.29	0.028
SLT-01A-55	7.95	38.4	0.053	0.926	0.0382	58.5	2.33	0.008	1.23	0.028
SLT-01A-56	8	20.9	0.167	3.09	0.249	32.2	8.71	0.009	-0.18	0.031
SLT-01A-57	8.1	10.9	0.250	2.89	0.254	17.0	8.16	0.013	-0.77	0.045
SLT-01A-58	8.15	39.4	0.101	0.159	0.0652	60.6	0.299	0.027	0.87	0.093
SLT-01A-59	8.2	39.3	0.117	0.146	0.0599	60.7	0.376	0.029	0.23	0.100
SLT-01A-60.1	8.25	36.5	0.142	0.645	0.425	57.2	1.76	0.025	0.54	0.087
SLT-01A-60.2	8.3	39.0	0.104	0.071	0.256	60.4	0.180	0.025	0.93	0.087
SLT-01A-60.3	8.35	39.0	0.079	0.089	0.0481	61.3	0.159	0.025	-1.51	0.087
SLT-01A-61	8.45	39.3	0.106	0.058	0.0404	60.5	0.140	0.025	0.53	0.087
SLT-01A-62	8.75	39.4	0.071	0.183	0.0325	60.5	0.453	0.016	0.76	0.055
SLT-01A-63	8.8	39.0	0.076	0.247	0.0434	60.8	0.636	0.019	-0.81	0.066
SLT-01A-64	8.85	38.6	0.092	0.472	0.0606	60.2	1.24	0.013	-0.82	0.045
SLT-01A-65.1	8.95	39.0	0.100	0.277	0.0543	60.6	0.751	0.014	-0.46	0.048
SLT-01A-65.2	9	36.3	0.585	0.873	0.279	56.9	3.36	0.023	-0.84	0.080
SLT-01A-66	9.2	38.0	0.172	0.399	0.102	59.5	1.27	0.012	-1.12	0.042
SLT-01A-67	9.25	38.6	0.109	0.088	0.0701	60.5	0.315	0.014	-1.23	0.048
SLT-01A-68	9.35	39.0	0.102	0.149	0.0689	60.0	0.461	0.01	0.59	0.035
SLT-01A-69	9.5	38.5	0.194	0.238	0.108	60.0	0.916	0.011	-0.59	0.038
SLT-01A-70	9.6	39.1	0.079	0.172	0.0451	60.7	0.482	0.01	-0.35	0.035
SLT-01A-71	9.75	38.4	0.200	0.331	0.102	59.8	1.10	0.01	-0.59	0.035
SLT-01A-72	9.8	38.4	0.342	0.378	0.151	59.0	1.60	0.011	0.76	0.038
SLT-01A-73.1	9.85	37.7	0.252	0.427	0.124	58.9	1.50	0.011	-0.89	0.038
SLT-01A-73.2	9.87	8.82	0.770	1.11	0.355	14.0	4.59	0.013	-0.61	0.045
SLT-01A-73.3	9.89	33.5	1.25	1.10	0.513	51.8	5.96	0.016	0.06	0.055
SLT-01A-73.4	9.91	38.1	0.067	0.511	0.0321	59.9	1.30	0.009	-1.76	0.031
SLT-01A-74	9.95	38.4	0.177	0.194	0.0870	59.8	0.741	0.009	-0.59	0.031
SLT-01A-75	10.15	37.8	0.338	0.365	0.152	58.3	1.53	0.01	0.48	0.035
SLT-01A-76	10.35	38.9	0.097	0.332	0.0767	60.3	0.823	0.009	-0.06	0.031
SLT-01A-77	10.4	35.2	1.12	1.20	0.438	55.2	5.72	0.011	-1.20	0.038
SLT-01A-78	10.45	33.5	1.79	1.67	0.648	52.8	8.63	0.01	-1.81	0.035
SLT-01A-80	10.55	9.20	0.371	3.97	0.399	14.5	10.9	0.023	0.63	0.080
SLT-01A-81	10.75	8.69	1.54	0.209	1.33	16.1	3.49	0.093	1.69	0.322
SLT-01A-82.1	10.9	7.35	1.05	4.51	1.01	13.0	14.2	0.058	-1.21	0.201
SLT-01A-84	11.1	38.9	0.094	0.100	0.0636	59.4	0.279	0.012	1.36	0.042
SLT-01A-85	11.25	39.0	0.193	0.161	0.102	60.3	0.702	0.015	0.06	0.052

Sample	Depth [m]	Na	K	Ca	Mg	Cl	SO_4	Br	Error	D_{Br}
		%	%	%	%	%	%	‰	%	
SLT-01A-86	11.3	37.9	0.355	0.478	0.184	58.2	1.90	0.014	0.89	0.048
SLT-01A-88	11.75	35.6	1.20	1.11	0.450	55.4	5.71	0.009	-0.60	0.031
SLT-01A-89	12.1	38.0	0.334	0.715	0.151	58.6	2.44	0.01	0.35	0.035
SLT-01A-90	12.3	37.3	0.505	0.868	0.203	57.8	3.32	0.01	-0.24	0.035

Table A3: Mineralogic composition of samples from drilling core SLT-01A in weight% (samples in grey colour were not completely decomposed and serve only as a rough estimation); w.i.r. = water insoluble rest

Sample	Depth [m]	Mineral content [wt%]							
		Halite	Gypsum	Poly-halite	Kieserite	Carnallite	Sylvite	Sum	w.i.r. [wt%]
SLT-01A-1.1	0.02	97.1	0.01	0.00	0.15	0.00	0.16	97.4	2.6
SLT01A-1.2	0.05	98.1	0.09	0.00	0.05	0.52	0.02	98.8	1.2
SLT-01A-1.3	0.07	99.1	0.12	0.00	0.05	0.63	0.01	100.0	0.0
SLT-01A-1.4	0.1	98.3	0.17	0.00	0.03	0.70	0.00	99.2	0.8
SLT-01A-2	0.19	98.7	0.01	0.03	0.00	0.00	0.00	98.8	1.2
SLT-01A-3	0.5	98.1	0.04	0.00	0.14	0.00	0.08	98.4	1.6
SLT-01A-4	0.85	97.9	0.00	0.10	0.00	0.00	0.00	98.0	2.0
SLT-01A-5	1	97.9	0.02	0.00	0.08	0.35	0.02	98.3	1.7
SLT-01A-6	1.2	98.1	0.00	0.17	0.00	0.00	0.00	98.3	1.7
SLT-01A-7	1.25	98.9	0.00	0.00	0.07	0.00	0.07	99.0	1.0
SLT-01A-8	1.35	98.9	0.01	0.00	0.05	0.00	0.07	99.0	1.0
SLT-01A-9	1.5	98.4	0.00	0.08	0.00	0.00	0.00	98.5	1.5
SLT-01A-10	1.6	99.7	0.00	0.07	0.00	0.00	0.00	99.8	0.2
SLT-01A-11	1.75	99.7	0.00	0.00	0.13	0.00	0.12	99.9	0.1
SLT-01A-12	1.9	98.2	0.11	0.32	0.09	0.00	0.00	98.8	1.2
SLT-01A-13	2.15	97.6	0.58	0.00	0.15	0.00	0.08	98.4	1.6
SLT-01A-14	2.35	97.1	1.03	0.00	0.17	0.00	0.08	98.4	1.6
SLT-01A-15.1	2.45	98.1	0.41	0.00	0.08	0.38	0.03	99.0	1.0
SLT-01A-15.2	2.6	98.9	0.00	0.32	0.00	0.00	0.00	99.2	0.8
SLT-01A-16	2.75	96.1	2.23	0.00	0.22	0.00	0.11	98.7	1.3
SLT-01A-17	2.8	93.3	5.44	0.00	0.08	0.31	0.03	99.2	0.8
SLT-01A-18	2.9	96.1	2.91	0.00	0.11	0.47	0.02	99.6	0.4
SLT-01A-19	3.1	99.5	0.23	0.00	0.19	0.00	0.10	100.0	0.0
SLT-01A-20	3.25	93.0	6.65	0.00	0.19	0.00	0.10	100.0	0.0
SLT-01A-21	3.35	95.4	3.83	0.35	0.11	0.00	0.00	99.7	0.3
SLT-01A-22.1	3.5	96.1	1.25	0.47	0.11	0.00	0.00	97.9	2.1
SLT-01A-22.2	3.55	94.0	5.06	0.00	0.13	0.75	0.04	100.0	0.0
SLT-01A-23.1	3.75	98.0	1.66	0.00	0.19	0.00	0.10	99.9	0.1
SLT-01A-23.2	3.8	94.3	3.66	0.00	0.18	0.54	0.03	98.7	1.3
SLT-01A-24	3.85	95.6	4.19	0.00	0.16	0.00	0.09	100.0	0.0
SLT-01A-25	3.9	98.8	0.20	0.09	0.05	0.38	0.00	99.5	0.5
SLT-01A-26	4.1	98.5	0.87	0.00	0.06	0.53	0.00	100.0	0.0
SLT-01A-27	4.5	97.6	1.44	0.00	0.05	0.49	0.02	99.6	0.4
SLT-01A-28	4.6	98.2	0.15	0.32	0.09	0.00	0.00	98.8	1.2
SLT-01A-29.1	4.7	96.5	2.89	0.47	0.11	0.00	0.00	100.0	0.0
SLT-01A-29.2	4.75	97.6	0.93	0.29	0.07	0.00	0.00	98.9	1.1
SLT-01A-30	4.8	97.4	1.76	0.00	0.17	0.00	0.10	99.4	0.6
SLT-01A-31	4.9	94.6	5.06	0.00	0.14	0.00	0.09	99.9	0.1
SLT-01A-32	5	96.3	2.42	0.00	0.07	0.34	0.04	99.2	0.8

Sample	Depth [m]	Mineral content [wt%]							
		Halite	Gypsum	Poly-halite	Kieserite	Carnallite	Sylvite	Sum	w.i.r. [wt%]
SLT-01A-33	5.05	95.3	2.75	0.00	0.18	0.00	0.11	98.4	1.6
SLT-01A-34	5.1	97.9	0.29	0.00	0.11	0.34	0.05	98.7	1.3
SLT-01A-35.1	5.15	93.8	4.70	0.00	0.33	0.34	0.06	99.2	0.8
SLT-01A-35.2	5.2	97.5	2.13	0.00	0.21	0.00	0.13	100.0	0.0
SLT-01A-35.3	5.25	98.6	0.18	0.32	0.06	0.00	0.00	99.1	0.9
SLT-01A-35.4	5.3	97.9	0.18	0.00	0.15	0.00	0.10	98.3	1.7
SLT-01A-36.1	5.35	96.1	3.38	0.35	0.10	0.00	0.02	99.9	0.1
SLT-01A-36.2	5.4	98.6	0.01	0.00	0.12	0.00	0.09	98.9	1.1
SLT-01A-36.3	5.45	92.5	0.56	0.00	0.22	0.77	0.00	**94.1**	5.9
SLT-01A-37.1	5.5	74.7	15.58	0.00	0.36	0.55	0.07	**91.3**	8.7
SLT-01A-37.2	5.55	96.6	0.49	0.00	0.17	0.44	0.03	97.7	2.3
SLT-01A-38	5.8	97.6	1.32	0.00	0.06	0.52	0.04	99.6	0.4
SLT-01A-39	6	97.6	1.25	0.34	0.04	0.00	0.00	99.2	0.8
SLT-01A-40	6.1	98.6	1.06	0.00	0.20	0.00	0.12	100.0	0.0
SLT-01A-41.1	6.3	95.9	3.61	0.08	0.03	0.43	0.00	100.0	0.0
SLT-01A-41.2	6.4	92.7	3.77	0.18	0.12	0.42	0.00	97.2	2.8
SLT-01A-42	6.5	98.1	1.30	0.42	0.15	0.00	0.00	100.0	0.0
SLT-01A-43	6.65	98.3	1.23	0.35	0.11	0.00	0.00	100.0	0.0
SLT-01A-44	6.7	98.9	0.00	0.27	0.00	0.00	0.00	99.2	0.8
SLT-01A-45	6.75	95.6	3.86	0.00	0.07	0.33	0.02	99.9	0.1
SLT-01A-46	6.9	95.8	3.03	0.00	0.14	0.00	0.08	99.1	0.9
SLT-01A-47	7.1	97.8	1.17	0.13	0.04	0.00	0.00	99.1	0.9
SLT-01A-48	7.15	98.7	0.02	0.14	0.03	0.00	0.00	98.9	1.1
SLT-01A-49	7.25	97.4	1.97	0.00	0.22	0.00	0.13	99.7	0.3
SLT-01A-50.1	7.35	99.4	0.34	0.00	0.06	0.00	0.05	99.9	0.1
SLT-01A-50.2	7.5	95.9	3.57	0.09	0.07	0.38	0.00	100.0	0.0
SLT-01A-51	7.75	96.5	2.96	0.41	0.11	0.00	0.00	100.0	0.0
SLT-01A-52	7.8	98.5	0.99	0.41	0.12	0.00	0.00	100.0	0.0
SLT-01A-53	7.85	97.5	1.99	0.00	0.09	0.45	0.01	100.0	0.0
SLT-01A-54	7.9	98.6	0.93	0.37	0.09	0.00	0.00	100.0	0.0
SLT-01A-55	7.95	95.9	3.56	0.41	0.12	0.00	0.00	100.0	0.0
SLT-01A-56	8	53.0	12.64	1.10	1.08	0.17	0.00	68.0	32.0
SLT-01A-57	8.1	27.5	11.81	1.04	0.80	0.82	0.00	42.0	58.0
SLT-01A-58	8.15	99.2	0.01	0.39	0.06	0.35	0.00	100.0	0.0
SLT-01A-59	8.2	99.0	0.20	0.37	0.05	0.42	0.00	100.0	0.0
SLT-01A-60.1	8.25	92.8	0.53	0.00	2.11	0.62	0.10	96.2	3.8
SLT-01A-60.2	8.3	99.1	0.01	0.00	0.25	0.23	0.14	99.8	0.2
SLT-01A-60.3	8.35	99.1	0.11	0.00	0.14	0.27	0.08	99.7	0.3
SLT-01A-61	8.45	99.6	0.00	0.22	0.00	0.24	0.00	100.0	0.0
SLT-01A-62	8.75	99.2	0.18	0.47	0.08	0.00	0.00	100.0	0.0
SLT-01A-63	8.8	98.5	1.01	0.00	0.10	0.29	0.07	100.0	0.0
SLT-01A-64	8.85	97.4	2.02	0.00	0.11	0.46	0.05	100.0	0.0
SLT-01A-65.1	8.95	98.2	1.18	0.00	0.12	0.38	0.09	100.0	0.0
SLT-01A-65.2	9	92.3	3.51	0.40	0.64	1.71	0.56	99.1	0.9
SLT-01A-66	9.2	96.6	1.71	0.00	0.25	0.66	0.15	99.4	0.6
SLT-01A-67	9.25	98.1	0.34	0.00	0.18	0.44	0.09	99.2	0.8
SLT-01A-68	9.35	98.6	0.45	0.23	0.08	0.51	0.00	99.9	0.1
SLT-01A-69	9.5	97.9	1.01	0.00	0.34	0.55	0.22	100.0	0.0
SLT-01A-70	9.6	98.8	0.71	0.00	0.12	0.27	0.08	100.0	0.0
SLT-01A-71	9.75	97.5	1.42	0.00	0.36	0.44	0.26	100.0	0.0
SLT-01A-72	9.8	96.9	0.34	2.07	0.13	0.52	0.00	100.0	0.0
SLT-01A-73.1	9.85	95.8	1.81	0.00	0.71	0.00	0.48	98.8	1.2

Sample	Depth [m]	Mineral content [wt%]							
		Halite	Gypsum	Poly-halite	Kieserite	Carnallite	Sylvite	Sum	w.i.r. [wt%]
SLT-01A-73.2	9.87	22.4	3.30	2.55	1.44	0.00	0.84	**30.5**	69.5
SLT-01A-73.3	9.89	84.6	0.03	8.20	0.45	1.18	0.00	**94.5**	5.5
SLT-01A-73.4	9.91	96.9	2.10	0.00	0.18	0.00	0.13	99.3	0.7
SLT-01A-74	9.95	97.6	0.83	0.00	0.30	0.40	0.23	99.4	0.6
SLT-01A-75	10.15	95.7	0.40	1.90	0.14	0.58	0.00	98.8	1.2
SLT-01A-76	10.35	98.2	1.14	0.00	0.27	0.33	0.10	100.0	0.0
SLT-01A-77	10.4	89.5	3.72	2.50	1.54	0.77	1.31	99.3	0.7
SLT-01A-78	10.45	85.2	3.98	5.58	2.07	0.68	1.85	99.3	0.7
SLT-01A-80	10.55	22.9	16.42	1.09	1.21	1.63	0.00	43.2	56.8
SLT-01A-81	10.75	22.1	0.01	0.00	5.02	4.77	1.66	33.5	66.5
SLT-01A-82	10.9	18.7	18.98	0.68	4.05	3.11	1.00	46.5	53.5
SLT-01A-83	11	18.5	0.47	0.00	0.34	2.54	0.00	21.8	78.2
SLT-01A-84	11.1	97.7	0.00	0.35	0.08	0.35	0.00	98.5	1.5
SLT-01A-85	11.25	98.5	0.01	0.88	0.19	0.37	0.03	100.0	0.0
SLT-01A-86	11.3	95.6	0.74	2.02	0.29	0.59	0.00	99.2	0.8
SLT-01A-88	11.75	90.5	1.24	6.16	0.86	0.57	0.59	99.9	0.1
SLT-01A-89	12.1	95.6	1.65	2.19	0.18	0.36	0.00	100.0	0.0
SLT-01A-90	12.3	94.8	3.70	0.03	0.00	0.39	0.28	99.2	0.8

Table A4: Technical parameters used for computer tomographic analyses of two core samples

Parameter		Core sample	
		SLT-03_K2	SLT-03_Crust
Channel	voltage	210 kV	170 kV
	amperage	450 µA	250 µA
	power	84,1 W	38,5 W
Detector	averaging	4 pictures	
	skip	1 picture	
	exposure time	499 ms	
Reconstruction	number of angles	400	
	cross section	50%	
	bit depth	16 bit	
Position of the manipulator		600 mm	
Magnification		5,16	
Edge length of a voxel		76,16 nm	76,12 nm

Table A5: Overview of the sampled brines and performed laboratory analyses

(Drilling) Location	Nr. of bore hole	Brine sampling depth [m]	Name of brine sample	Laboratory analyses				
				IC	TIC	ICP-MS	Viscosity	Density
SLT-01	A	-	-	-	-	-	-	-
	B	4.50 – 5.50	SLT-01B_5m-20909	x	x	x	x	x
	C	7.00 – 8.00	SLT-01C_7.5m-200909	x	x	x	-	x
	E	6.40 – 7.40	SLT-01E_7m-200909	x	x	x	-	x
	F	2.00 – 3.00	SLT-01F_2.5m-200909	x	x	x	-	x
SLT-03	A	2.50 – 3.50	SLT-03A_3m-260909	x	x	x	x	x
	B	3.50 – 4.50	SLT-03B_4m-260909	x	x	x	-	x
	C	4.30 – 5.30	SLT-03C_4.7m-260909	x	x	x	-	x
	E	1.50 – 2.50	SLT-03E_2m-260909	x	x	x	-	x
SLT-S	-	0.10	SLT-S_0m-280909	x	x	x	-	x

Table A6: On-site parameters of the brine samples obtained in September 2009 (EMF is the electromotive force measured in the field, E_h shows the redox potentials corrected with regard to a temperature of 25°C and the potential of a standard hydrogen electrode)

Sample	Sampling day	T	pH	$EC_{25°C}$	O_2		EMF	E_h	Fe_{total}	Fe^{2+}	S^{2-}	NO_2^-	NH_4^+
		°C		mS/cm	mg/L	%	mV	mV	mg/L	mg/L	mg/L	mg/L	mg/L
SLT-01B_5m-200909	20.09.2009	5.1	7.12	242	3.99	49.0	-115	95.9	0.05	<0.03	<0.01	0.024	2.3
SLT-01C_7.5m-200909	20.09.2009	4.6	7.11	234	3.19	38.2	-73	138	0.03	<0.03	<0.01	0.022	2.1
SLT-01E_7m-200909	20.09.2009	4.6	7.09	238	6.24	75.6	-81	130	0.04	<0.03	<0.01	0.017	1.9
SLT-01F_2.5m-200909	20.09.2009	7.4	7.09	227	3.68	47.7	-133	77.5	0.03	0.04	<0.01	0.020	1.5
SLT-03A_3m-260909	26.09.2009	7.1	6.88	194	6.99	89.5	-276	-65.4	<0.03	0.07	<0.01	0.137	2.8
SLT-03B_4m-260909	26.09.2009	8.2	6.84	202	6.30	83.7	-279	-68.7	<0.03	<0.03	0.05	0.075	2.2
SLT-03C_4.7m-260909	26.09.2009	9.2	6.92	211	6.86	93.6	-270	-59.9	<0.03	0.10	0.03	0.158	1.7
SLT-03E_2m-260909	26.09.2009	7.0	6.94	209	6.94	89.4	-264	-53.4	<0.03	<0.03	0.01	0.090	1.4
SLT-S_0m-280909	28.09.2009	12.4	5.84	230	0.38	-	4	210	31.4	28	<0.01	0.019	75

Table A7: Main and cations and anions in brine samples obtained by ion chromatography (contents of HCO_3^- obtained by calculation from TIC values)

Sample	Charge error	Cations [mg/L]				Anions [mg/L]				TDS
	[%]	Ca^{2+}	Mg^{2+}	Na^+	K^+	Cl^-	SO_4^{2-}	Br^-	HCO_3^-	[g/L]
SLT-01B_5m-200909	-1.18	650.7	5,414	103,753	6,386	182,541	7,931	85.96	50.7	306.8
SLT-01C_7.5m-200909	-1.02	644.9	5,540	105,197	6,410	184,450	8,099	90.13	49.2	310.5
SLT-01E_7m-200909	1.95	644.0	5,492	105,355	6,453	173,562	8,112	96.75	46.3	299.8
SLT-01F_2.5m-200909	0.44	658.1	5,501	106,564	6,453	181,004	8,046	82.36	47.6	308.4
SLT-03A_3m-260909	0.42	85.26	21,137	77932	20,202	184,694	23,854	202.6	139.3	328.2
SLT-03B_4m-260909	0.73	170.5	21,305	77,315	20,243	182,675	24,215	196.5	144.3	326.3
SLT-03C_4.7m-260909	0.23	249.0	19,164	80,314	19,792	184,884	21,044	186.4	144.7	325.8
SLT-03E_2m-260909	0.12	217.6	20,137	78,711	19,997	184,945	22,306	189.2	136.6	326.6
SLT-S_0m-280909	0.78	814.5	5,525	90,842	7,918	157,483	7,443	152.5	633.7	270.8

Table A8: Concentrations of elements obtained by ICP-MS measurements (alphabetical order) with lower detection limit (DL), dilution factor and the measure mode of the instrument for every element (S = standard mode, C = collision mode)

Element	Ag	Al	As	B	Ba	Be	Bi	Br	Cd	Co	Cr	Cs	Cu	Fe	Ga	I	In
DL [µg/L]	0.005	0.12	0.025	0.3	0.001	0.0013	0.0001	0.5	0.0005	0.0007	0.004	0.0001	0.02	0.05	0.001	0.004	0.0002
Unit	µg/L	µg/L	µg/L	mg/L	µg/L	µg/L	µg/L	mg/L	µg/L	µg/L	µg/L	µg/L	µg/L	µg/L	µg/L	µg/L	µg/L
SLT-01B	11.1	127	579	203	80.9	< 0.65	0.362	86.0	1.61	0.223	1.73	176	8.94	118	0.405	18.2	0.093
SLT-01C	9.13	99.3	640	212	91.1	< 0.65	0.287	90.1	1.40	0.208	0.802	184	10.4	121	0.275	24.8	0.160
SLT-01E	7.93	128	624	213	73.8	< 0.65	0.240	96.8	1.64	0.172	0.740	182	10.9	125	0.291	52.0	0.210
SLT-01F	6.34	109	613	208	61.5	< 0.65	0.243	82.4	1.01	0.186	0.773	177	12.4	126	0.287	15.6	0.232
SLT-03A	8.69	186	5,441	1,055	37.1	< 0.65	0.185	203	0.941	0.094	1.74	514	20.2	82.0	0.502	200	1.85
SLT-03B	17.0	186	4,526	1,059	29.6	< 0.65	0.234	197	1.04	0.187	1.44	568	16.5	92.2	0.458	84.1	0.825
SLT-03C	8.11	216	4,293	856	31.8	< 0.65	0.188	186	0.963	0.184	1.70	554	18.1	97.3	0.436	77.7	1.13
SLT-03E	8.44	211	5,760	962	37.6	< 0.65	0.181	189	0.788	0.134	1.86	467	19.0	89.2	0.512	55.7	1.51
SLT-S	7.39	106	339	421	57.9	< 0.65	0.204	153	1.02	3.81	0.978	1,177	15.0	40,610	0.410	1,135	0.345
Mode	S	C	C	S	S	S	S	S	C	C	C	S	C	C	S	S	S
Dilution	100	100	100	500	100	500	100	100	100	100	100	100	100	100	100	100	100

Element	Li	Mn	Mo	Ni	P	Pb	Rb	Sb	Se	Si	Sn	Sr	Te	Tl	U	V	Zn
DL [µg/L]	0.01	0.003	0.0025	0.0075	2.8	0.001	0.002	0.0002	0.61	40	0.008	0.0025	0.005	0.0001	0.00015	0.0025	0.09
Unit	mg/L	µg/L	µg/L	µg/L	µg/L	µg/L	µg/L	µg/L	µg/L	µg/L	µg/L	µg/L	µg/L	µg/L	µg/L	µg/L	µg/L
SLT-01B	263	1,020	14.9	3.59	< 280	1.75	5,452	1.52	351	< 3,800	< 0.8	17,180	2.01	0.105	2.94	13.9	< 8.5
SLT-01C	268	1,047	21.3	2.99	< 280	1.38	5,548	1.80	357	< 3,800	< 0.8	18,360	3.25	0.073	3.30	12.1	< 8.5
SLT-01E	259	1,057	28.2	2.83	< 280	1.41	5,626	1.84	409	5,353	< 0.8	18,160	3.91	0.055	0.798	10.7	< 8.5
SLT-01F	260	1,024	31.9	2.24	< 280	1.14	5,510	1.99	452	6,309	< 0.8	17,430	4.61	0.054	0.250	11.1	< 8.5
SLT-03A	1,023	1,613	278	4.41	450	1.43	17,270	8.75	1,011	9,563	< 0.8	1,112	19.0	0.061	1.26	17.3	< 8.5
SLT-03B	995	1,313	128	4.19	287	1.21	17,400	8.52	1,025	8,934	< 0.8	552	16.2	0.071	0.703	13.7	< 8.5
SLT-03C	897	1,198	188	2.51	341	1.09	15,920	8.54	1,039	8,118	< 0.8	317	16.6	0.038	0.424	16.1	< 8.5
SLT-03E	955	1,845	233	2.88	250	1.11	17,590	8.34	957	9,432	< 0.8	1,843	17.4	0.056	1.41	16.1	< 8.5
SLT-S	331	2,003	44.0	7.23	511	1.07	8,692	2.24	643	23,560	< 0.8	18,700	7.77	0.158	0.065	12.4	123
Mode	S	C	S	C	C	S	S	S	C	C	S	S	S	S	S	C	C
Dilution	2,000	100	100	100	100	100	100	100	100	100	100	100	100	100	100	100	100

Table A9: Results of hydrochemical analyses of the brine samples from SLT-01 and SLT-03 performed by the BGR (values are in mg/L)

Sample	Ca^{2+}	Mg^{2+}	Na^{+}	K^{+}	Cl^{-}	SO_4^{2-}	Br^{-}	HCO_3^{-}	NH_4^{+}
SLT-01B	731	5,884	115,333	6,729	190,131	8,431	72	326	2.2
SLT-01C	707	5,754	114,535	6,664	190,565	8,429	60	332	2.1
SLT-01E	700	5,692	114,924	6,605	191,507	8,347	58	328	1.9
SLT-01F	715	5,719	115,286	6,598	193,702	8,363	56	322	2.1
SLT-03A	246	21,203	83,923	21,288	193,409	25,255	161	1,971	26.1
SLT-03B	222	21,258	81,841	21,196	193,117	25,658	158	1,948	27.9
SLT-03C	293	18,875	85,884	20,530	196,205	21,839	151	1,620	18.4
SLT-03E	265	19,727	83,622	20,702	187,734	23,077	150	1,804	20.5

Sample	Ba	B	Li	Si	Sr
SLT-01B	0.39	813	264	8	16.7
SLT-01C	0.38	817	259	6	16.9
SLT-01E	0.40	802	258	4	16.5
SLT-01F	0.43	804	259	6	16.4
SLT-03A	0.38	3930	990	6	0.90
SLT-03B	0.32	3943	997	5	0.48
SLT-03C	0.36	3345	910	7	1.95
SLT-03E	0.39	3610	938	7	1.23

Table A10: Densities of the brine samples obtained with pyknometry performed by the BGR and calculated densities at the temperatures measured in the field

Brine sample	Density (25°C) [kg/m³]	Density (T_{field}) [kg/m³]	T_{field} [°C]
SLT-01B_5m-200909	1206.8	1224.9	5.1
SLT-01C_7.5m-200909	1207.1	1225.2	4.6
SLT-01E_7m-200909	1207.1	1225.2	4.6
SLT-01F_2.5m-200909	1207.6	1223.4	7.4
SLT-03A_3m-260909	1229.6	1235.7	7.1
SLT-03B_4m-260909	1229.5	1235.1	8.2
SLT-03C_4.7m-260909	1226.9	1234.4	9.2
SLT-03E_2m-260909	1227.4	1235.8	7.0

Table A11: Reference values of density and TDS content of concentrated seawater samples from Mc Caffrey et al. (1987) and brines from the Salar de Uyuni by Risacher & Fritz (1991b)

concentrated seawater (McCaffrey et al. 1987)			Salar de Uyuni brines (Risacher & Fritz 1991b)		
Sample number	Density [kg/m³]	TDS [g/L]	Sample number	Density [kg/m³]	TDS [g/L]
w61	1,187	278.0	US	1,201	320.9
w46	1,214	318.0	UA	1,211	325.0
w43	1,223	324.8	UO	1,231	356.8
w36	1,249	357.8	UB	1,248	359.5
36#5	1,319	433.0	RZ	1,279	389.8
36#4	1,334	448.7			
40#6	1,310	423.7			

Table A12: Mean saturation indices of the brines from different locations modelled by PhreeqC using PITZER

Phase	Formula	SLT-01		SLT-03		SLT-S
		mean	std.dev.	mean	std.dev.	
Anhydrite	$CaSO_4$	0.48	0.065	0.52	0.037	0.16
Aragonite	$CaCO_3$	0.24	0.082	-0.01	0.081	0.42
Arcanite	K_2SO_4	-2.53	0.017	-1.14	0.043	-2.54
Bischofite	$MgCl_2{:}6H_2O$	-3.27	0.085	-2.42	0.041	-3.73
Bloedite	$Na_2Mg(SO_4)_2{:}4H_2O$	-1.70	0.083	-0.28	0.075	-2.32
Borax	$Na_2(B_4O_5(OH)_4){:}8H_2O$	-3.37	0.046	-1.52	0.088	-4.57
Brucite	Mg(OH)2	-3.44	0.114	-2.86	0.067	-5.99
Burkeite	$Na_6CO_3(SO_4)_2$	-6.11	0.121	-5.33	0.024	-6.7
Calcite	$CaCO_3$	0.44	0.082	0.20	0.081	0.62
Carnallite	$KMgCl_3{:}6H_2O$	-3.06	0.109	-1.56	0.058	-3.62
Celestite	$SrSO_4$	0.59	0.057	-0.16	0.353	0.3
Dolomite	$CaMg(CO_3)_2$	2.29	0.171	2.98	0.097	2.63
Epsomite	$MgSO_4{:}7H_2O$	-1.46	0.046	-0.54	0.057	-1.71
Gaylussite	$CaNa_2(CO_3)_2{:}5H_2O$	-4.27	0.102	-4.63	0.131	-3.82
Glaserite	$NaK_3(SO_4)_2$	-3.62	0.041	-1.29	0.059	-3.63
Glauberite	$Na_2Ca(SO_4)_2$	0.42	0.095	0.83	0.033	-0.21
Gypsum	$CaSO_4{:}2H_2O$	0.40	0.053	0.38	0.035	0.18
Halite	NaCl	0.33	0.039	0.44	0.010	0
Hexahydrite	$MgSO_4{:}6H_2O$	-1.57	0.048	-0.61	0.060	-1.85
Kainite	$KMgClSO_4{:}3H_2O$	-2.71	0.083	-0.97	0.068	-3.11
Kalicinite	$KHCO_3$	-5.05	0.022	-4.29	0.042	-3.24
Kieserite	$MgSO_4{:}H_2O$	-2.46	0.067	-1.31	0.060	-2.86
Leonhardite	$MgSO_4{:}4H_2O$	-2.20	0.055	-1.15	0.053	-2.48
Leonite	$K_2Mg(SO_4)2{:}4H_2O$	-3.74	0.062	-1.25	0.088	-3.91
Magnesite	$MgCO_3$	1.33	0.083	2.23	0.006	1.36
Mirabilite	$Na_2SO_4{:}10H_2O$	-0.44	0.073	-0.54	0.047	-0.76
Misenite	$K_8H_6(SO_4)_7$	-60.39	0.120	-52.57	0.425	-52.09
Nahcolite	$NaHCO_3$	-2.53	0.030	-2.30	0.044	-0.95
Natron	$Na_2CO_3{:}10H_2O$	-5.82	0.022	-6.10	0.068	-5.34
Nesquehonite	$MgCO_3{:}3H_2O$	-1.76	0.071	-0.98	0.008	-1.64
Pentahydrite	$MgSO_4{:}5H_2O$	-1.97	0.047	-0.95	0.053	-2.21
Pirssonite	$Na_2Ca(CO_3)_2{:}2H_2O$	-3.95	0.113	-4.21	0.127	-3.62
Polyhalite	$K_2MgCa_2(SO_4)_4{:}2H_2O$	-1.38	0.194	1.28	0.087	-2.2
Portlandite	$Ca(OH)_2$	-10.83	0.122	-11.36	0.148	-13.14
Schoenite	$K_2Mg(SO_4)_2{:}6H_2O$	-3.73	0.049	-1.30	0.081	-3.82
Sylvite	KCl	-0.66	0.025	-0.04	0.021	-0.83
Syngenite	$K_2Ca(SO_4)_2{:}H_2O$	-1.23	0.068	0.23	0.028	-1.36
Teepleite	$Na_2B(OH)_4Cl$	-2.52	0.065	-2.02	0.026	-3.88
Trona	$Na_3H(CO_3)_2{:}2H_2O$	-7.19	0.064	-6.97	0.080	-5.44

Table A13: Results of the pumping test in well SLT-03C at the 25th September 2009, the drawdown h_s was measured in the observation wells SLT-03E and SLT-03B in differing time intervals after starting the pump

t	h_s [m]		t	h_s [m]		t	h_s [m]	
[min]	SLT-03E	SLT-03B	[min]	SLT-03E	SLT-03B	[min]	SLT-03E	SLT-03B
0	0	0	19	0	0.042	46	0.006	0.058
1	0	0.03	20	0	0.045	48	0.01	0.058
2	0	0.02	21	0	0.045	50	0.005	0.058
3	0	0.04	22	0	0.045	55	0.008	0.059
4	0	0.04	23	0	0.045	60	0.008	0.057
5	0	0.04	24	0	0.047	65	0.008	0.061
6	0	0.04	25	0	0.045	70	0.008	0.063
7	0	0.04	26	0	0.048	75	0.008	0.062
8	0	0.04	27	0	0.049	80	0.005	0.062
9	0	0.04	28	0	0.049	90	0.005	0.06
10	0	0.04	29	0	0.05	100	0.005	0.07
11	0	0.04	30	0	0.05	110	0.008	0.07
12	0	0.04	32	0	0.05	115	0.008	0.07
13	0	0.04	34	0	0.05	120	0.005	0.07
14	0	0.04	36	0.002	0.05	130	0.005	0.07
15	0	0.04	38	0.004	0.051	140	0.008	0.07
16	0	0.04	40	0.004	0.051	150	0.008	0.07
17	0	0.04	42	0.004	0.054	160	0.008	0.07
18	0	0.04	44	0.006	0.055			

Table A14: Results of the recovery test in SLT-01A at the 26th September 2009, the decreasing drawdown h_s was measured in SLT-01A in differing time intervals after switching off the pump

t [s]	h_s [m]		t [s]	h_s [m]		t [s]	h_s [m]
10	3.29		900	1.18		1,620	0.25
120	2.89		960	1.04		1,680	0.19
180	2.74		1,020	0.98		1,740	0.15
240	2.57		1,080	0.88		1,800	0.12
300	2.42		1,140	0.79		1,860	0.09
360	2.26		1,200	0.71		1,980	0.06
420	2.14		1,260	0.64		2,100	0.04
540	1.87		1,320	0.55		2,220	0.03
600	1.77		1,380	0.47		2,400	0.02
720	1.54		1,440	0.41		2,700	0.01
840	1.29		1,500	0.33			

Appendix B: Drilling profiles

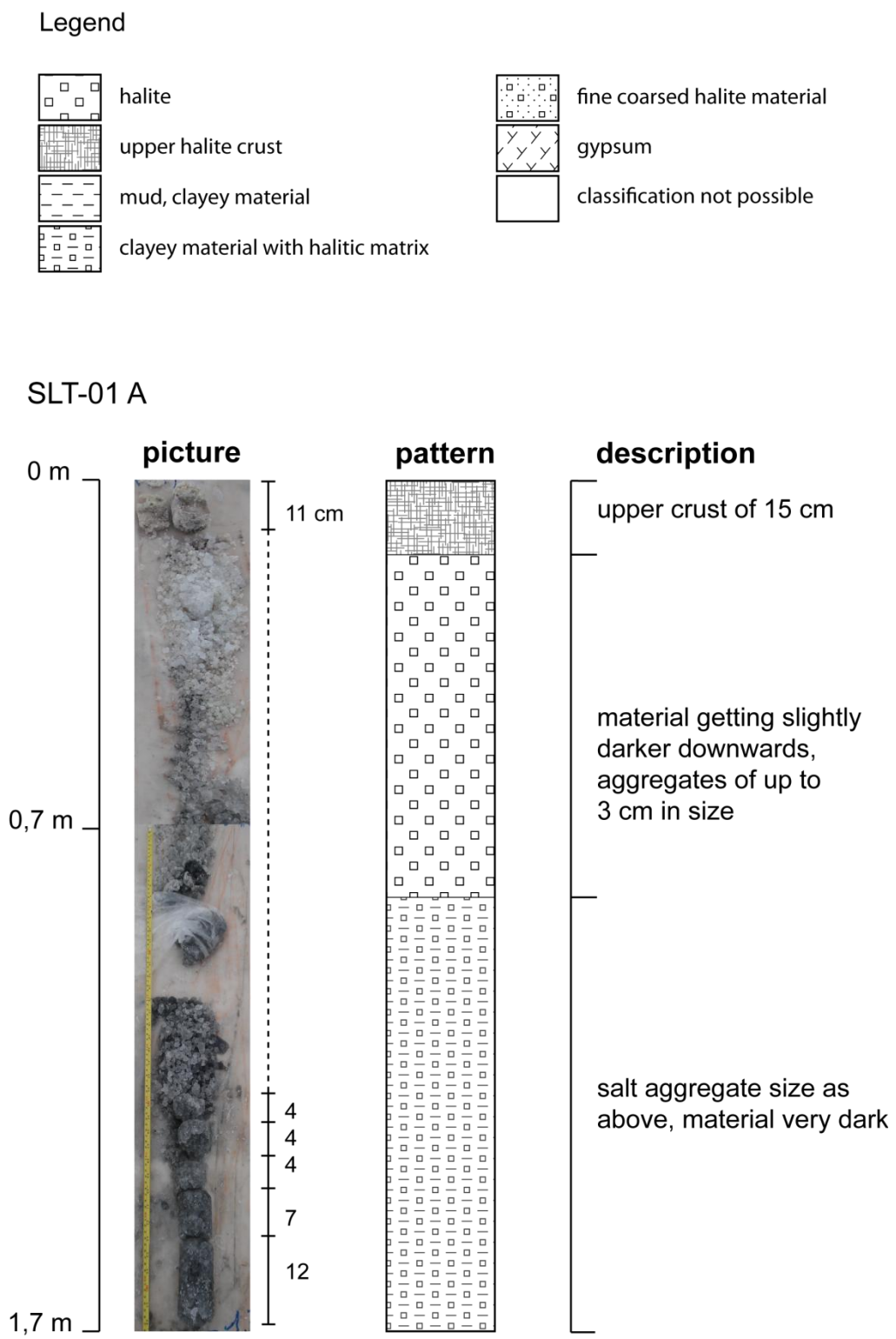

Fig. B1: Drilling profile for SLT-01A between a depth of 0 and 1.70 m and legend for the schematic illustration of the stratigraphy

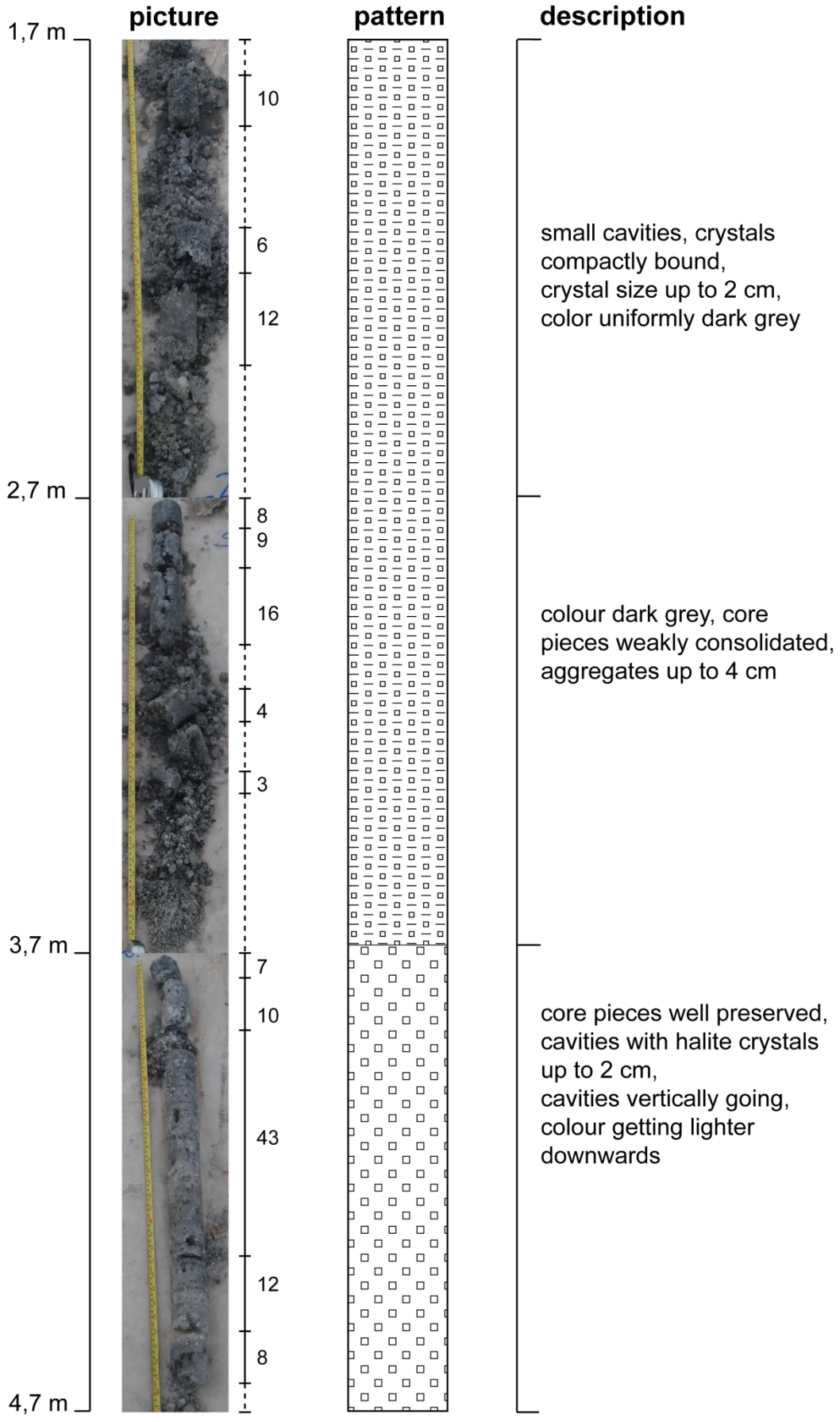

Fig. B2: Drilling profile for SLT-01A between a depth of 1.70 and 4.70 m

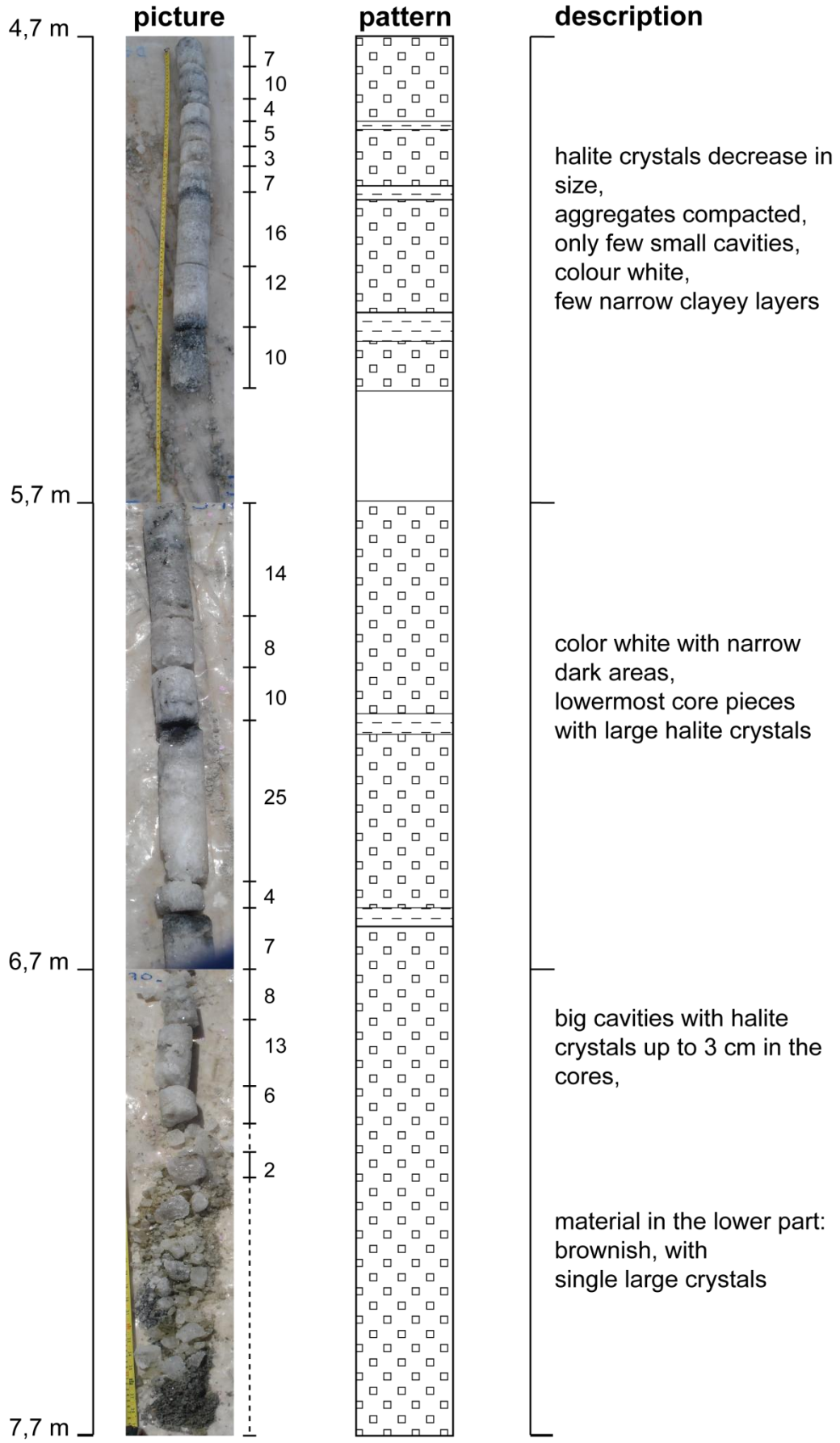

Fig. B3: Drilling profile for SLT-01A between a depth of 4.70 and 7.70 m

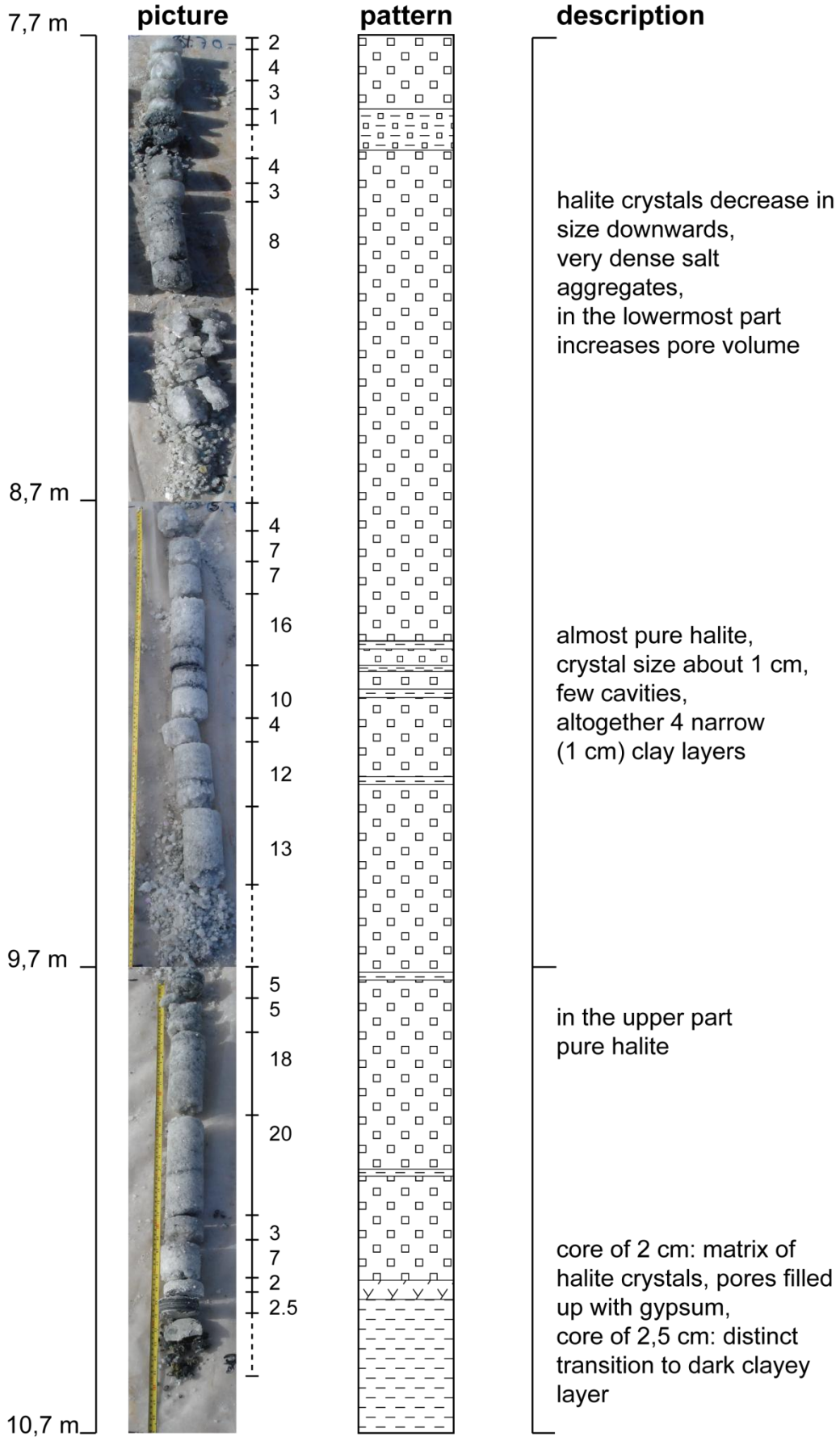

Fig. B4: Drilling profile for SLT-01A between a depth of 7.70 and 10.70 m

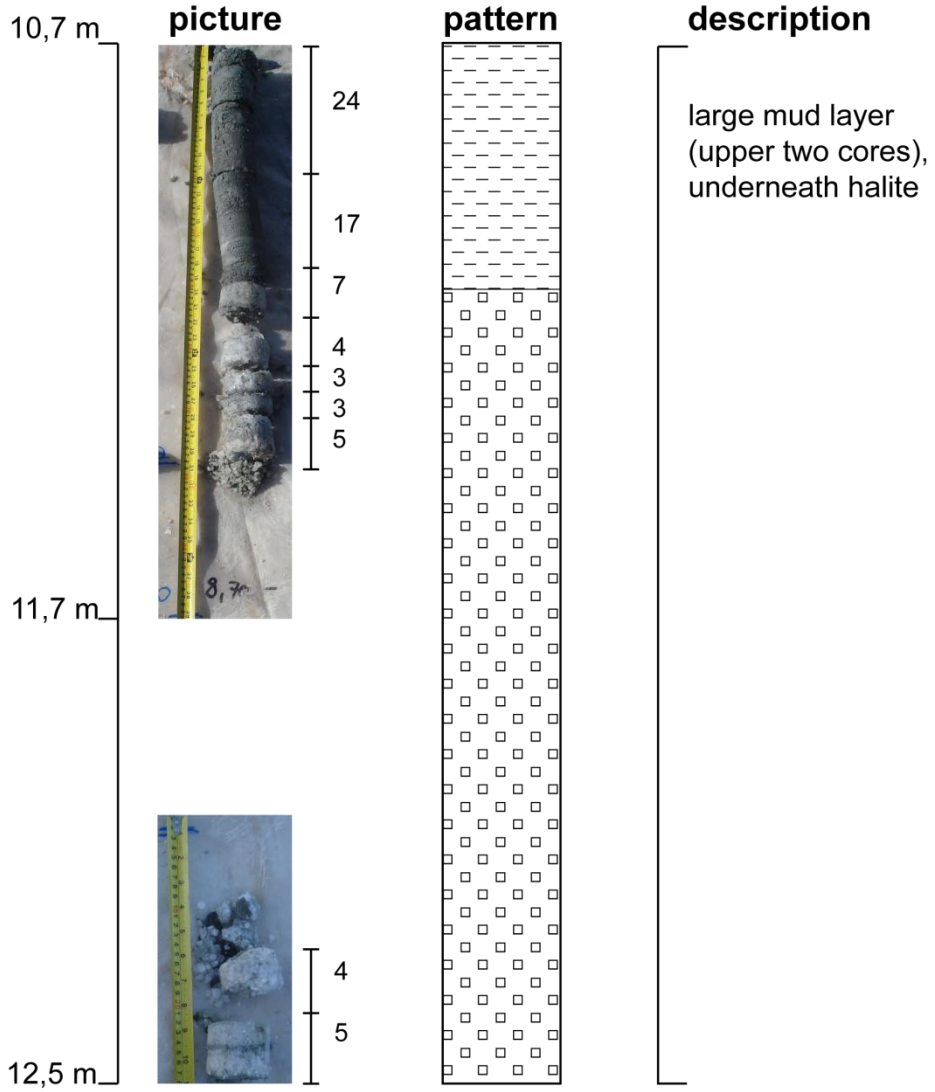

Fig. B5: Drilling profile for SLT-01A between a depth of 10.70 and 12.50 m

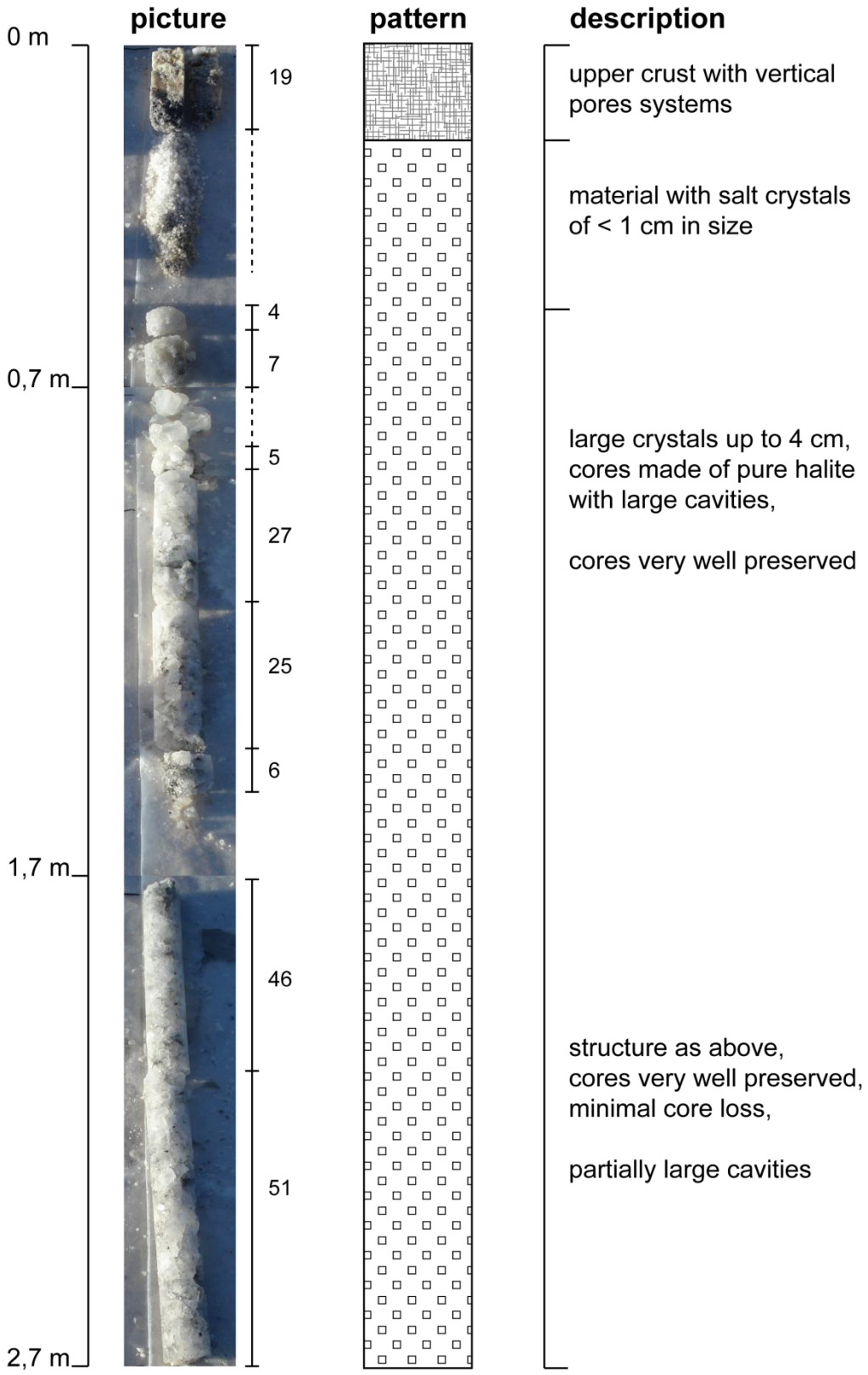

Fig. B6: Drilling profile for SLT-01E between a depth of 0 and 2.70 m

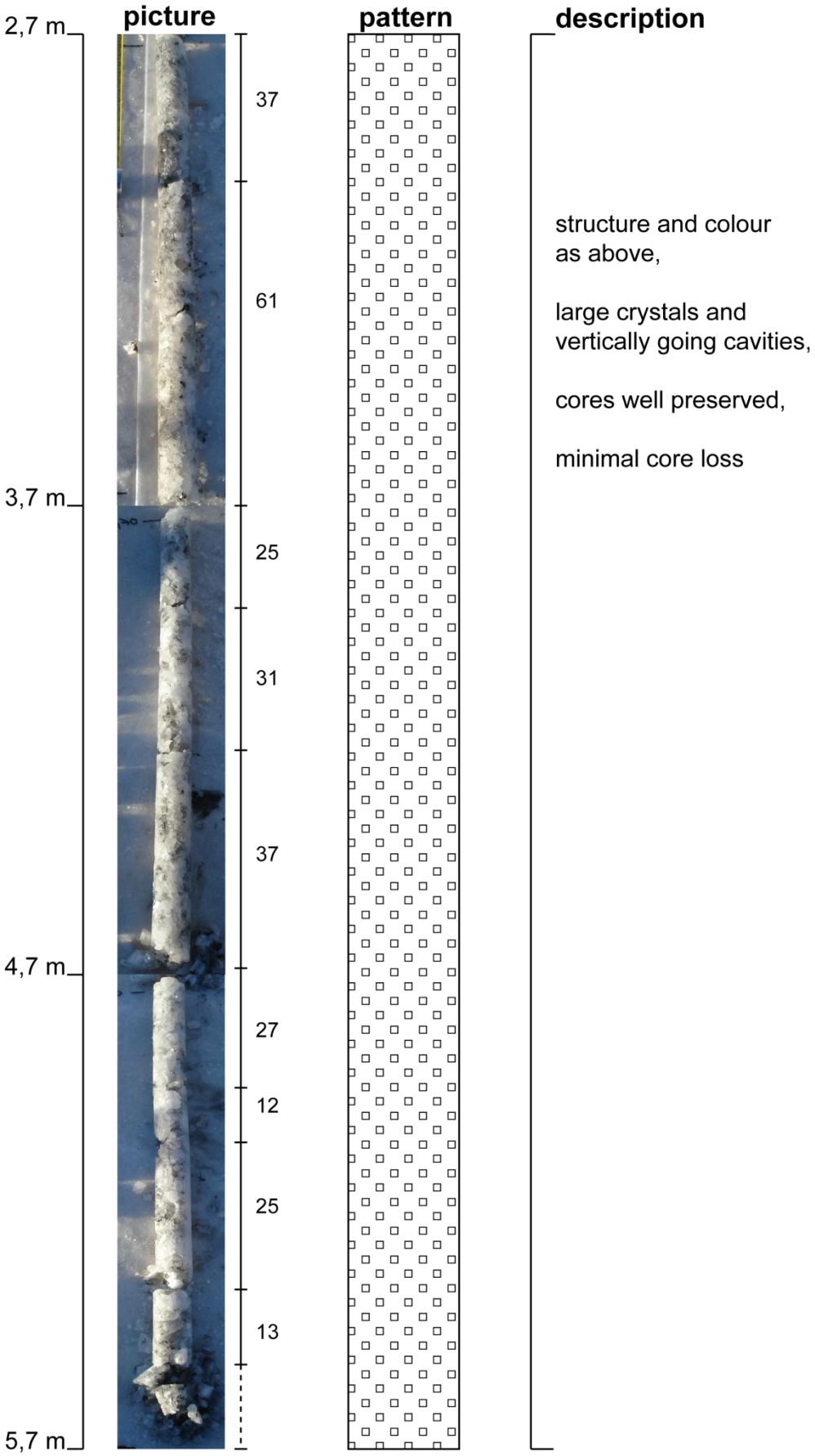

Fig. B7: Drilling profile for SLT-01E between a depth of 2.70 and 5.70 m

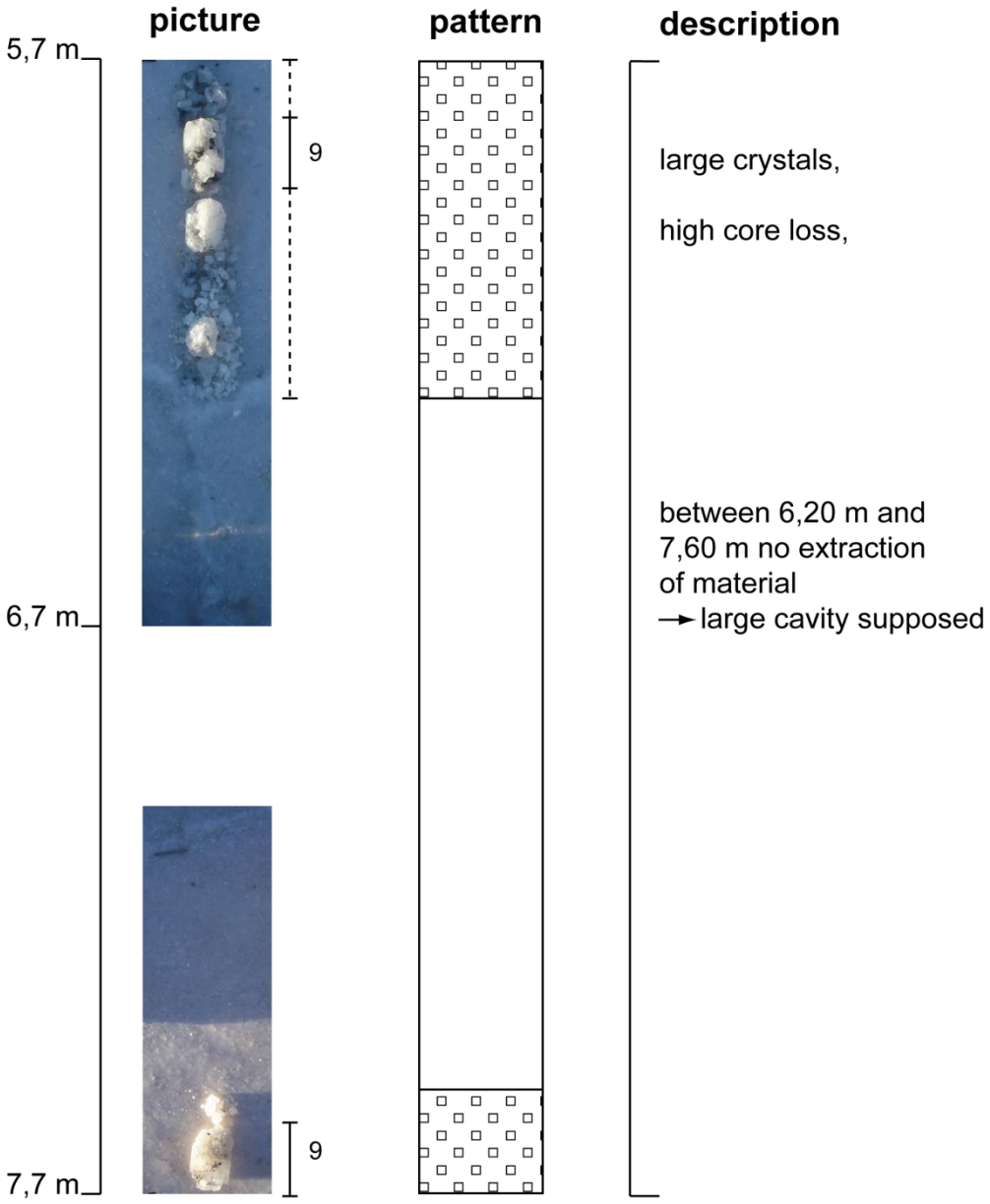

Fig. B8 : Drilling profile for SLT-01E between a depth of 5.70 and 7.70 m

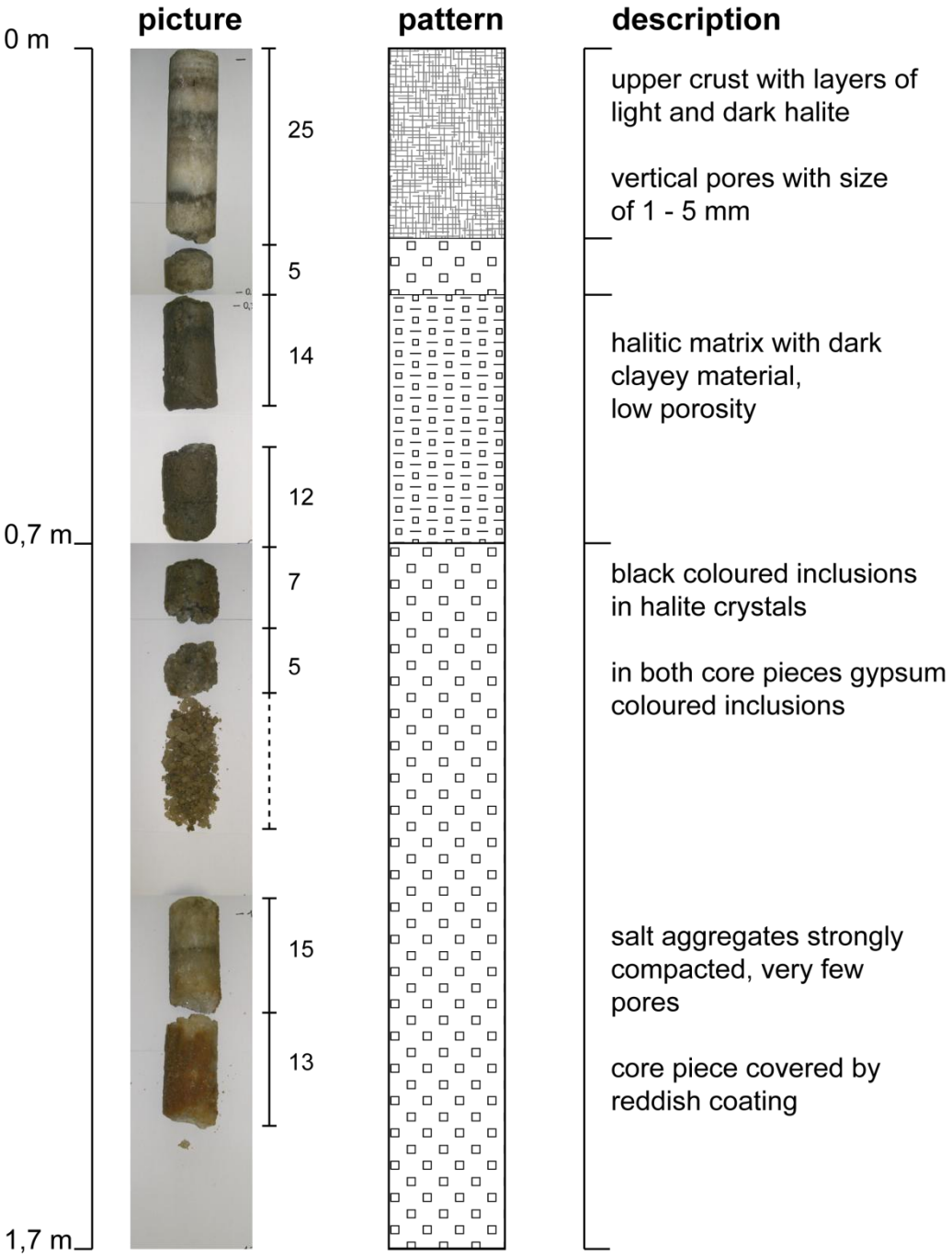

Fig. B9: Drilling profile for SLT-03A between a depth of 0 and 1.70 m

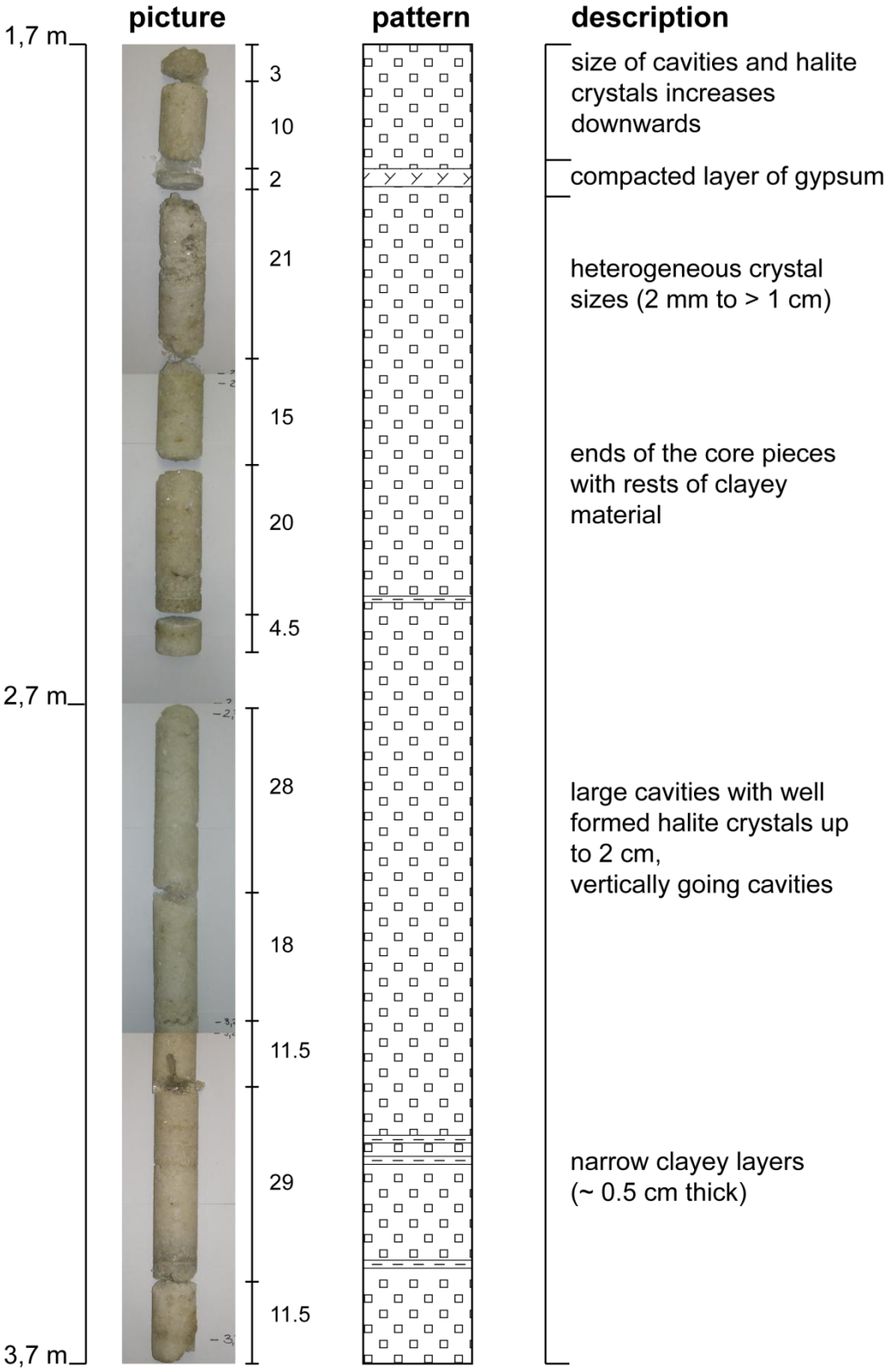

Fig. B10: Drilling profile for SLT-03A between a depth of 1.70 and 3.70 m

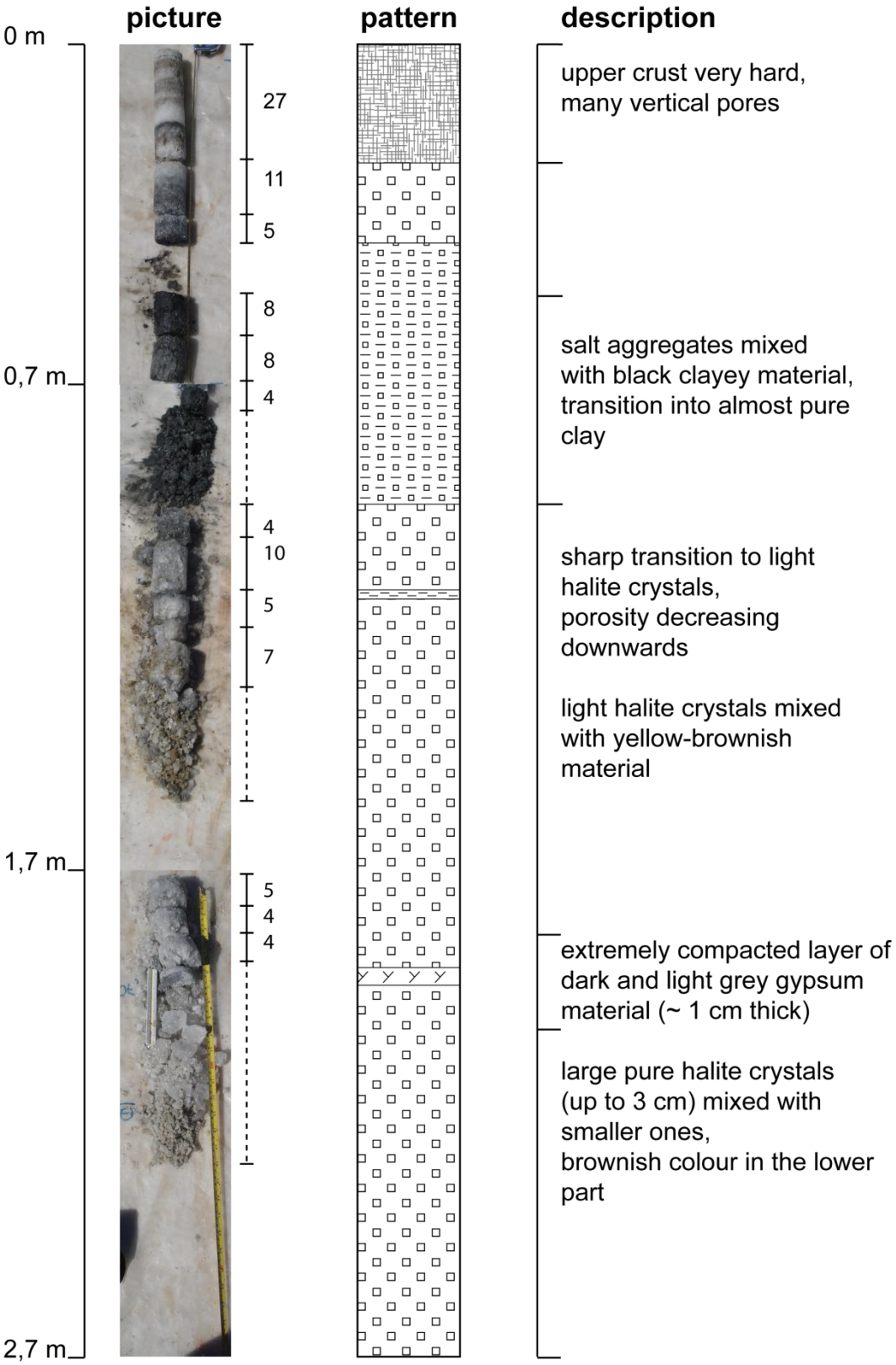

Fig. B11: Drilling profile for SLT-03C between a depth of 0 and 2.70 m

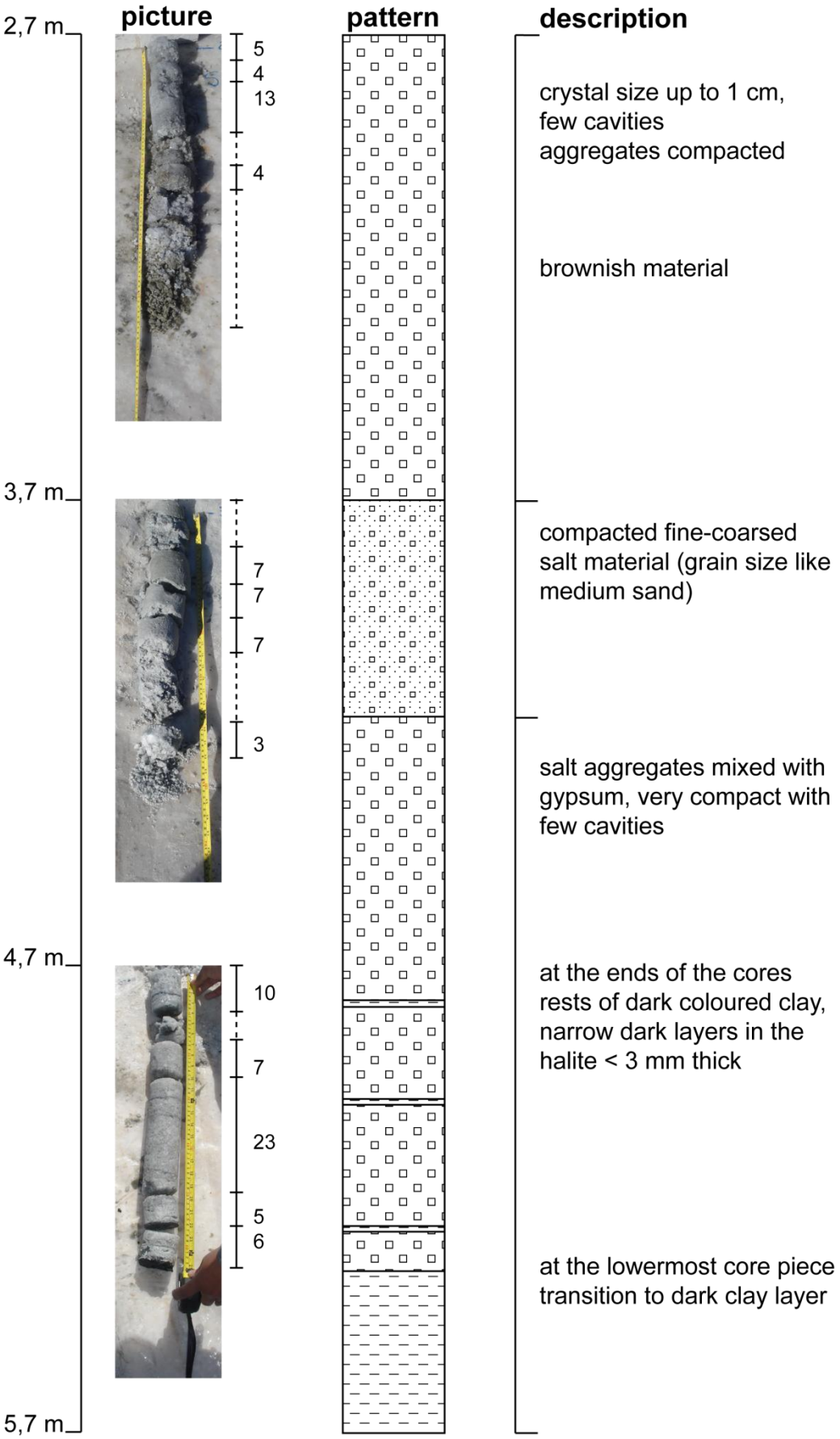

Fig. B12: Drilling profile for SLT-03C between a depth of 2.70 and 5.70 m

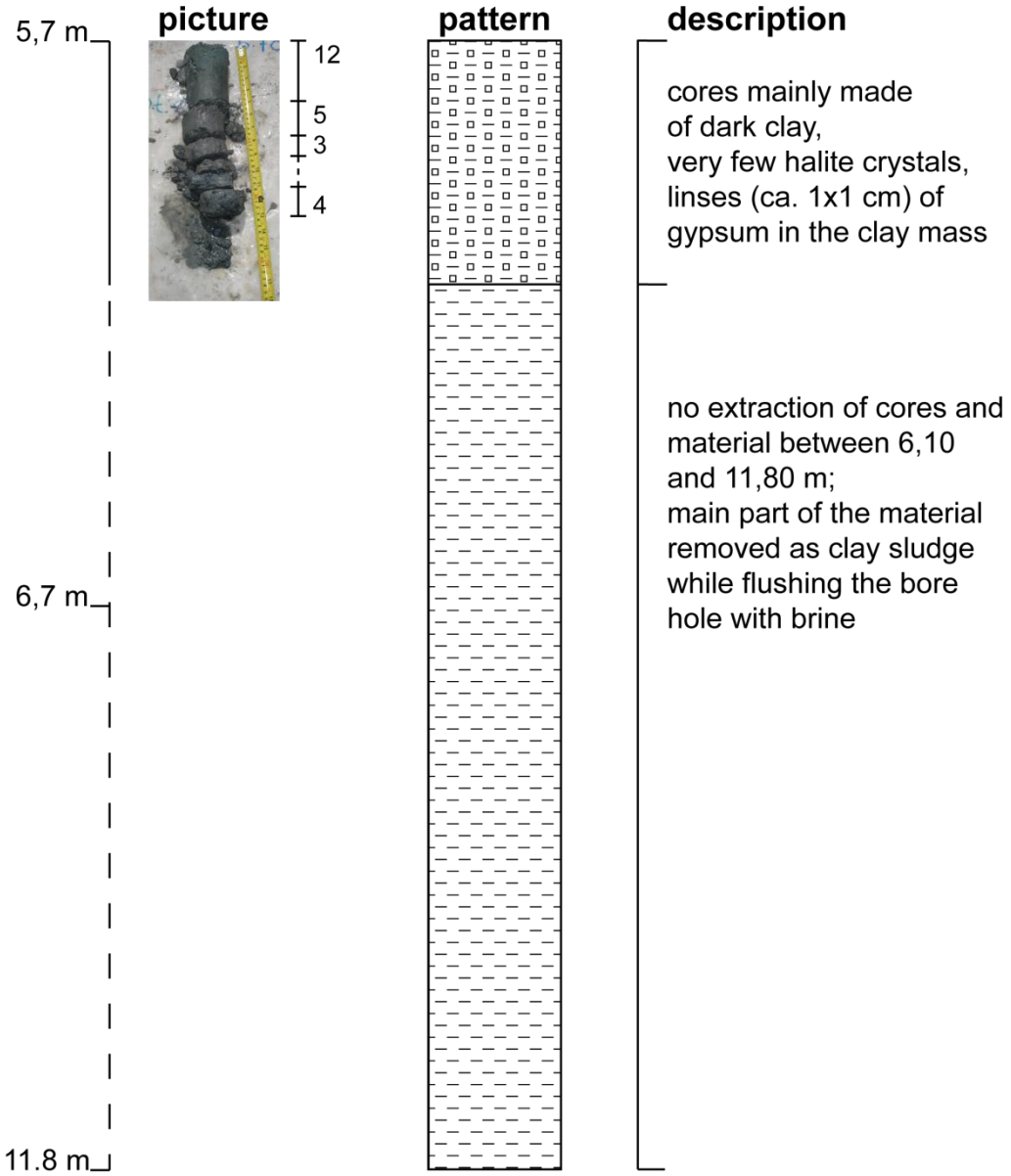

Fig. B13: Drilling profile for SLT-03C between a depth of 5.70 and 11.80 m

Appendix C: Others

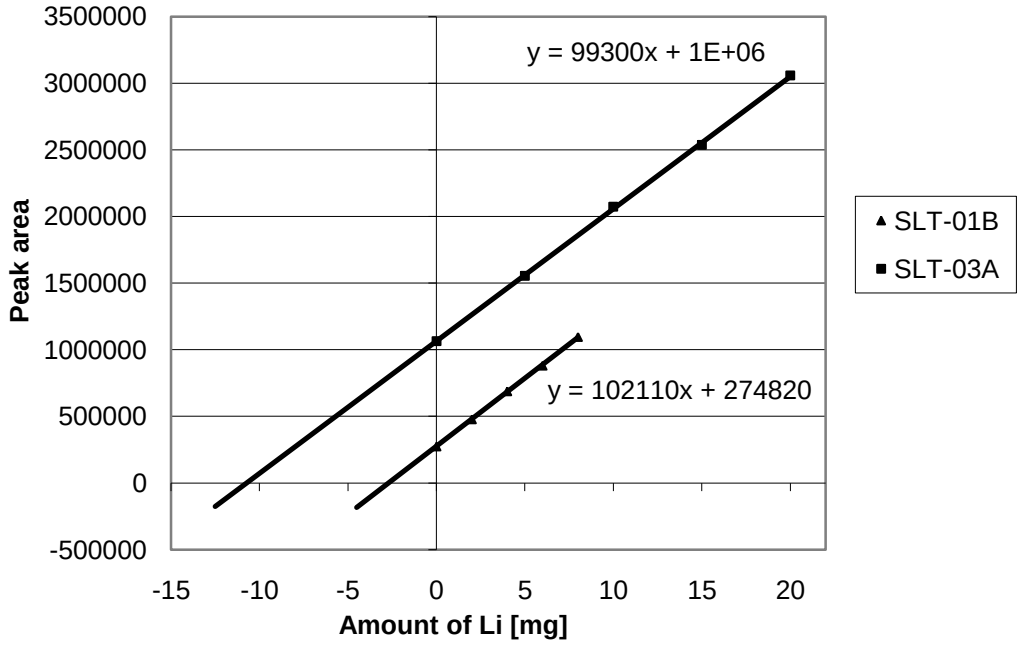

Fig. C1: Results of the standard addition for two samples (the Y-intercept corresponds to the amount of lithium in the original solution)